Construction and Testing of Large-Area GEM Detectors for the Forward Muon Endcap Upgrade of the CMS Experiment and Vector-Portal Search for Dark Matter Particles with Dimuon Pairs at $\sqrt{s}$ = 13 TeV

A Dark Matter Search at the LHC

Dissertation Defense

Mehdi Rahmani
Florida Institute of Technology

Contact: mrahmani2015@my.fit.edu

Apr 19, 2022

FLORIDA TECH

Compact Muon Solenoid

Layout

1. The Experimental Apparatus

The Experimental Apparatus

The Large Hadron Collider

- The principal idea behind the Large Hadron Collider (**LHC**) is utilizing the electromagnetic field to accelerate and steer particles
- At the LHC, proton beams are injected into Radiofrequency (RF) cavities and boosted to the desired energies.

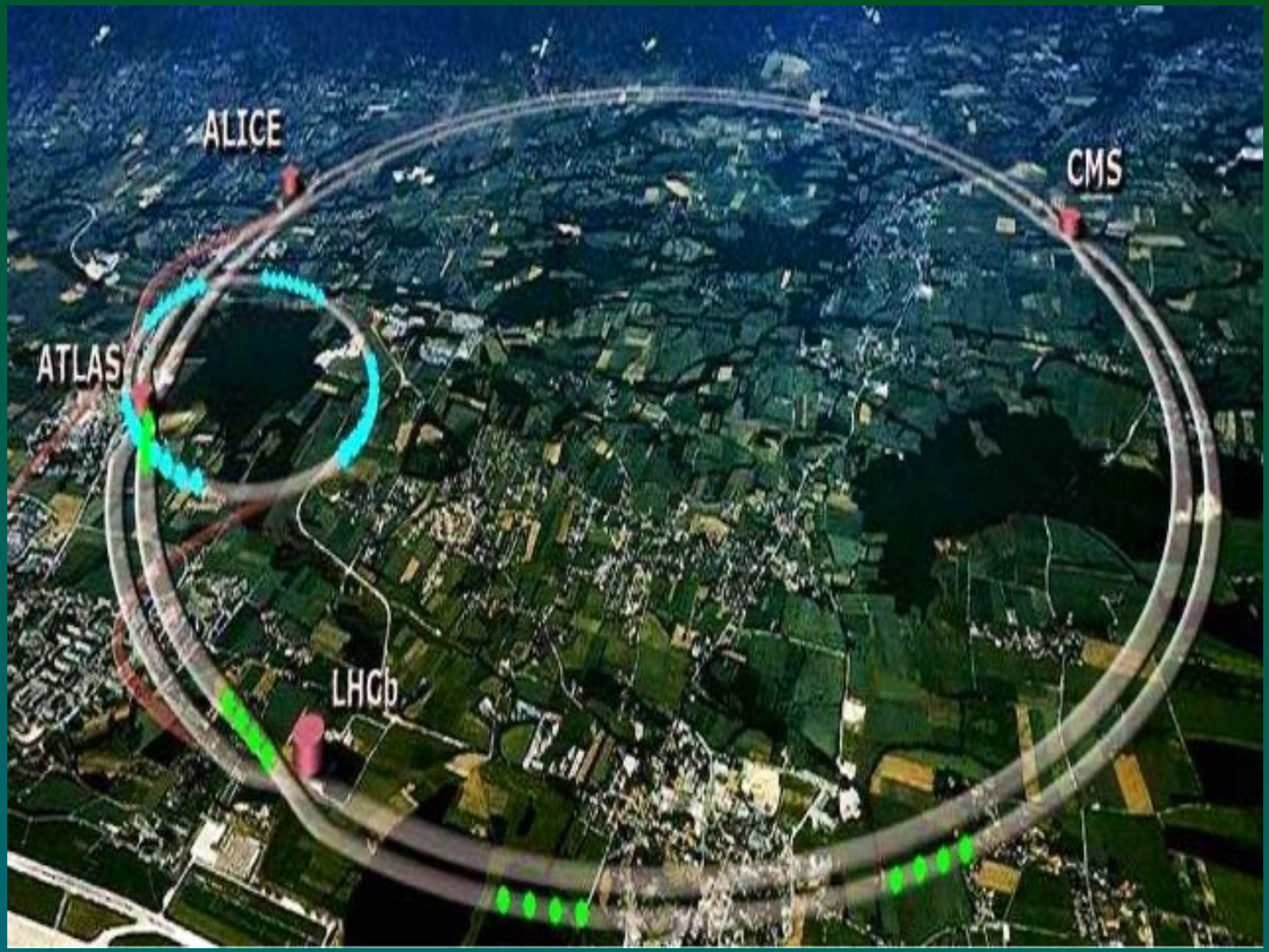

The CERN complex

The Experimental Apparatus

The Large Hadron Collider

- The principal idea behind the Large Hadron Collider (**LHC**) is utilizing the magnetic field to accelerate and steer particles
- At the LHC, proton beams are injected into Radiofrequency (RF) cavities and boosted to the desired energies.
- Groups of protons are then sorted into packs of protons called "***bunches***."
- Once boosted, the beams are guided and focused by superconducting electromagnets at the near speed of light.
- The two largest detectors are built around intersections

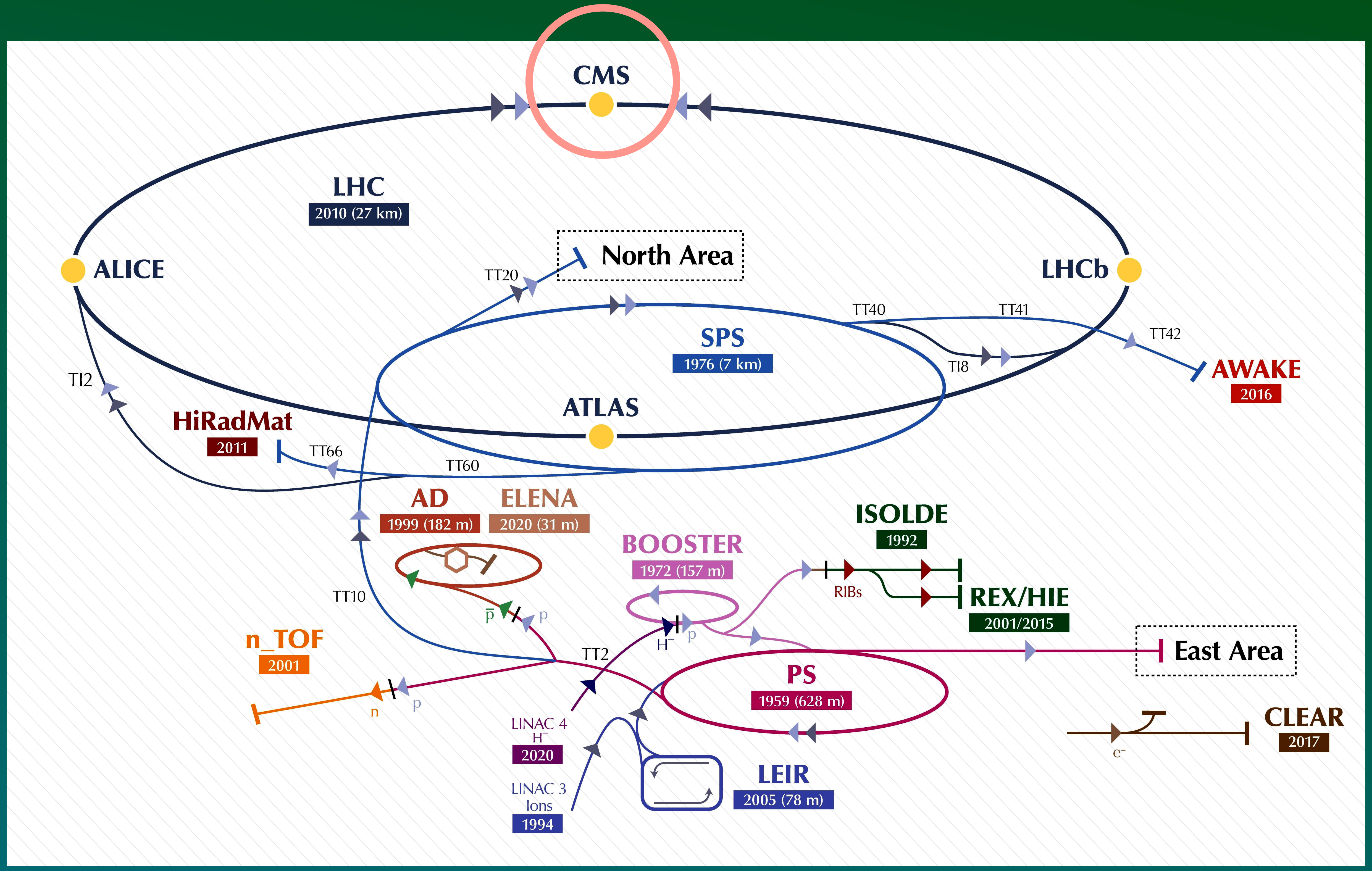

The CERN complex

The Experimental Apparatus

The Compact Muon Solenoid

- The Compact Muon Solenoid (**CMS**) detector utilizes magnetic system for muon detection

- A superconducting solenoid with 13 m of length and 5.9 m of radius produces a uniform magnetic field of **4 Tesla** in the core and 2 Tesla outside the solenoid

Source: CMS-OUTREACH-2019-001, 2019

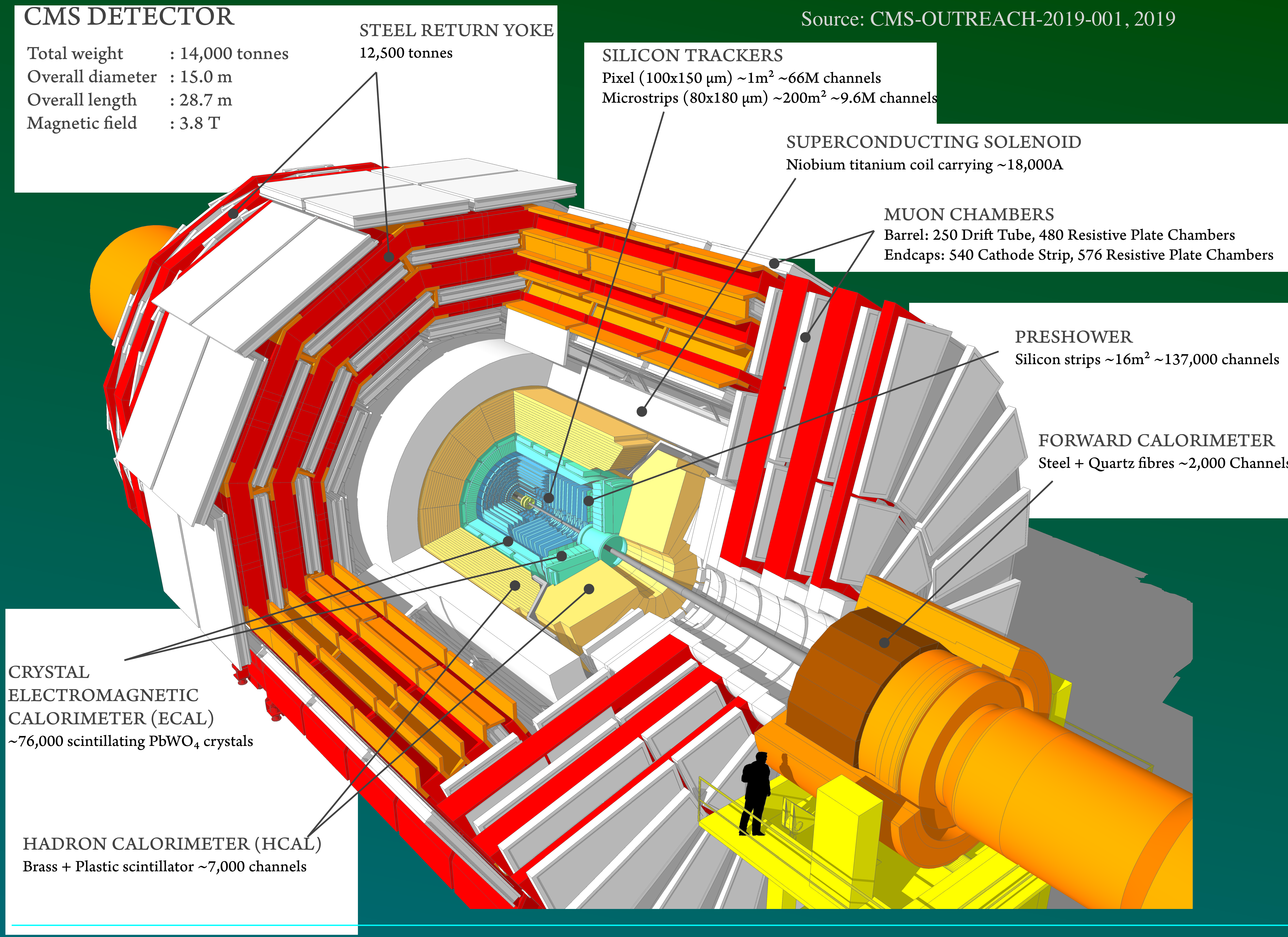

The CMS detector

The Experimental Apparatus

The Compact Muon Solenoid

- The Compact Muon Solenoid (**CMS**) detector utilizes magnetic system for muon detection

- A superconducting solenoid with 13 m of length and 5.9 m of radius produces a uniform magnetic field of **4 Tesla** in the core and 2 Tesla outside the solenoid

- Major components:
    - **Magnet and Muon System**
    - **Tracking**
    - **and Calorimetry**

Source: CMS-OUTREACH-2019-001, 2019

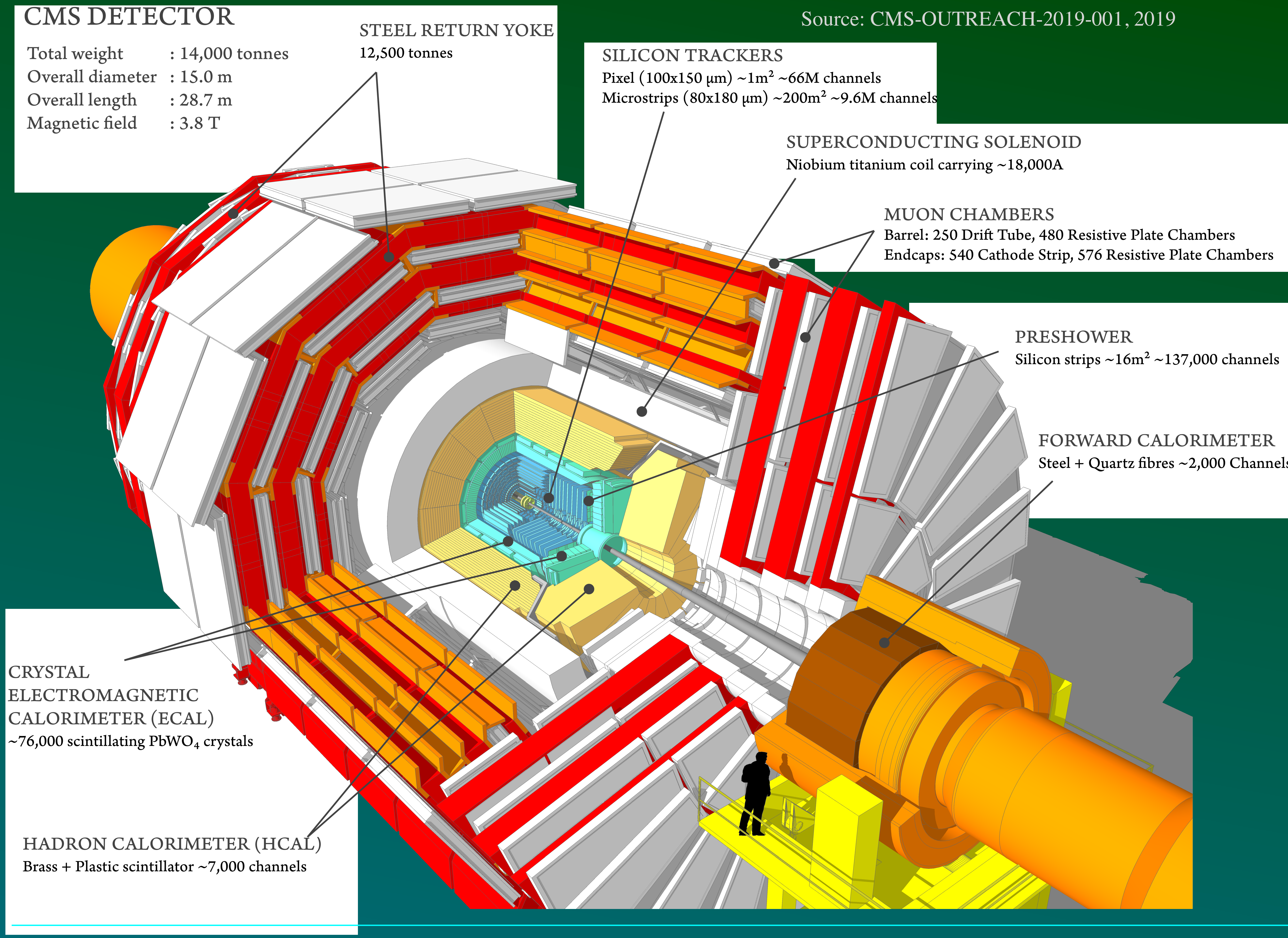

The CMS detector

The Experimental Apparatus

Bending Muons

- The magnetic field, produced by superconducting solenoid, facilities precise measurements of the momentum of the muon tracks.

- The magnetic flux **bends muon** tracks in the **transverse plane.**

- The bending and the direction of the tracks can be parametrized (sagitta) and used to solve the equation of motion

- The **momentum** and the **charge** of the of particles are determined via measuring this angle

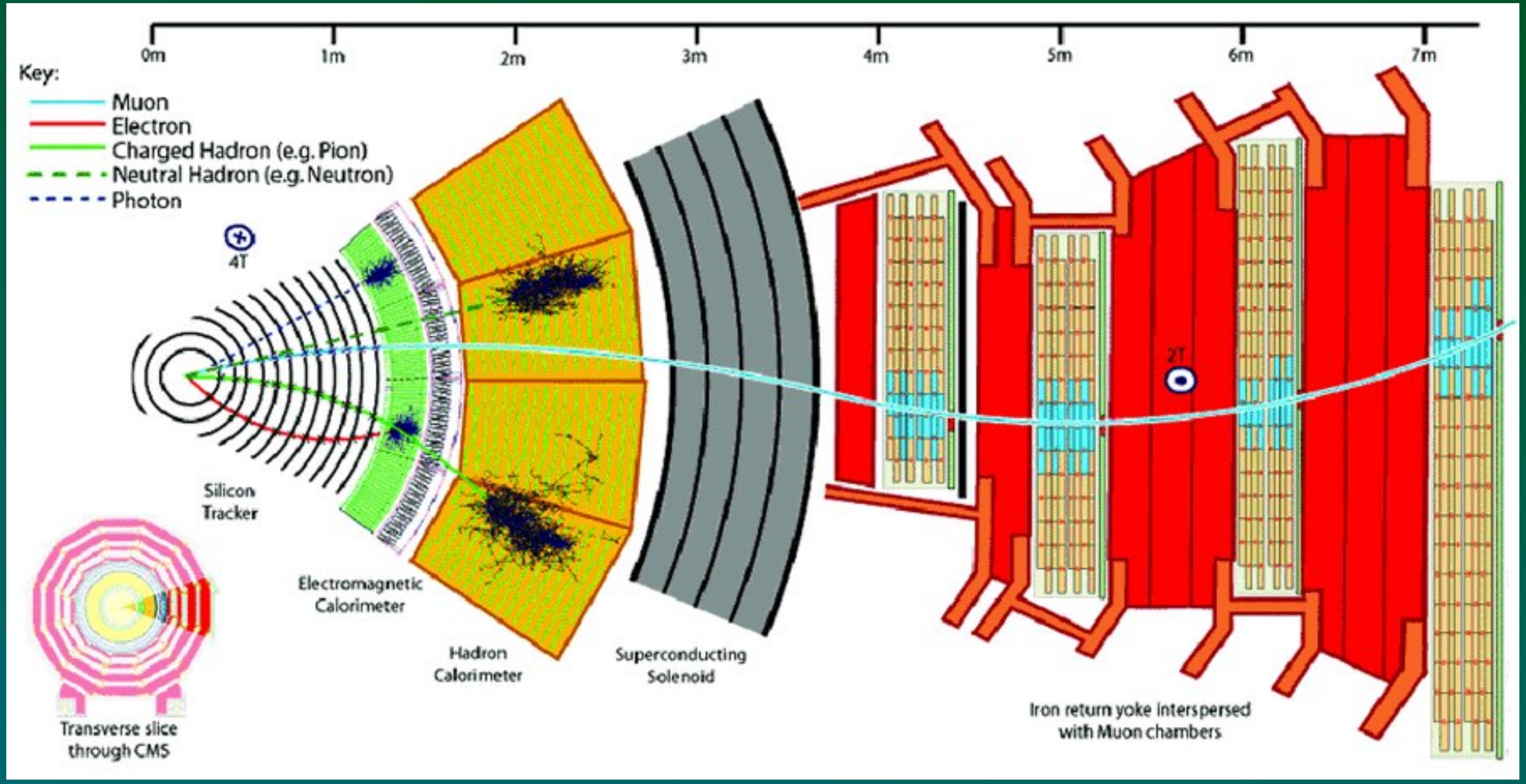

The bending of the an electromagnetic particle

The Experimental Apparatus

Identifying Tracks

- The tracking task at the CMS is shared by two major systems
  - **the inner trackers**
  - **the muon system**

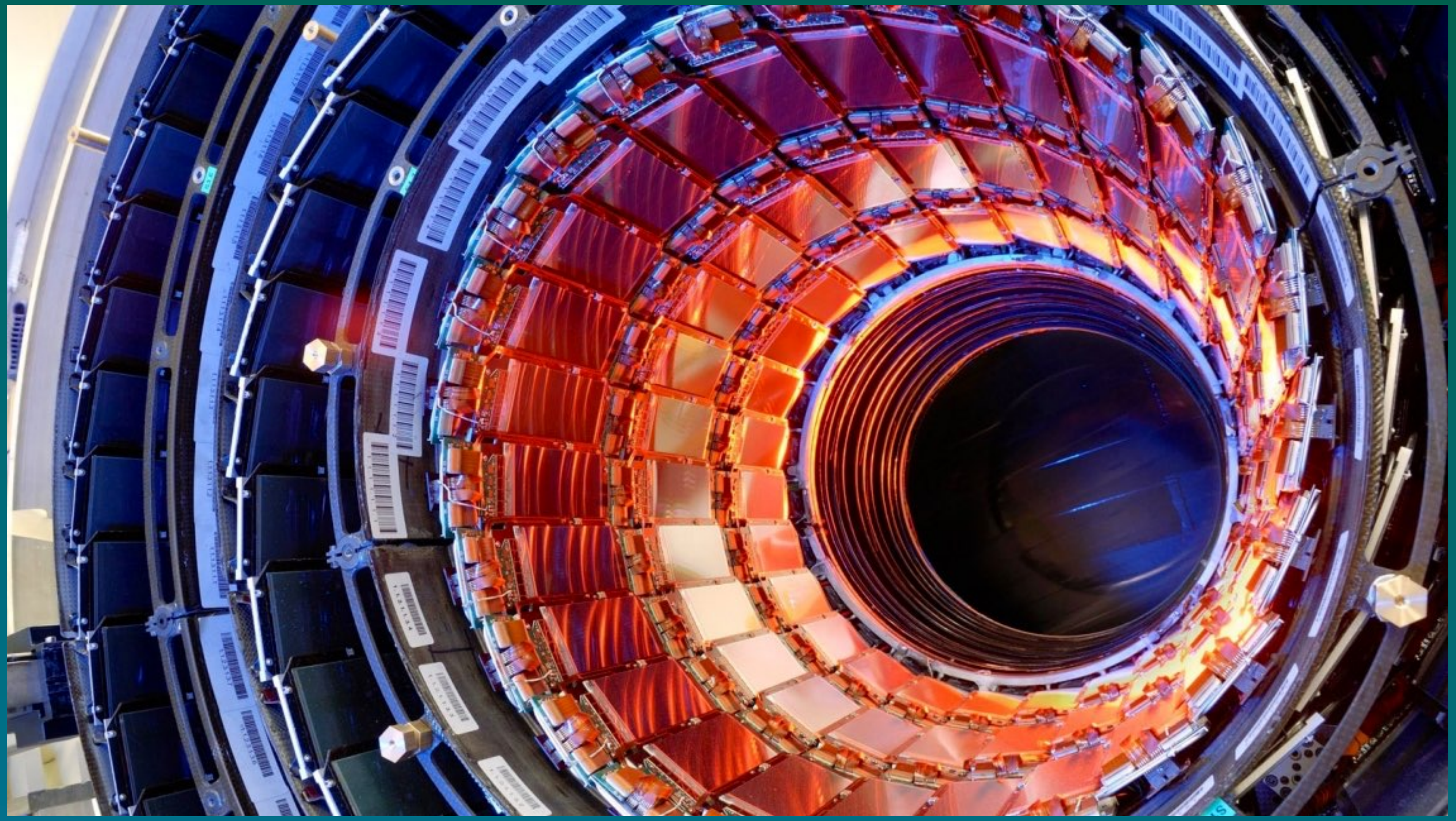

The strip tracker

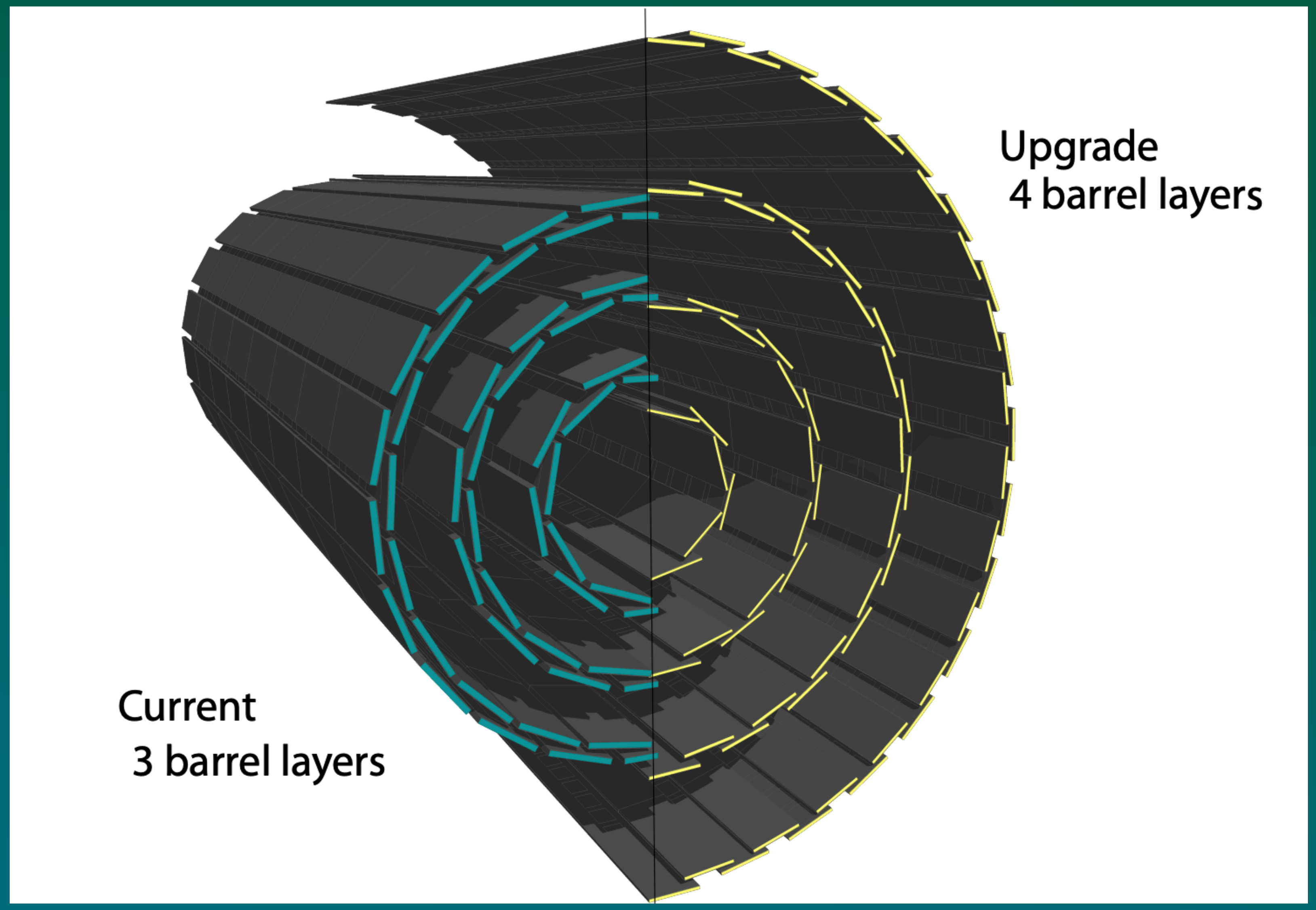

The silicon pixels

The Experimental Apparatus

Identifying Tracks

- The tracking task at the CMS is shared by two major systems
  - **the inner trackers**
  - **the muon system**

- The inner tracker detectors: semiconductor-based
  - **the pixel detectors** (went through upgrade in 2016)
  - **strip detectors**
- Muon system: gaseous detectors

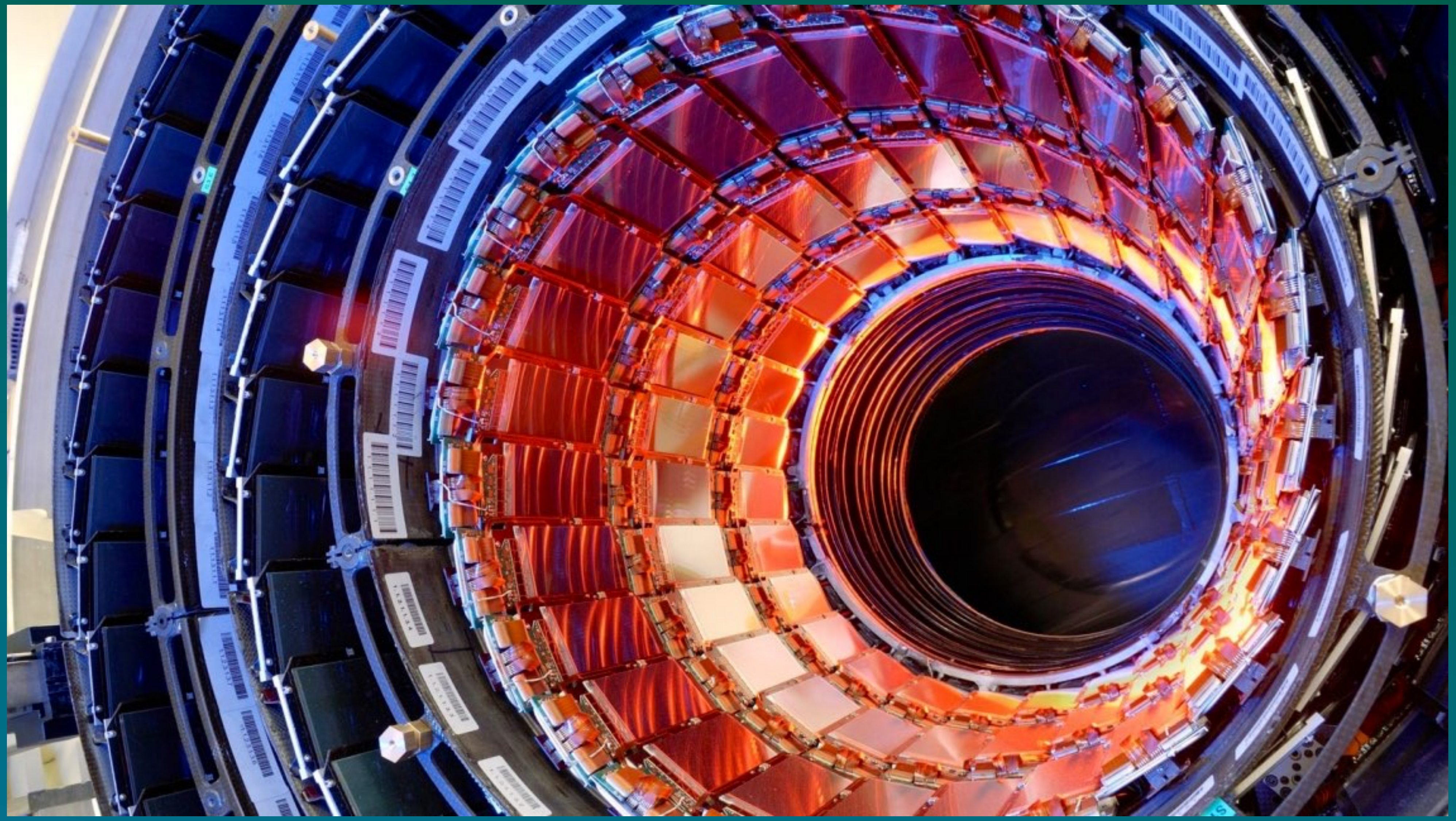

The strip tracker

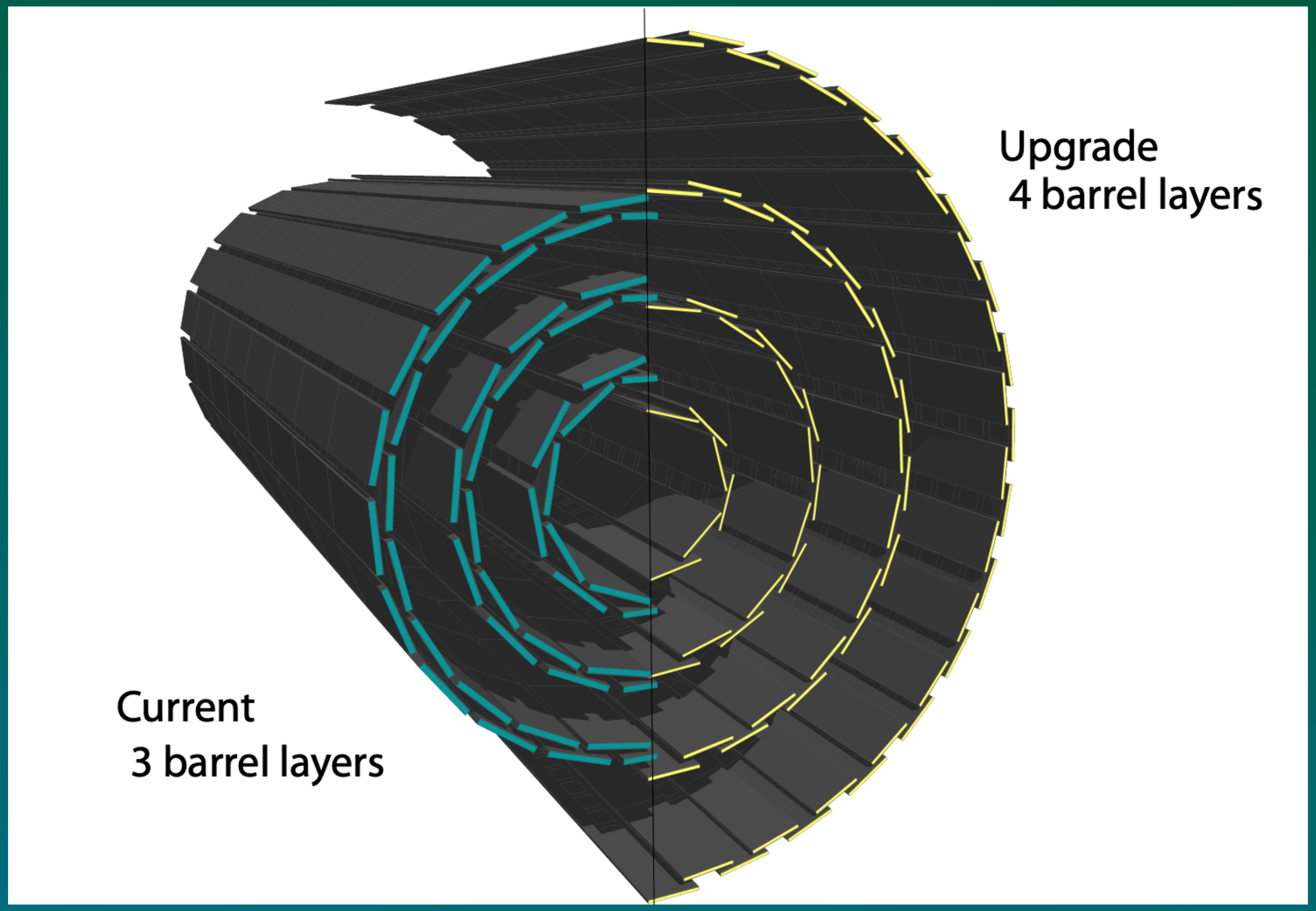

The silicon pixels

The Experimental Apparatus

Measuring Energy: Calorimetry

- At the CMS, calorimetry is done on electromagnetic particles
  - e, e^+, γ: measured by **electromagnetic** calorimeter (**ECAL**)
  - p, n, $\pi^\pm$, $\mathscr{K}^\pm$: measured by **hadronic** calorimeter (**HCAL**)

The Experimental Apparatus

Measuring Energy: Calorimetry

- At the CMS, calorimetry is done on electromagnetic particles
    - e, e^+, γ: measured by electromagnetic calorimeter (**ECAL**)
    - p, n, $\pi^{\pm}$, $\mathscr{K}^{\pm}$: measured by hadronic calorimeter (**HCAL**)

ECAL

- $PbWO_4$ crystals as scintillation materials
- High-energy electromagnetic particles produce ***showers*** in the crystals upon smashing into them

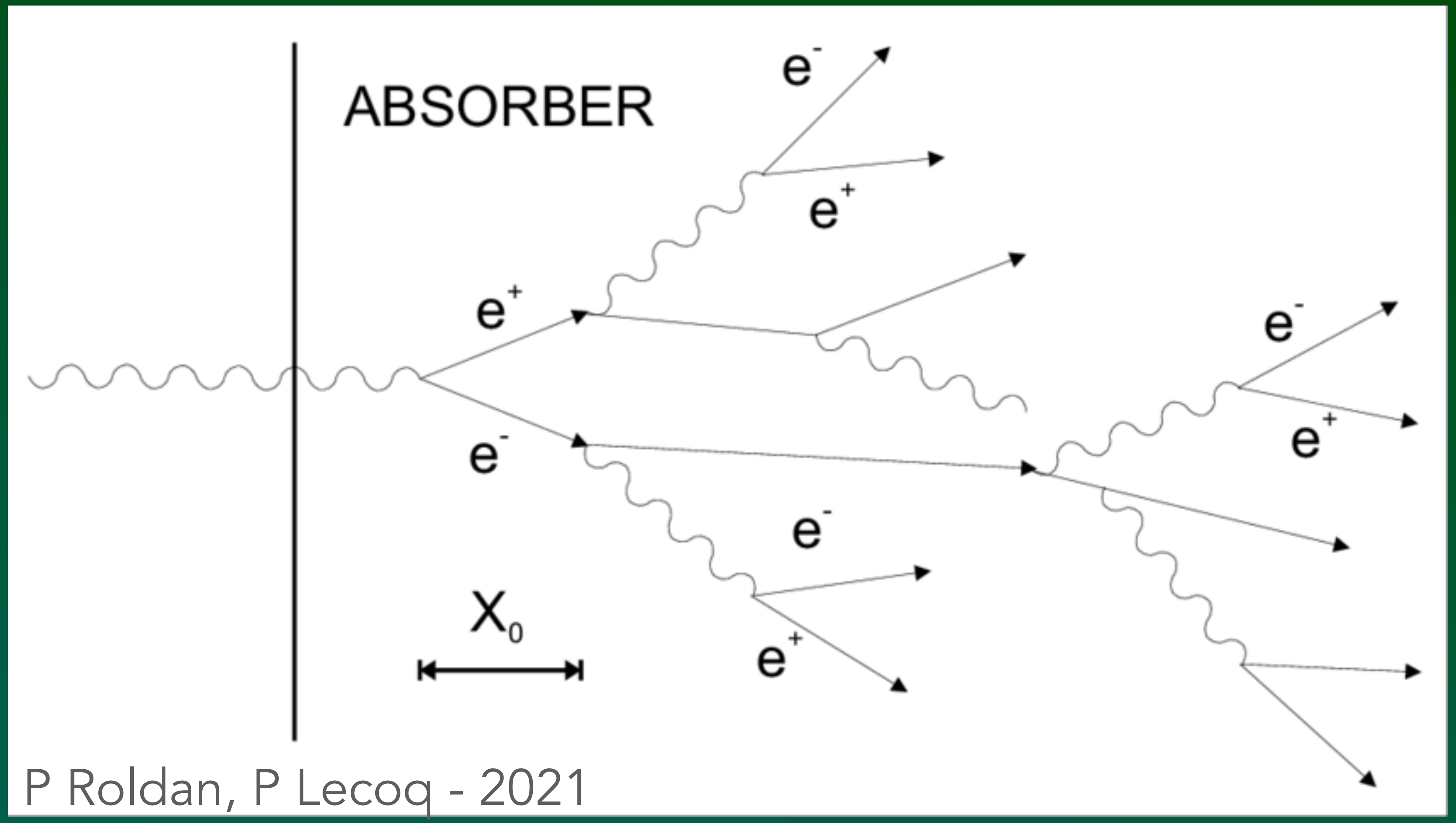

Electromagnetic shower

The Experimental Apparatus

Measuring Energy: Calorimetry

- At the CMS, calorimetry is done on electromagnetic particles
  - e, e^+, γ: measured by electromagnetic calorimeter (**ECAL**)
  - p, n, $\pi^{\pm}$, $\mathscr{K}^{\pm}$: measured by hadronic calorimeter (**HCAL**)

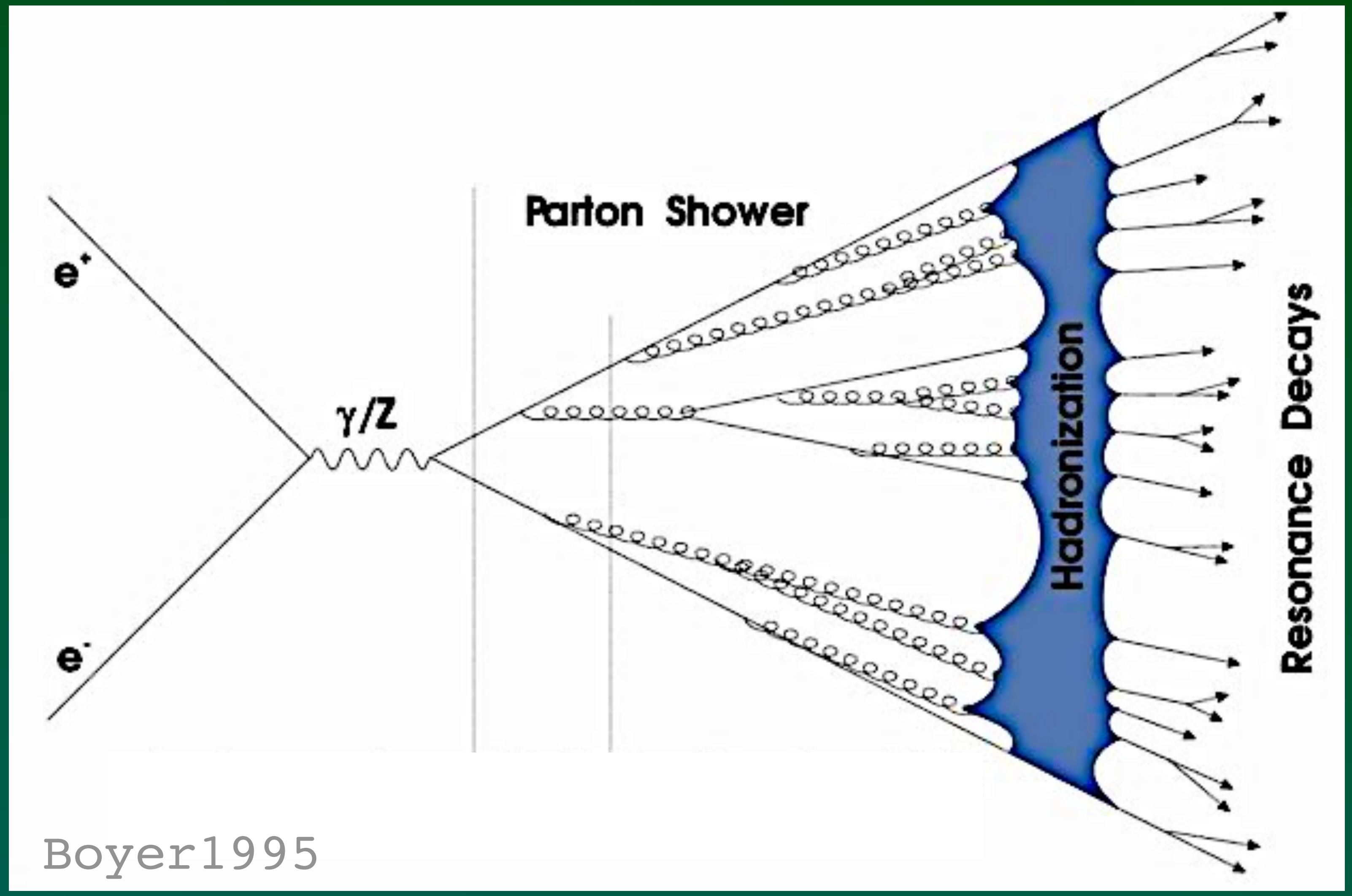

Parton showering and hadronization

ECAL

- $PbWO_4$ crystals as **scintillation materials**
- High-energy electromagnetic particles produce ***showers*** in the crystals upon smashing into them

HCAL

- Layers of **dense material** (brass or steel) interleaved with tiles of plastic **fluorescent scintillators**
- The incoming hadrons interact strongly with the nuclei of the calorimeters material, provoking a ***hadronic shower.***
- Once interaction energy scale falls, the **strong interaction** coupling rises, which triggers ***hadronization***

The Experimental Apparatus

Detecting Muons: The Muon System

- The muon system is tasked with three major functionalities: **muon identification, tracking, triggering**, and momentum measurement.
- The muon system has two main sections
  - The barrel
  - The endcaps

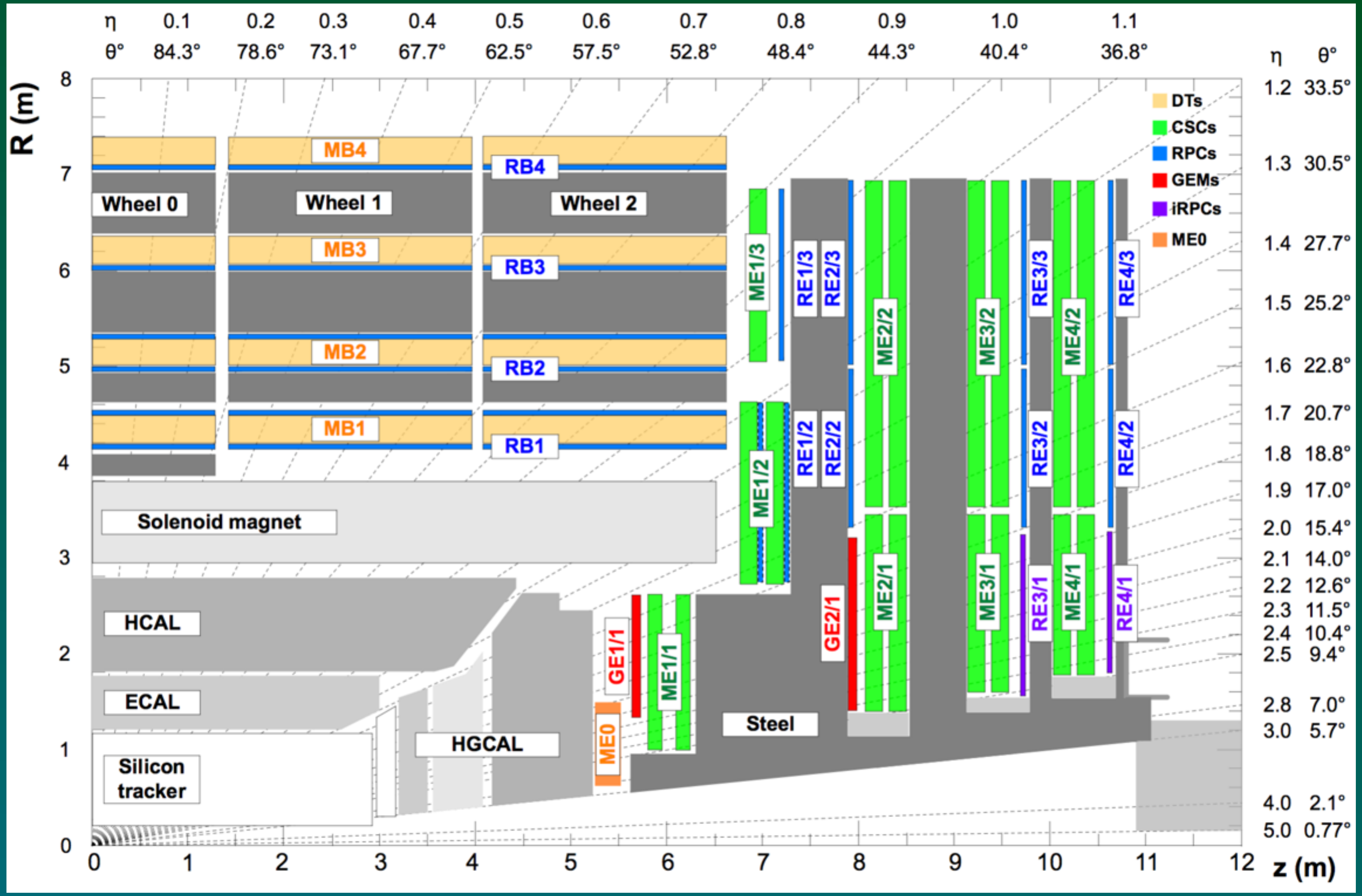

Quadrant overview of the CMS detector

The Experimental Apparatus

Detecting Muons: The Muon System

- The muon system is tasked with three major functionalities: muon identification, tracking, triggering, and momentum measurement.
- The muon system has two main sections
  - The barrel
  - The endcaps
- The barrel has Drift Tubes (DTs),Resistive Plate Chambers (RPCs), and the endcaps are armed with Cathode Strip Chambers (CSCs), RPCs, and **Gas Electron multiplier (GEMs)** [not operational for duration of this dissertation]
- Transverse momentum is measured based on the bending angle

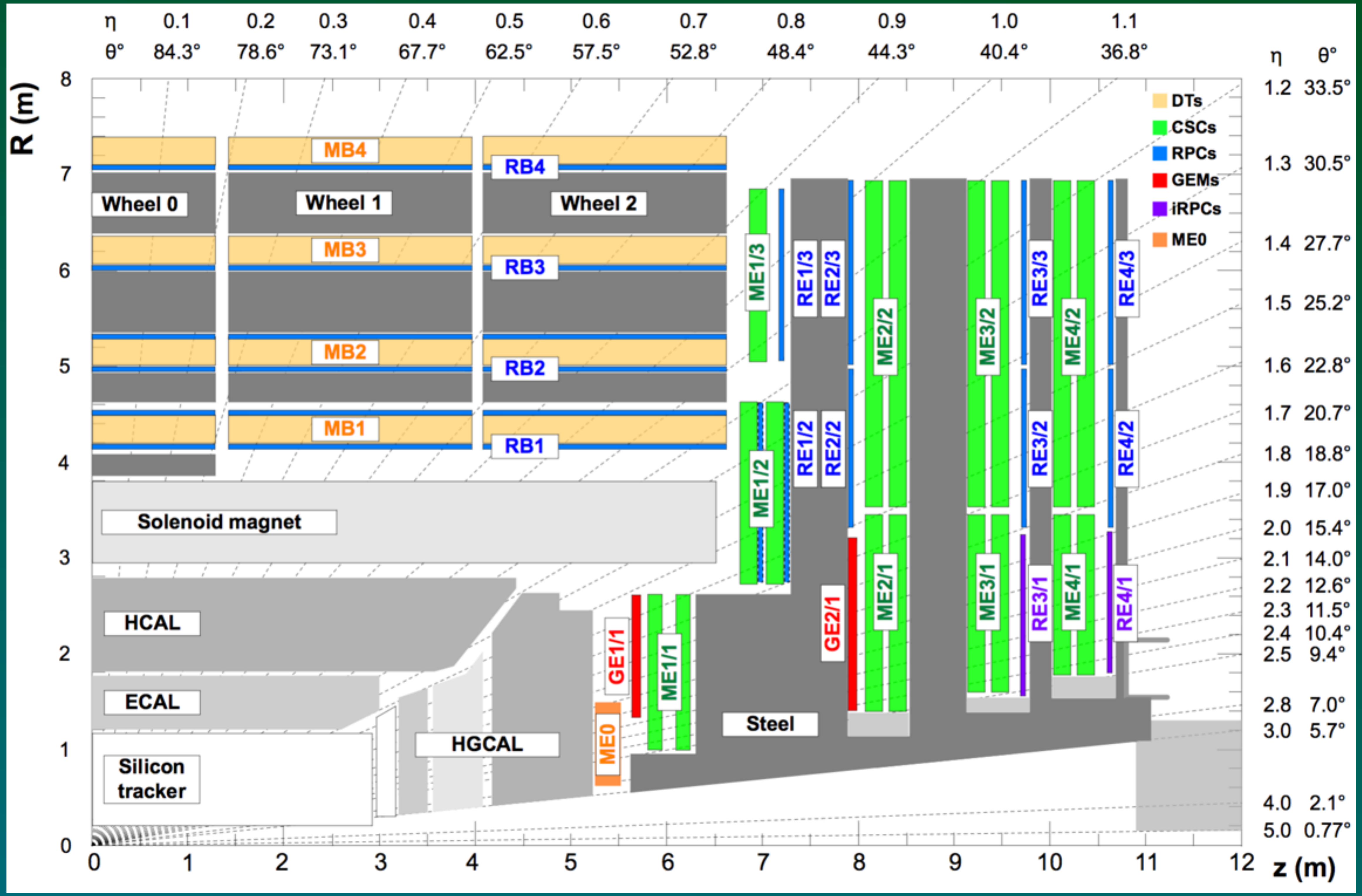

Quadrant overview of the CMS detector

The Experimental Apparatus

The Trigger System

- The CMS records only potentially ***interesting* events** with a **two-level tigger system**.

- **Level-1 (L1) trigger** utilizes a system of **synchronized hardware**

    - The muon system, HCAL, and ECAL participate in the L1 trigger

- **High-Level Triggering** (**HLT**) is purely **software-based**

    - The information from the **muon system and tracker** sub-detectors is **combined** to **identify the muons** and **determine their** p_t.

The Experimental Apparatus

The Trigger System

- The CMS records only potentially *interesting* events with a two-level tigger system.
- Level-1 (L1) trigger utilizes a system of synchronized hardware
  - The muon system, HCAL, and ECAL participate in the L1 trigger
- High-Level Triggering (HLT) is purely software-based
  - The information from the muon system and tracker sub-detectors is combined to identify the muons and determine their p_t.

- **Two-Level HLT**
  - **Level-2 (L2)** muon system: hits and segments patterns → seeds → Kalman filter → **reconstruction**
  - **Level-3 (L3) inner tracker** + **muon sub-detectors**: tracker seeds and muon system **seeds matchup** → maximize the reconstruction efficiency
- Main technique to determine **identity** of the particle and isolation : **Particle-Flow (PF)**

Layout

1. The Experimental Apparatus
2. Construction & Quality Control of GEM Detectors

GEMs: Introduction

Motivation

- Rate capability: >>10 kHz/cm2,
- time resolution of >~8 ns,
- spatial resolution ~200 μm.

- The LHC is being planned to transform into the **High Luminosity** Large Hadron Collider (HL LHC)

- Unprecedented luminosity of $2 - 3 \times 10^{34}$ cm^{2} s^{-1}

- The muon system is not able to keep up higher rates of **multiple scattering**: L1 trigger overwhelms the system at the forward region

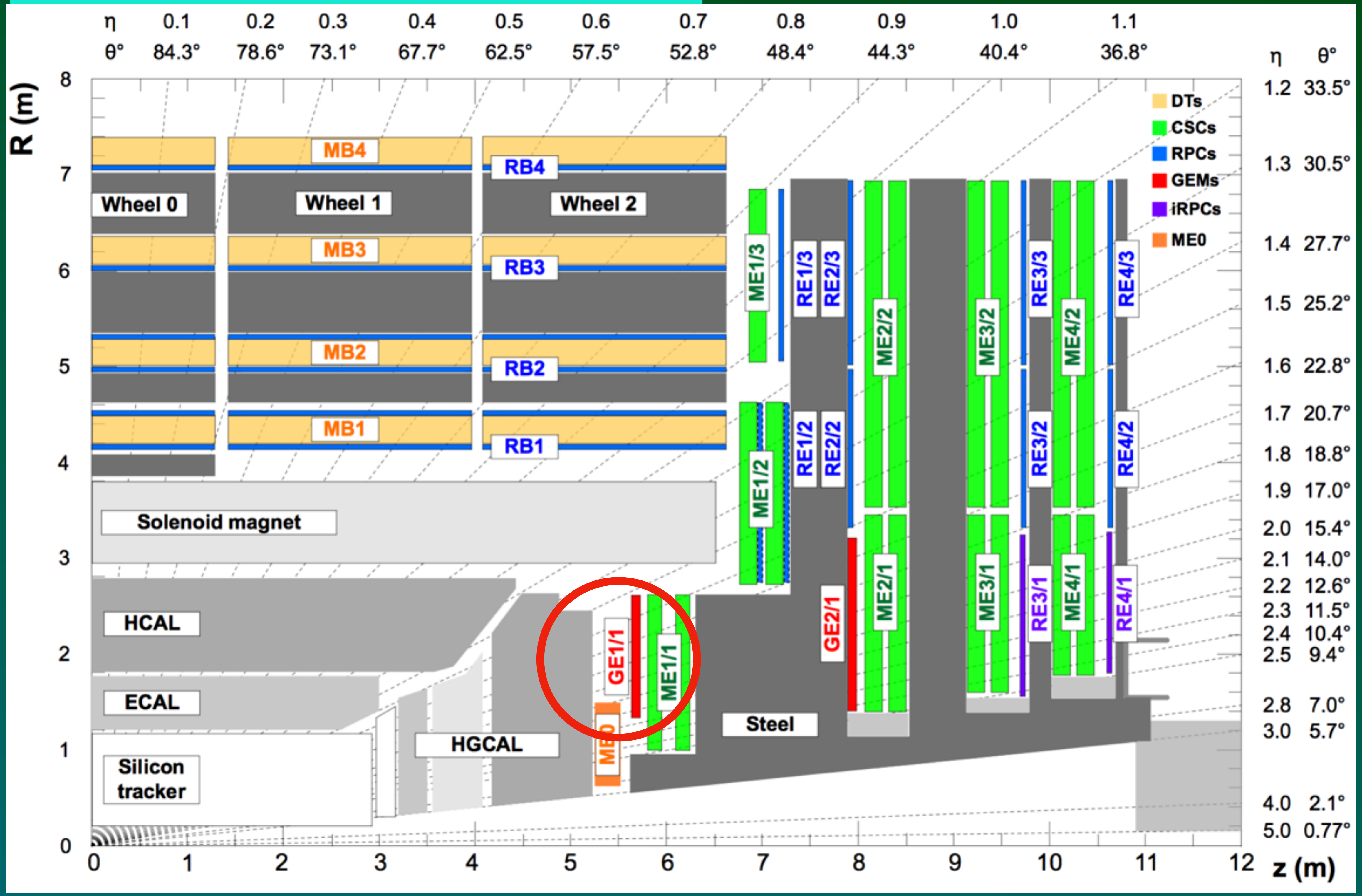

The GE1/1 station at the CMS

GEMs: $1.55 < |\eta| < 2.18$

GEMs: Introduction

Motivation

- The LHC is being planned to transform into the **High Luminosity** Large Hadron Collider (HL LHC)
- Unprecedented luminosity of $2 - 3 \times 10^{34}$ cm^{2} s^{-1}
- The muon system is not able to keep up higher rates of **multiple scattering**: L1 trigger overwhelms the system at the forward region
- Response: **Gas Electron Multiplier (GEM) technology** to be installed at the designated **GE1/1 endcap station**
- **Restore redundancy** for tracking and triggering in the muon system
- Improves muon **momentum resolution**, **unaffected by multiple scattering**

- Rate capability: >>10 kHz/cm2,
- time resolution of >~8 ns,
- spatial resolution ~200 μm.

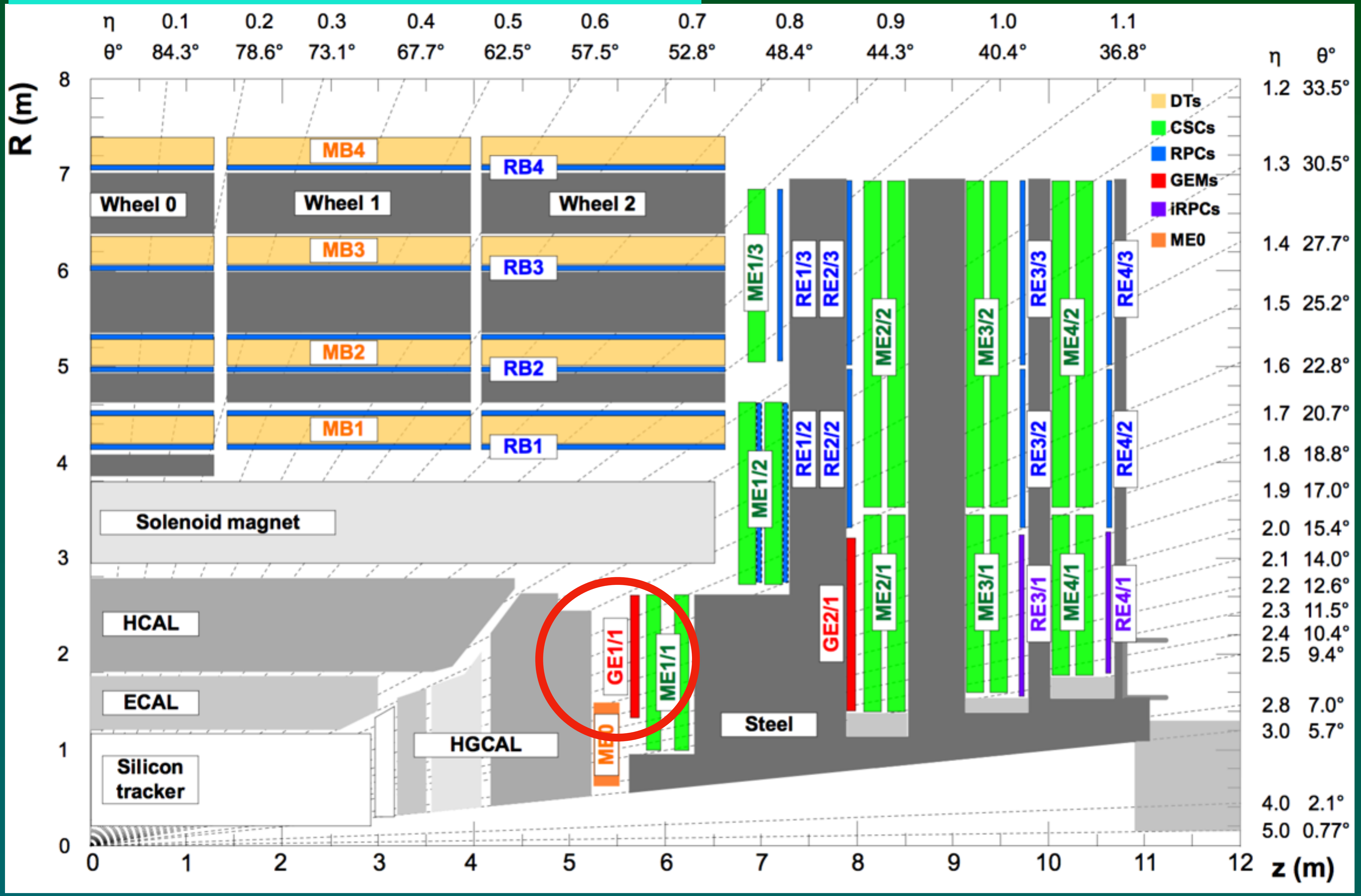

The GE1/1 station at the CMS

GEMs: $1.55 < |\eta| < 2.18$

GEMs: Introduction

The Operation Principals

- A *triple-GEM* chamber (detector) incorporates three GEM foils,
  - i.e., **Kapton foils** coated with **copper** on both sides
  - with an array of **microscopic holes** (typically 140 μm pitch),
  - separated by **spacers** and held between an **anode readout** board and a **cathode drift** board.

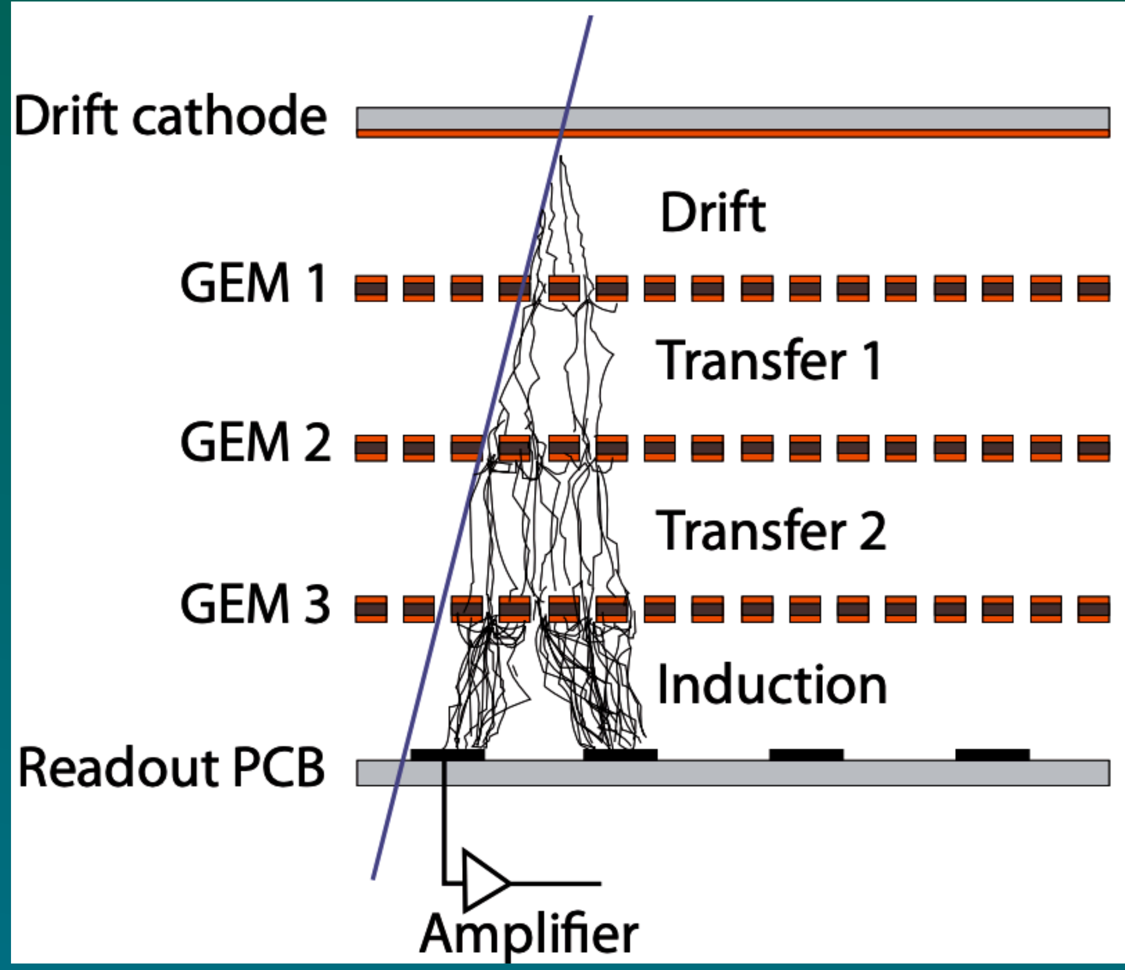

GE1/1 Gap Sizes	Typical Potentials	Typical Voltages	Typical El. Fields [kV/cm]
	3200 V		
3 mm		770 V	2.6
	2430 V		
		380 V	64.0
	2050 V		
1 mm		300 V	3.0
	1750 V		
		370 V	62.0
	1380 V		
2 mm		600 V	3.0
	780 V		
		350 V	60.0
	430 V		
1 mm		430 V	4.3
	0 V		

charge amplification: up to 10^5 (gain)

GEMs: Introduction

The Operation Principals

- A *triple-GEM* chamber (detector) incorporates three GEM foils,
  - i.e., Kapton foils coated with copper on both sides
  - with an array of microscopic holes (typically 140 μm pitch),
  - separated by spacers and held between an anode readout board and a cathode drift board.
- A GEM chamber utilizes **electron amplification** through microscopic holes within a gas medium (**Ar/CO_2** 70:30).

Applied Voltage → strong electric field (60-100 kV/cm) inside the holes

→ electron drift toward the holes →electron amplification (Townsend **avalanche**)

→ induce **electrical signal** readout anode

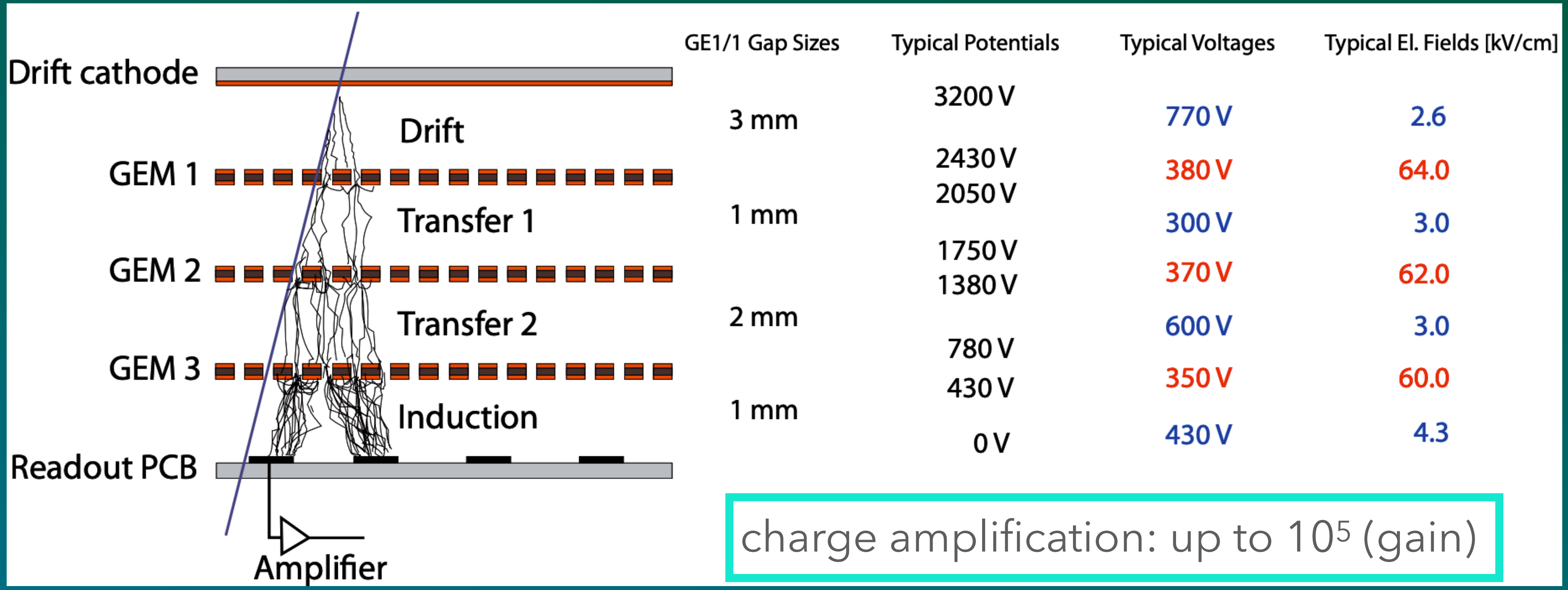

GEMs: Introduction

Components

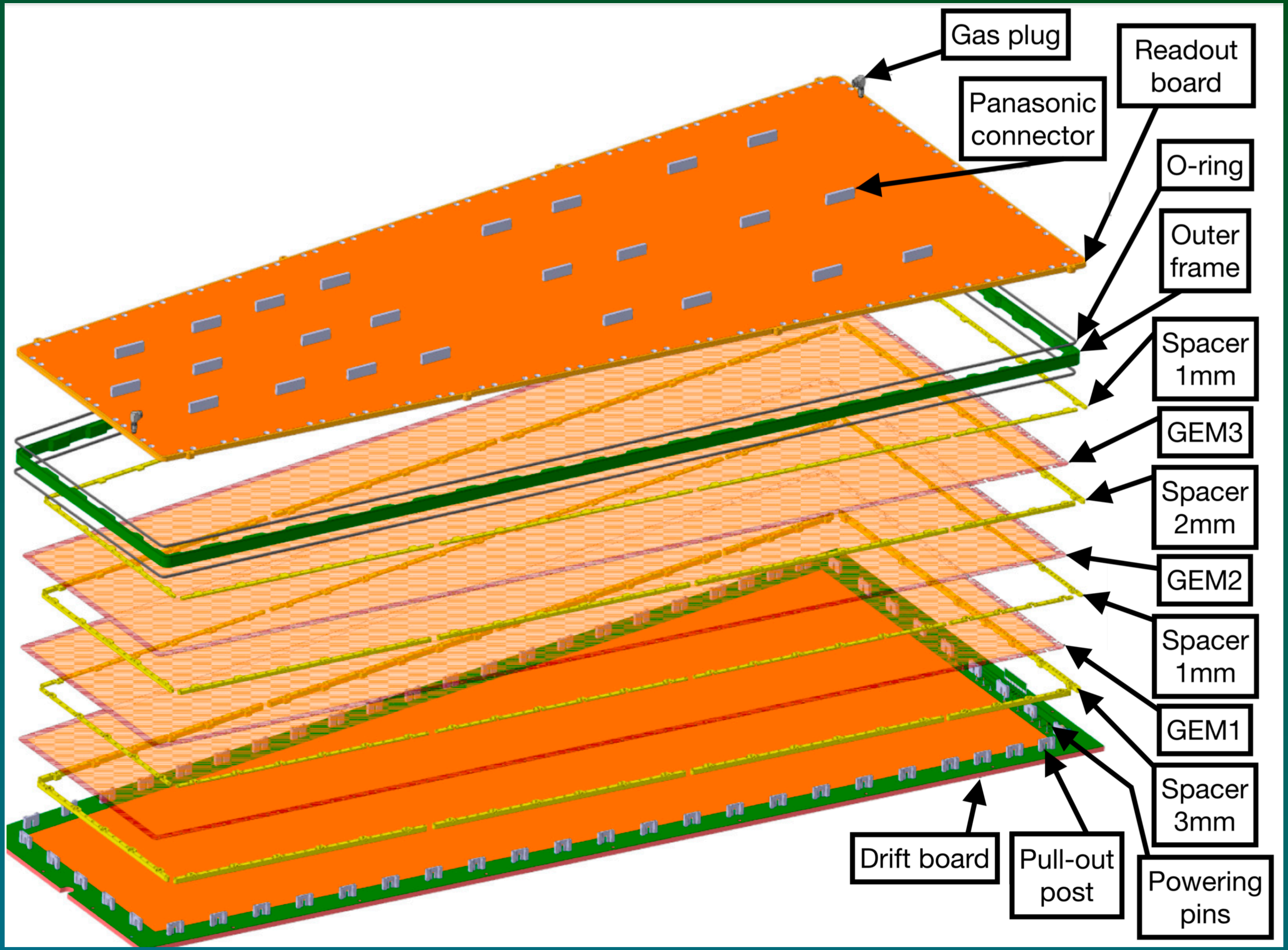

Exploded overview of a GEM chamber

GEMs: Assembly

Procedure Overview

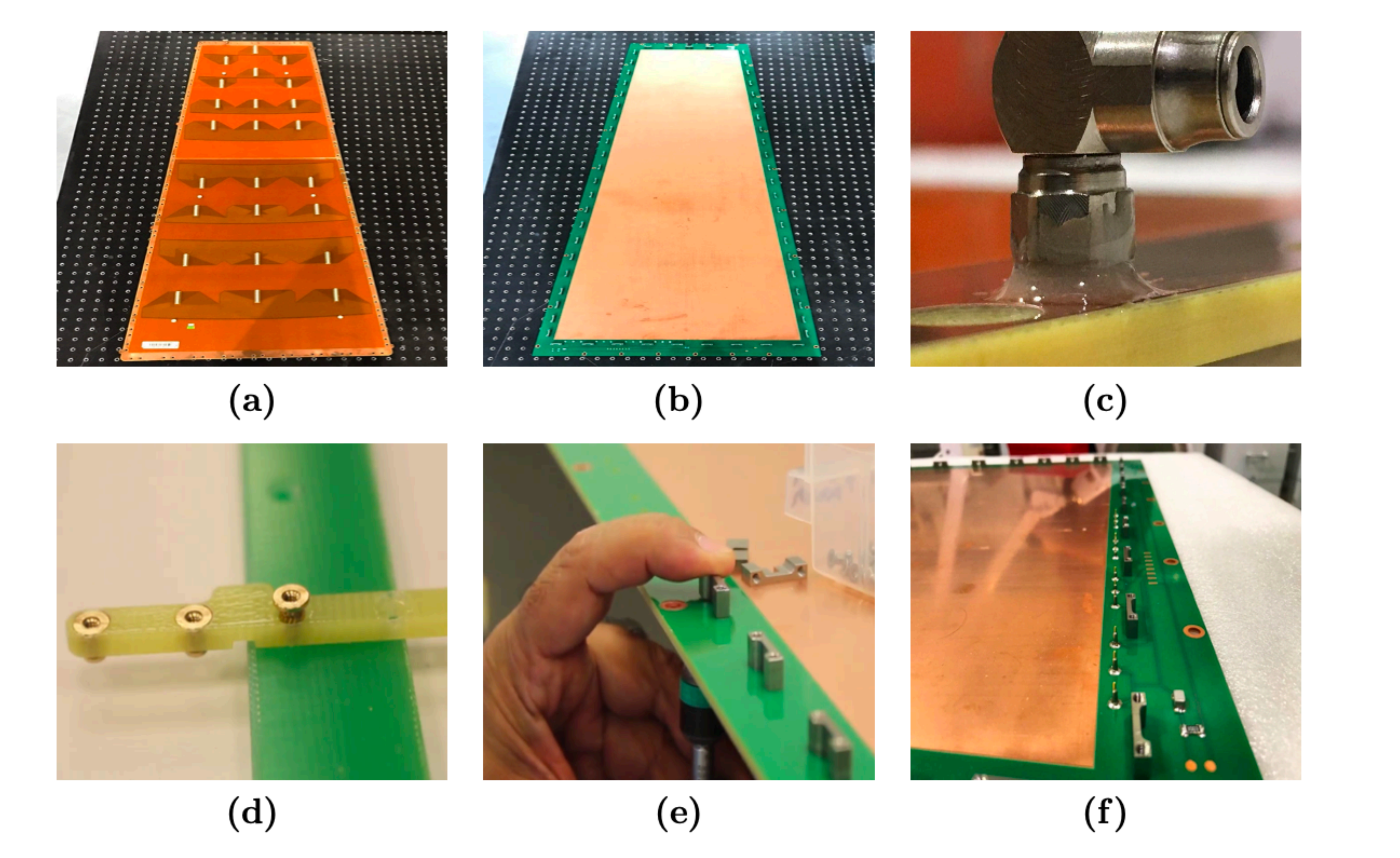

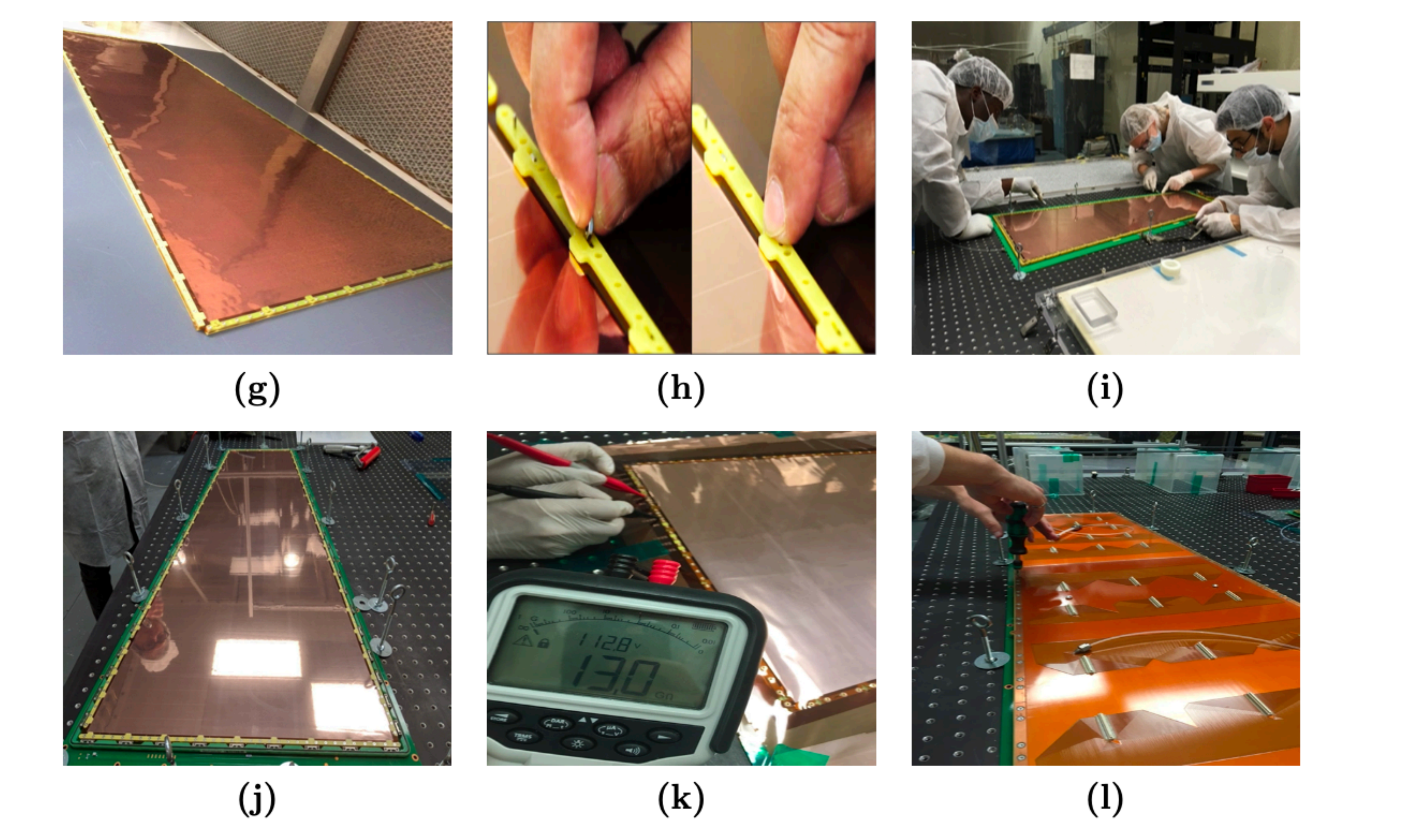

GEMs: Quality Control

Overview

QC Step	QC Procedure
1	Initial inspection of the chamber components
2	Electrical cleaning of the GEM foils and resistance check
3	Leak test of closed detector volume
4	Linearity test of high voltage divider and intrinsic noise rate measurement
5a	Effective gas gain measurement
5b	Response uniformity measurement

GEM: Production Line

FIT production line

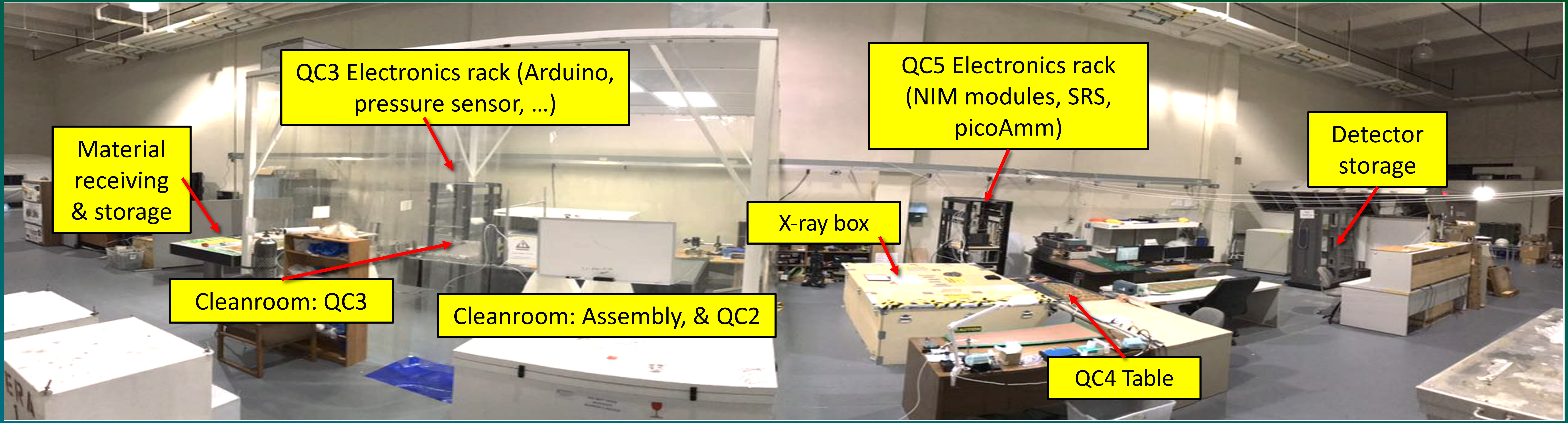

GEMs: QC Step 2
GEM Foil Resistance Check

- Applying 550 V to the GEM foils and measuring the **leakage current** between top and bottom electrodes

- The GEM foil is accepted if its **impedance** is above **10 $G\Omega$,** with relative humidity lower than 50% and the number of **sparks** per minutes is lower than **2-3** during the last three minute

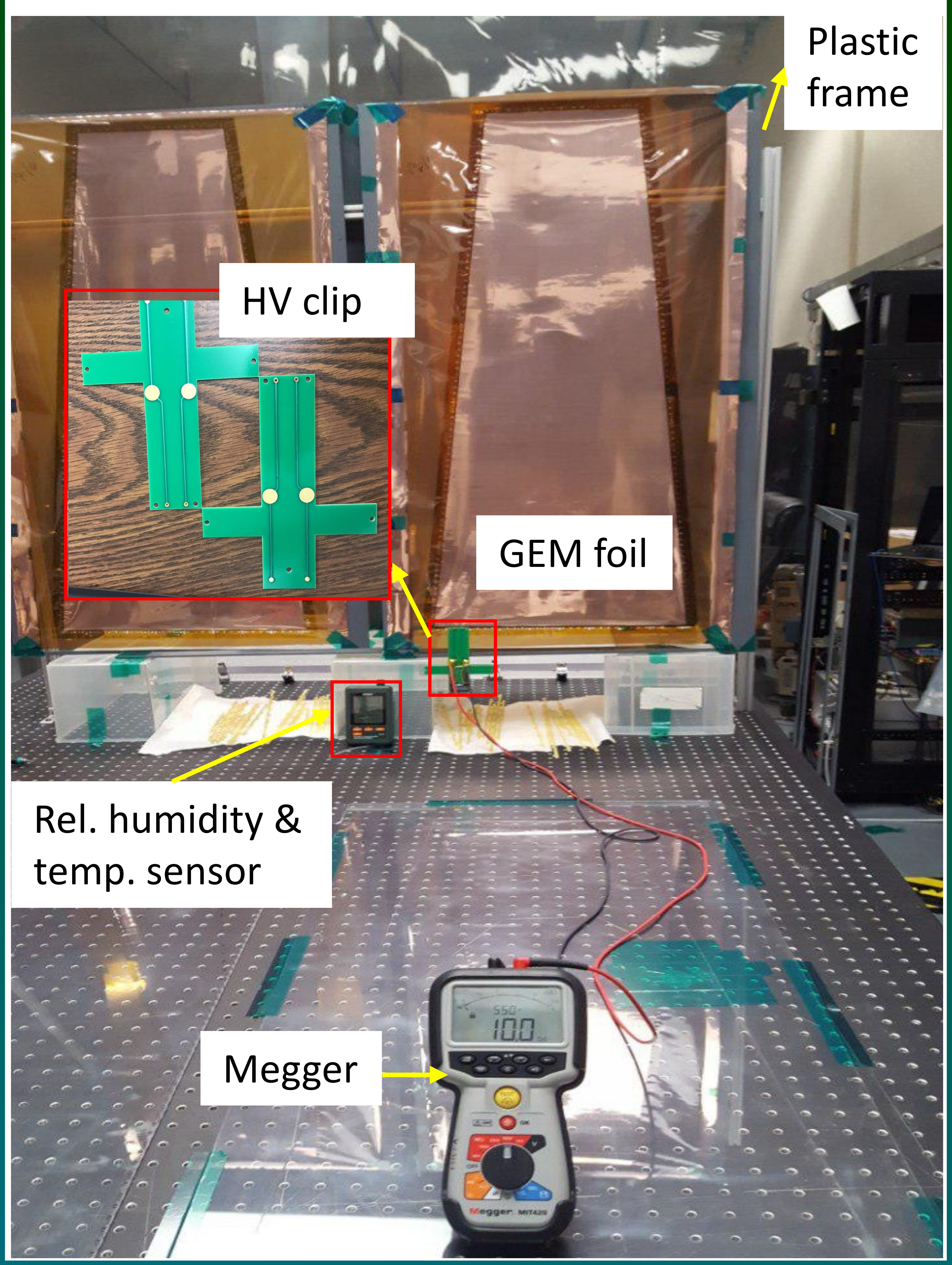

GEMs: QC Step 2

Typical Results

- Applying 550 V to the GEM foils and measuring the **leakage current** between top and bottom electrodes

- The GEM foil is accepted if its **impedance** is above **10 $G\Omega$,** with relative humidity lower than 50% and the number of **sparks** per minutes is lower than **2-3** during the last three minute

FOIL-BATCH-S-132/12					
Time [min]	Voltage [V]	Resistance [G ohm]	Current [nA]	Sparks	Total sparks
0.5	550	4	550	1	1
1	550	8	250	1	2
2	550	9.8	152	1	3
3	550	3.8	134	0	3
4	550	8.9	112.2	1	4
5	550	12.5	95	0	4
6	550	13.4	90	0	4
7	550	14	71	0	4
8	550	15.5	65	0	4
9	550	16	61	0	4
10	550	17	61	0	4

QC2 measurements a foil in FIT0002

GEMs: QC Step 2

Summary of Results

- Applying 550 V to the GEM foils and measuring the **leakage current** between top and bottom electrodes

- The GEM foil is accepted if its **impedance** is above **10 $G\Omega$,** with relative humidity lower than 50% and the number of **sparks** per minutes is lower than **2-3** during the last three minute

Chmaber SN	Foil ID	Resistance (MΩ)	Temp (C°)	RH %	Pressure (mbar)
FIT0001	172/15 168/15 137/13	12 14 13	26.3	53.6	1016.1
FIT0002	167/15 170/15 171/15	17 11 14	27	51.2	1017.3
FIT0003	175/15 125/12 133/12	11 11 13	26.3	53	1016.1
FIT0004	172/17 186/16 132/12	14 13 10	27.2	52	1015.2
FIT0005	171/15 226/19 228/19	15 13 11	26.3	53.6	1016.7
FIT0006	207/18 215/18 218/18	10 13 17	26.3	53	1016.4
FIT0007	213/18 217/18 194/17	13 8 11	25.2	56.3	1013.4
FIT0008	214/18 191/17 199/17	11 13 11	26.9	55.2	1014.1
FIT0009	205/18 206/18 209/18	11 14 15	27.2	48.4	1015.1
FIT0010	166/15 208/18 210/18	11 11 13	26.1	43.8	1017.9

QC2 summary

GEMs: QC Step 3

Gas Leakage Test

- Measure **gas leakage** of the closed chamber with both gas **input and output blocked**
- An **exponential** fit to the pressure drop against time to extract **time constant** τ
- $P_{int} = P_0 e^{-t/\tau}$
- The initial pressure P_0 is set to **25 millibar**
- Any chamber with a **time constant greater than 3.04 hours** passes the QC3 criteria to ensure that the **leak rate** remains **below 1%**

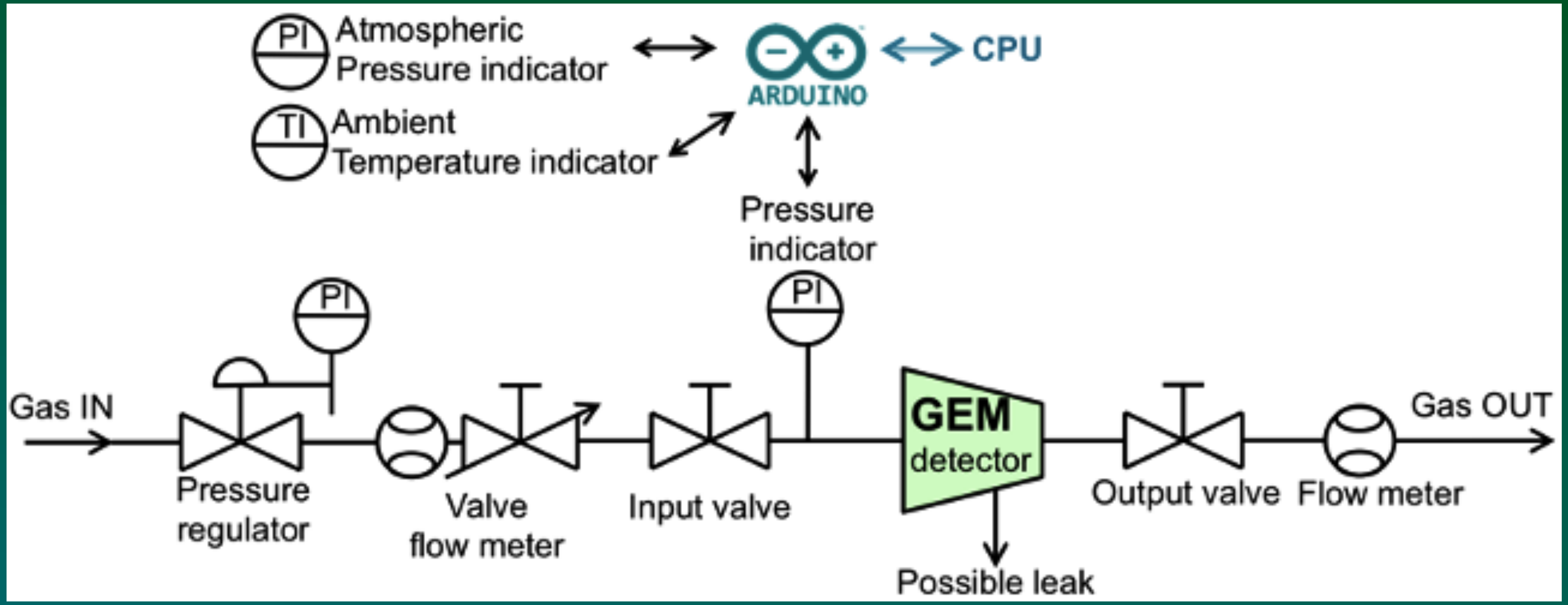

QC3 apparatus

GEMs: QC Step 3

Typical Results

- Measure **gas leakage** of the closed chamber with both gas **input and output blocked**
- An **exponential** fit to the pressure drop against time to extract **time constant** τ
- $P_{int} = P_0 e^{-t/\tau}$
- The initial pressure P_0 is set to **25 millibar**
- Any chamber with a **time constant greater than 3.04 hours** passes the QC3 criteria to ensure that the l**eak rate** remains **below 1%**

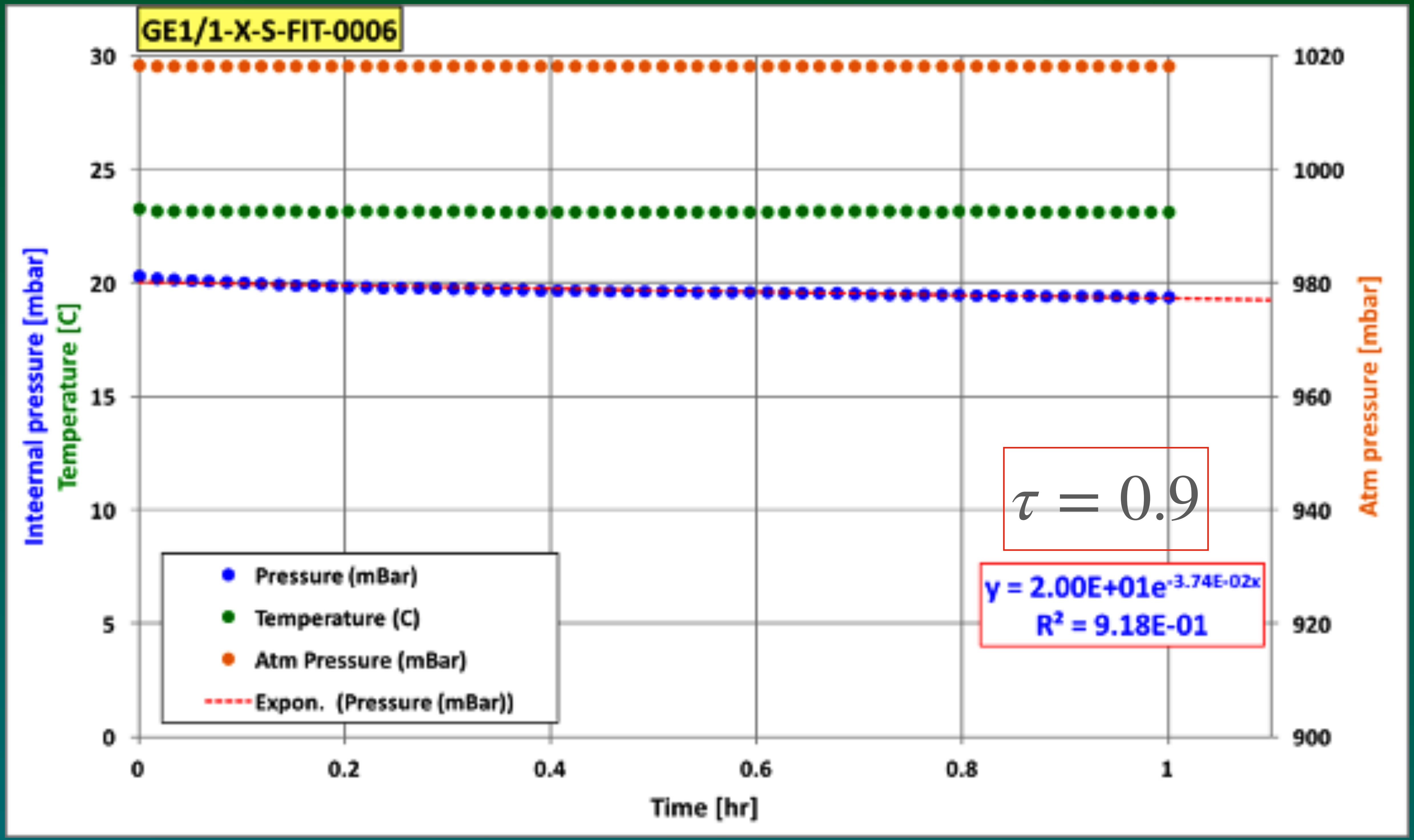

QC3 results for FIT0006

GEMs: QC Step 3

Summary of Results

- Measure **gas leakage** of the closed chamber with both gas **input and output blocked**
- An **exponential** fit to the pressure drop against time to extract **time constant** τ
- $P_{int} = P_0 e^{-t/\tau}$
- The initial pressure P_0 is set to **25 millibar**
- Any chamber with a **time constant greater than 3.04 hours** passes the QC3 criteria to ensure that the l**eak rate** remains **below 1%**

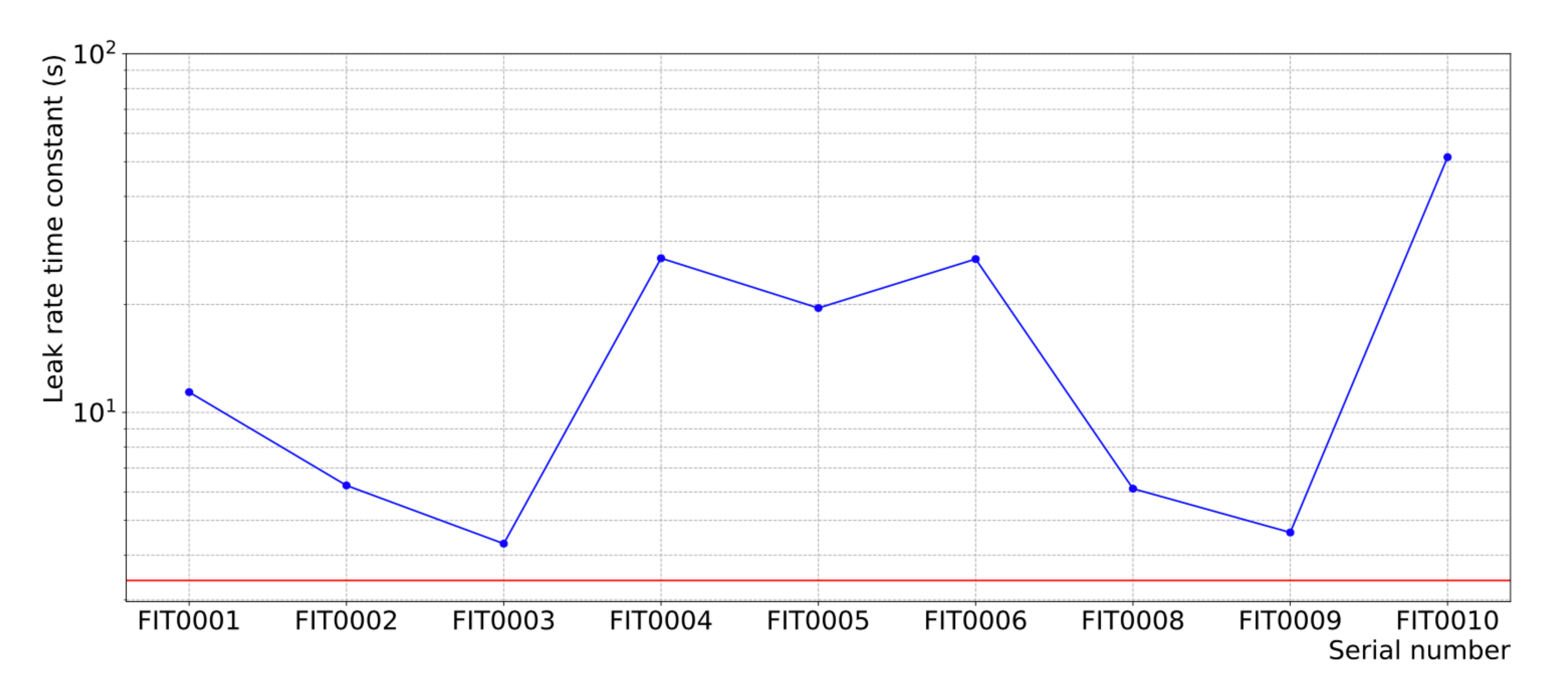

QC3 summary

GEMs: QC Step 4a

Linearity test of the HV divider

- The **HV** has to be appropriately distributed among the GEM foils and the drift board

- The QC4 is designed to test the functionality of **on-detector circuitry** that distributes the HV.

- The GE1/1 arranged in a **3/1/2/1 mm**

- **Ceramic HV** divider →appropriate **fields**

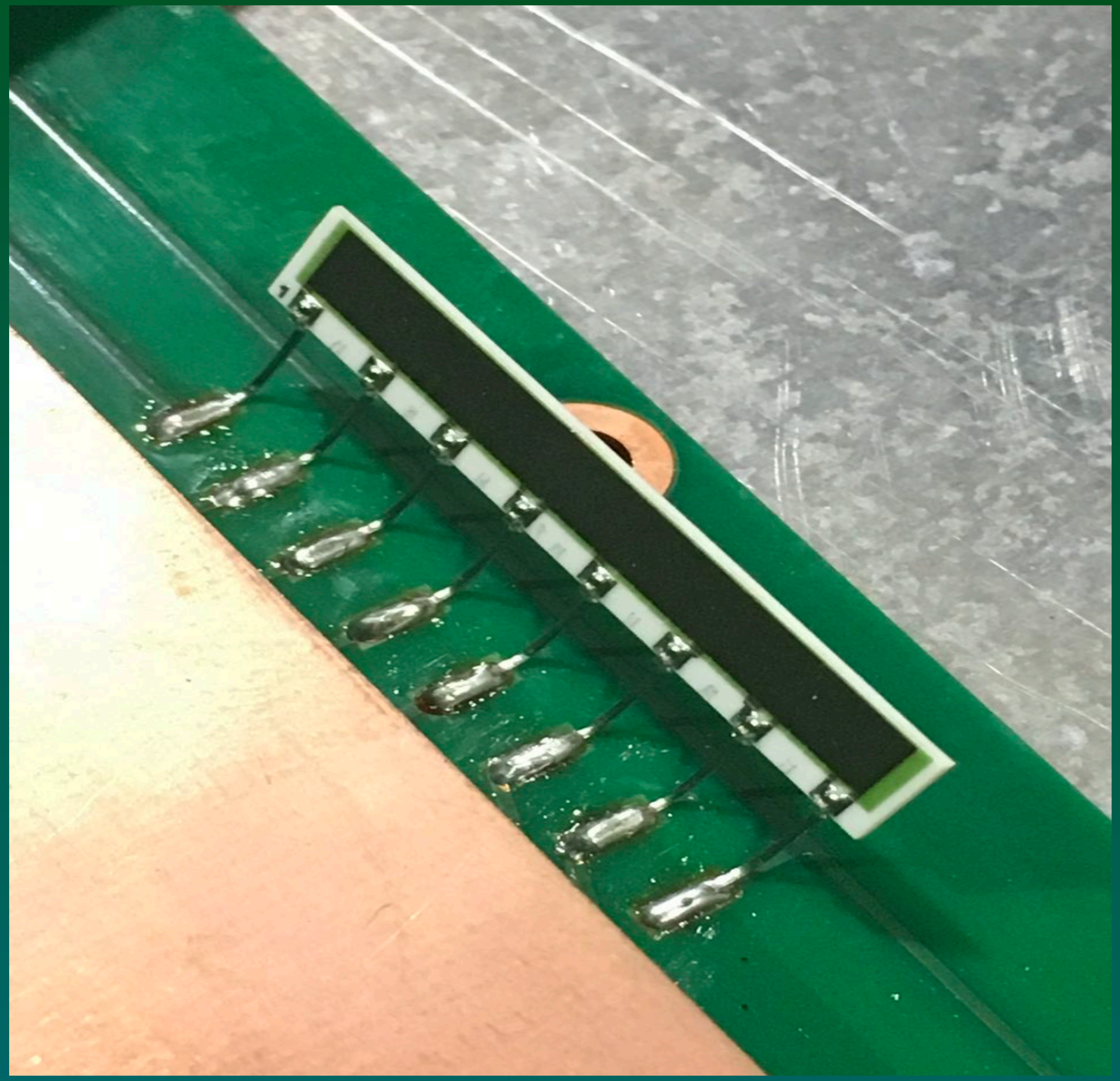

The ceramic HV divider

GEMs: QC Step 4a

Linearity test of the HV divider

- The **HV** has to be appropriately distributed among the GEM foils and the drift board
- The QC4 is designed to test the functionality of **on-detector circuitry** that distributes the HV.
- The GE1/1 arranged in a **3/1/2/1 mm**
- **Ceramic HV** divider →appropriate **fields**

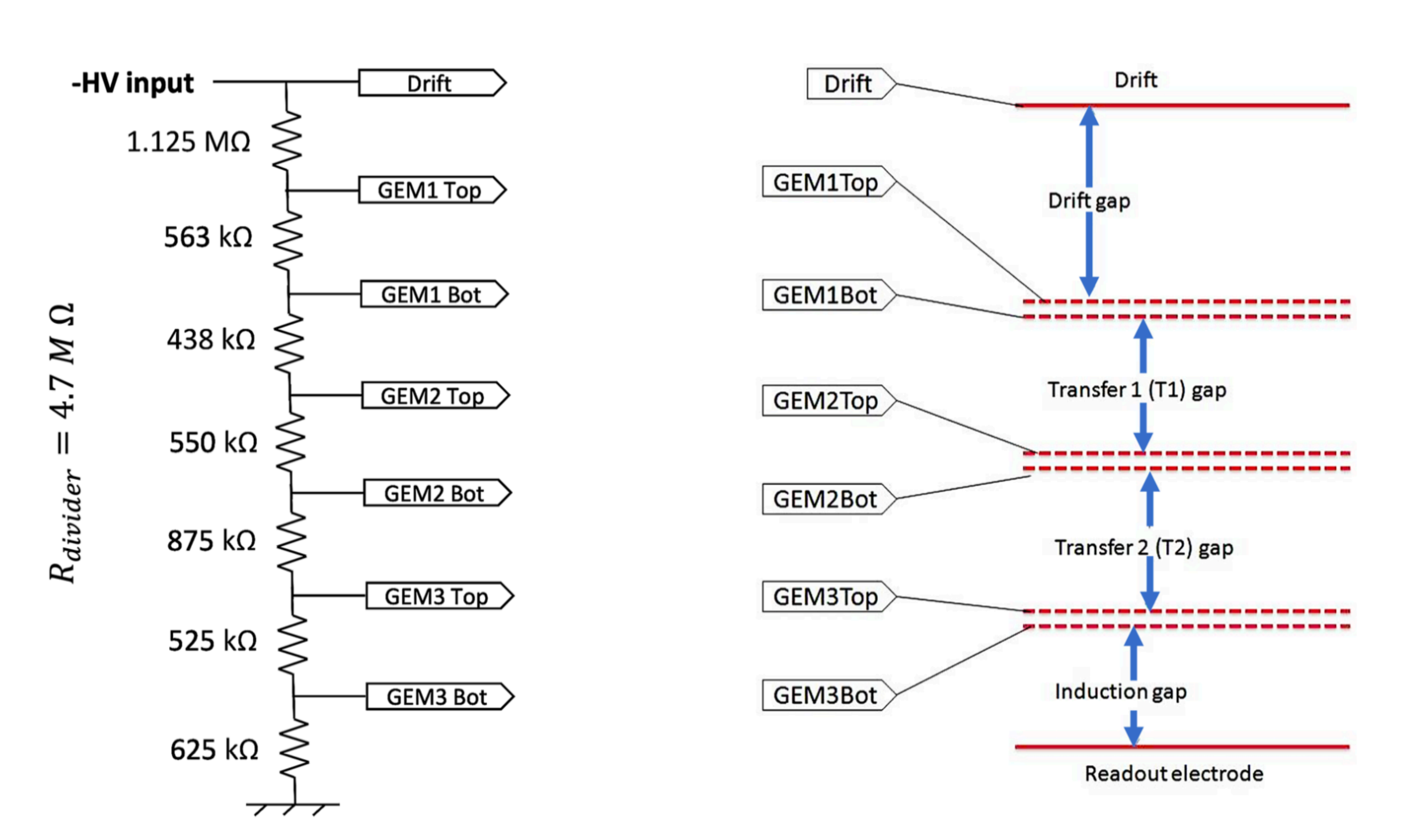

HV divider circuit diagram

GEMs: QC Step 4a

Typical Results

- The **HV** has to be appropriately distributed among the GEM foils and the drift board

- The QC4 is designed to test the functionality of **on-detector circuitry** that distributes the HV.

- The GE1/1 arranged in a **3/1/2/1 mm**

- **Ceramic HV** divider →appropriate **fields**

- Fit the **I-V curve** with a **linear** and compute the **deviation** of its slope with respect to the **nominal** resistance: $D_R = \dfrac{R_m - Rn}{R_n}$

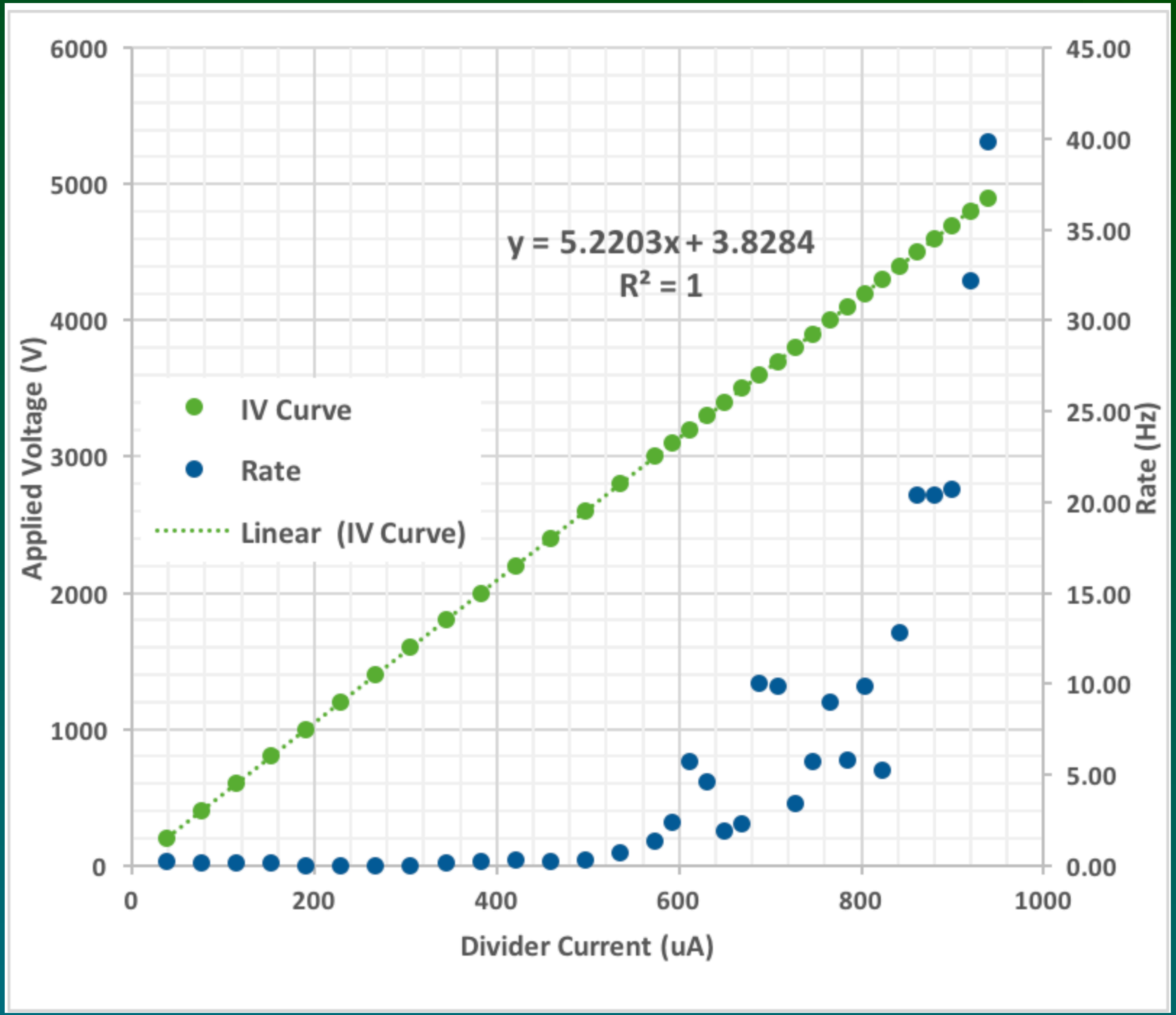

Typical results (FIT0006)

GEMs: QC Step 4a

Summary of Results

- The **HV** has to be appropriately distributed among the GEM foils and the drift board

- The QC4 is designed to test the functionality of **on-detector circuitry** that distributes the HV.

- The GE1/1 arranged in a **3/1/2/1 mm**

- **Ceramic HV** divider →appropriate **fields**

- Fit the **I-V curve** with a **linear** and compute the **deviation** of its slope with respect to the **nominal** resistance

- A chamber with a **resistance deviation** — between the nominal and measured resistances — **smaller than 3%** passes

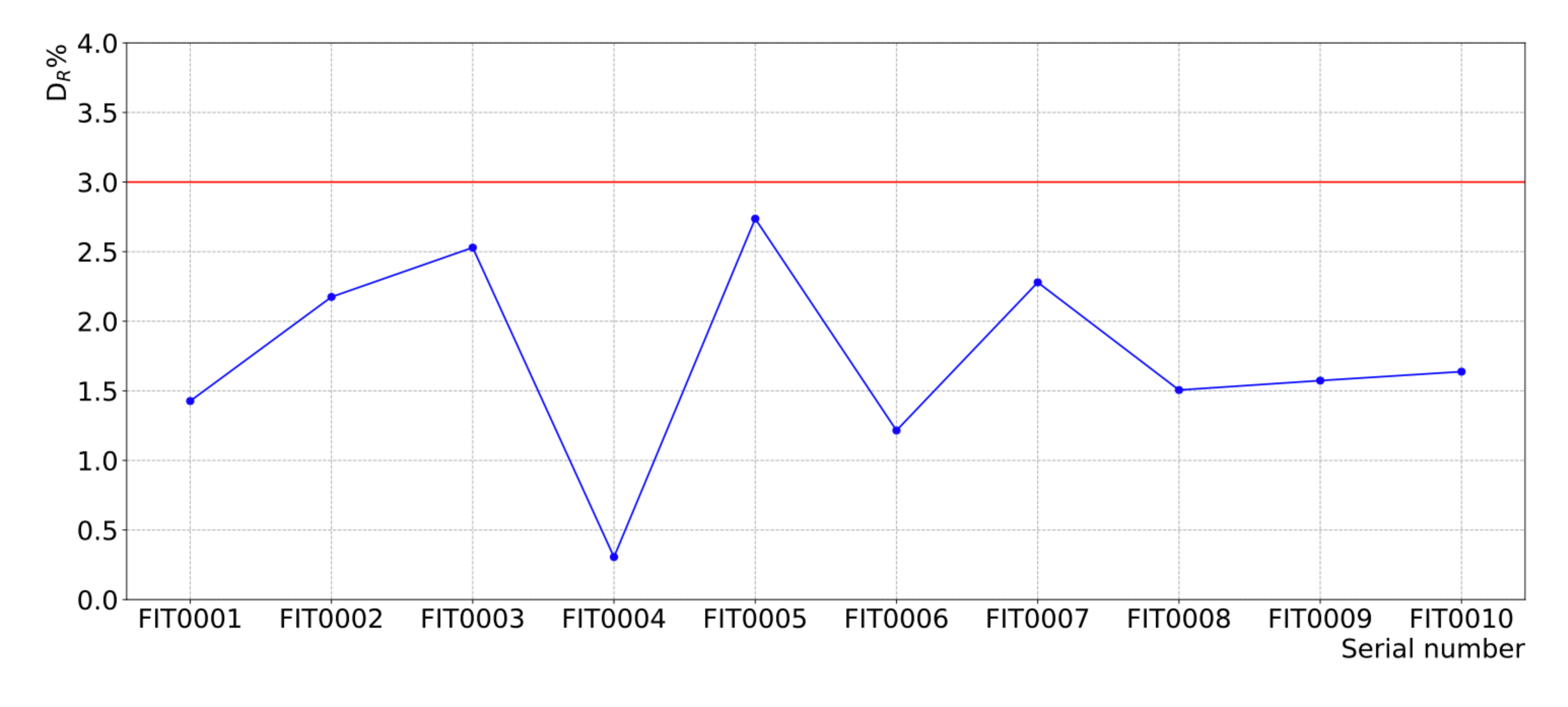

Summary of results for QC4a

GEMs: QC Step 4b

Intrinsic Noise Rate Measurement

- **Intrinsic noise** produced by **coronal discharges** rate per surface area
- Flushing the chamber with **CO_2**, which has high enough **ionizing energy** to be immune to ionization from the cosmic rays
- A detector passes the QC step 4 if the intrinsic noise rate for the entire detector does **not exceed 100 Hz.**

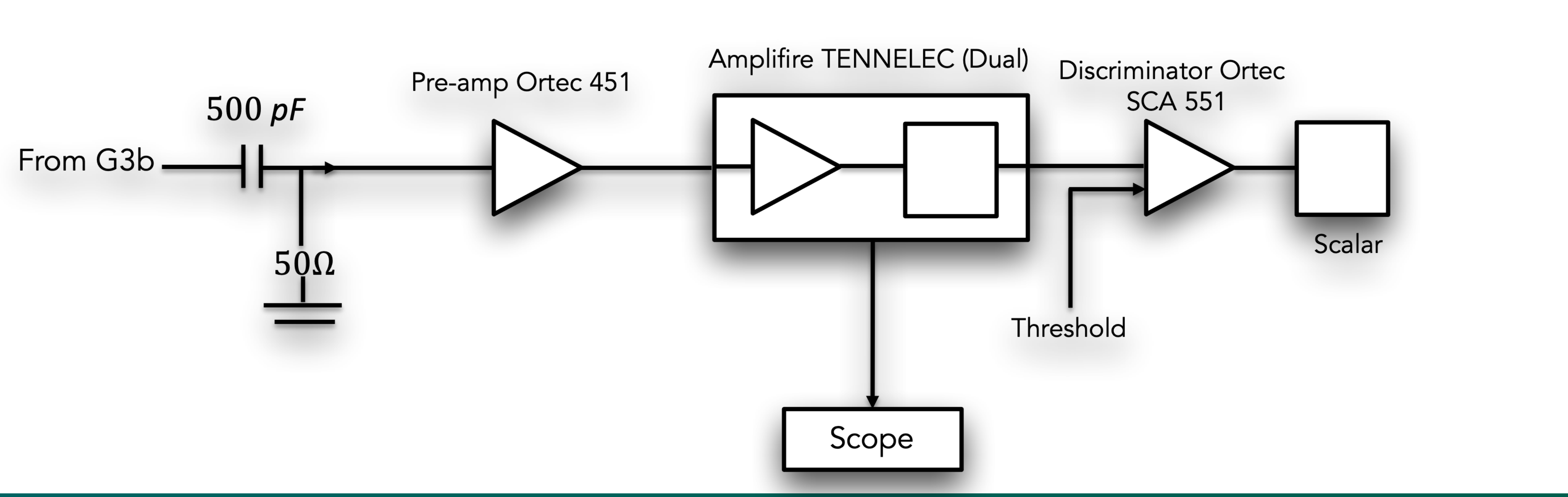

QC4 electric chain

GEMs: QC Step 4b

Typical Results

- **Intrinsic noise** produced by **coronal discharges** rate per surface area
- Flushing the chamber with **CO_2**, which has high enough **ionizing energy** to be immune to ionization from the cosmic rays
- A detector passes the QC step 4 if the intrinsic noise rate for the entire detector does **not exceed 100 Hz.**

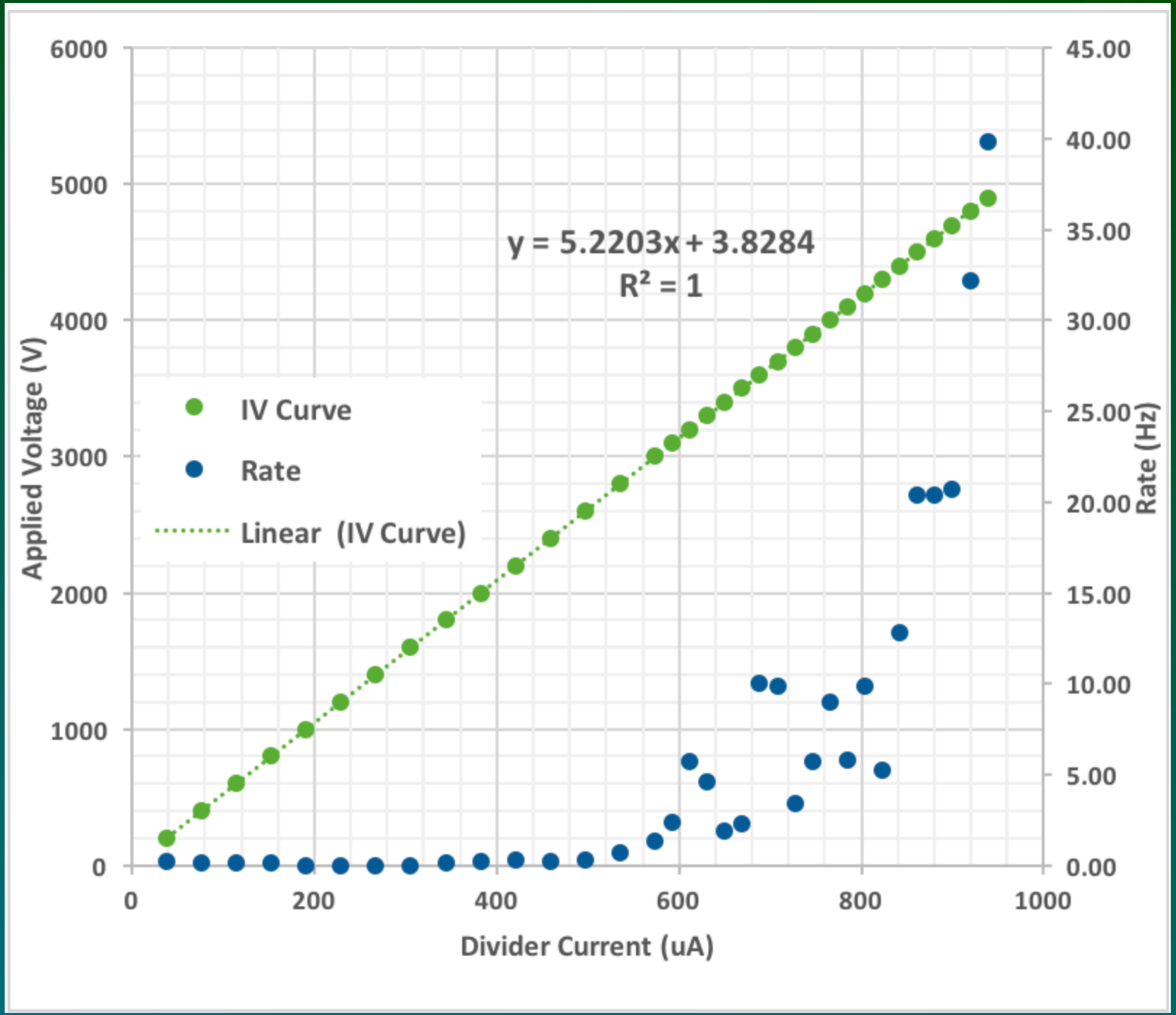

Typical results (FIT0006)

GEMs: QC Step 4b

Summary of Results

- **Intrinsic noise** produced by **coronal discharges** rate per surface area
- Flushing the chamber with **CO_2**, which has high enough **ionizing energy** to be immune to ionization from the cosmic rays
- A detector passes the QC step 4 if the intrinsic noise rate for the entire detector does **not exceed 100 Hz.**

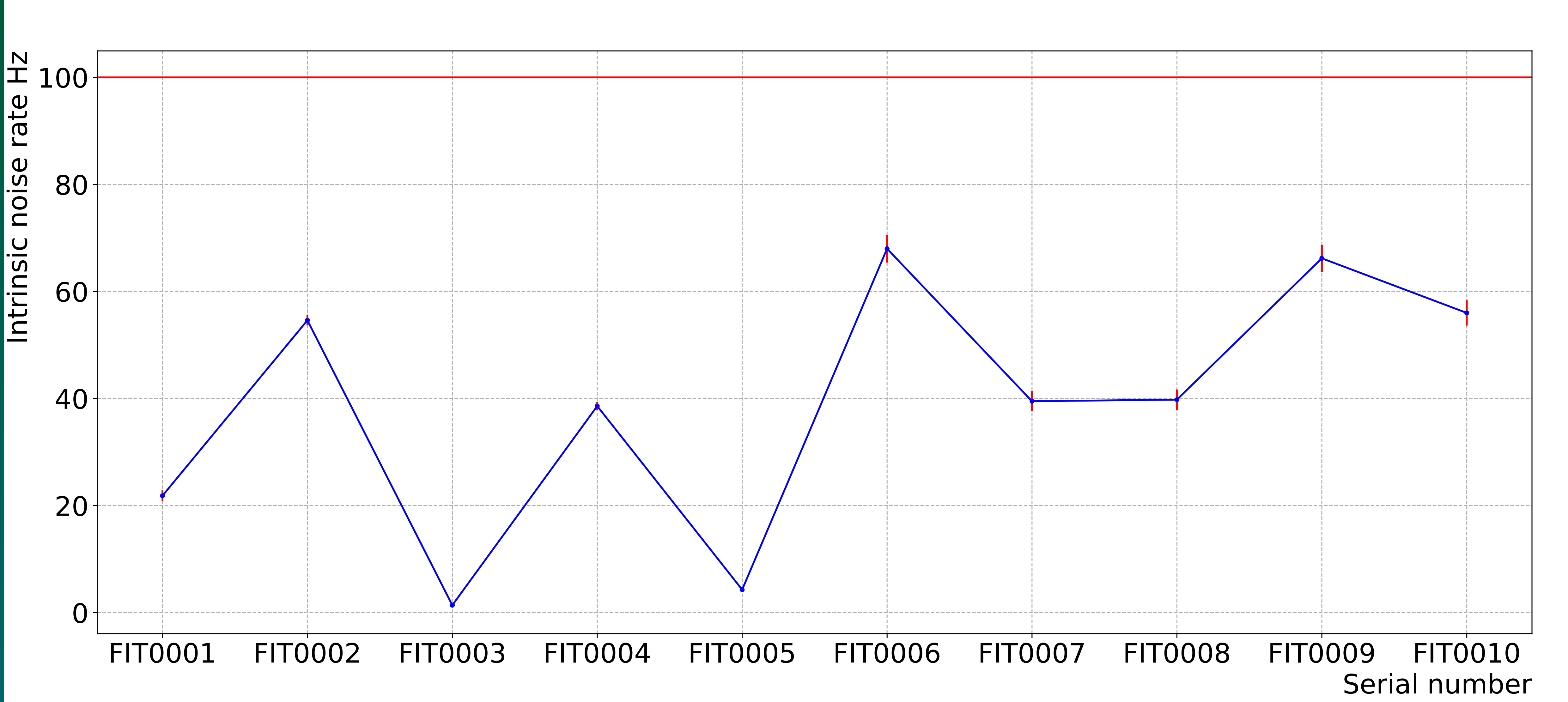

Summary of results for QC4b

GEMs: QC Step 5a

Effective Gain

- Measure the **gain** vs. **current in HV divider** (prop. to applied voltage) using **X-ray source** flushed under **Ar/CO_2**

- Comparing the **primary ionization charge** produced by the incoming charged particle in the drift gap to the final **amplified charge** on RO

- $G = \dfrac{I_{RO}}{R \cdot N_{primary} \cdot e}$

- Each chamber is required to have effective gain within $\pm 1.1\sigma \pm 37\,\%$ of the nominal effective gas gain value: 2×10^4

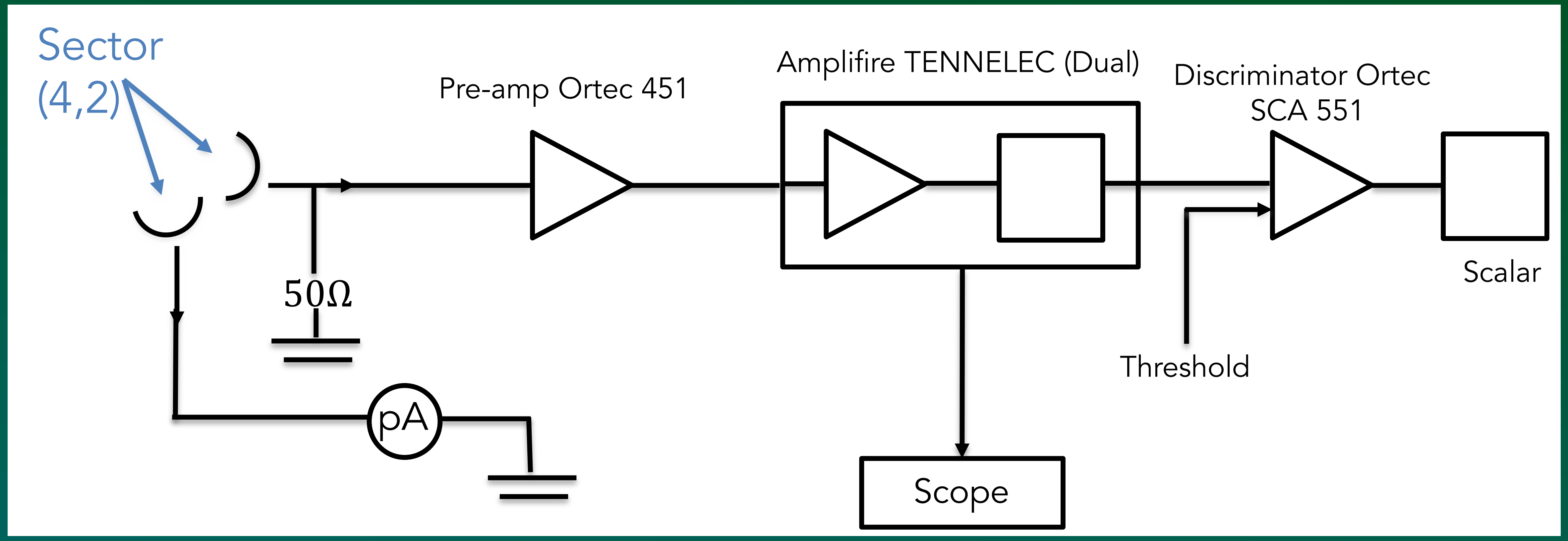

Electronics chain for QC5a

GEMs: QC Step 5a

Typical Results

- Measure the gain vs. current in HV divider (prop. to applied voltage) using X-ray source
- The gas gain is measured via the anode current produced in the chamber during this irradiation
- $G = \dfrac{I_{RO}}{R \cdot N_{primary} \cdot e}$
- Each chamber is required to have effective gain within $\pm 1.1\sigma \pm 37\ \%$ of the nominal effective gas gain value: 2×10^4

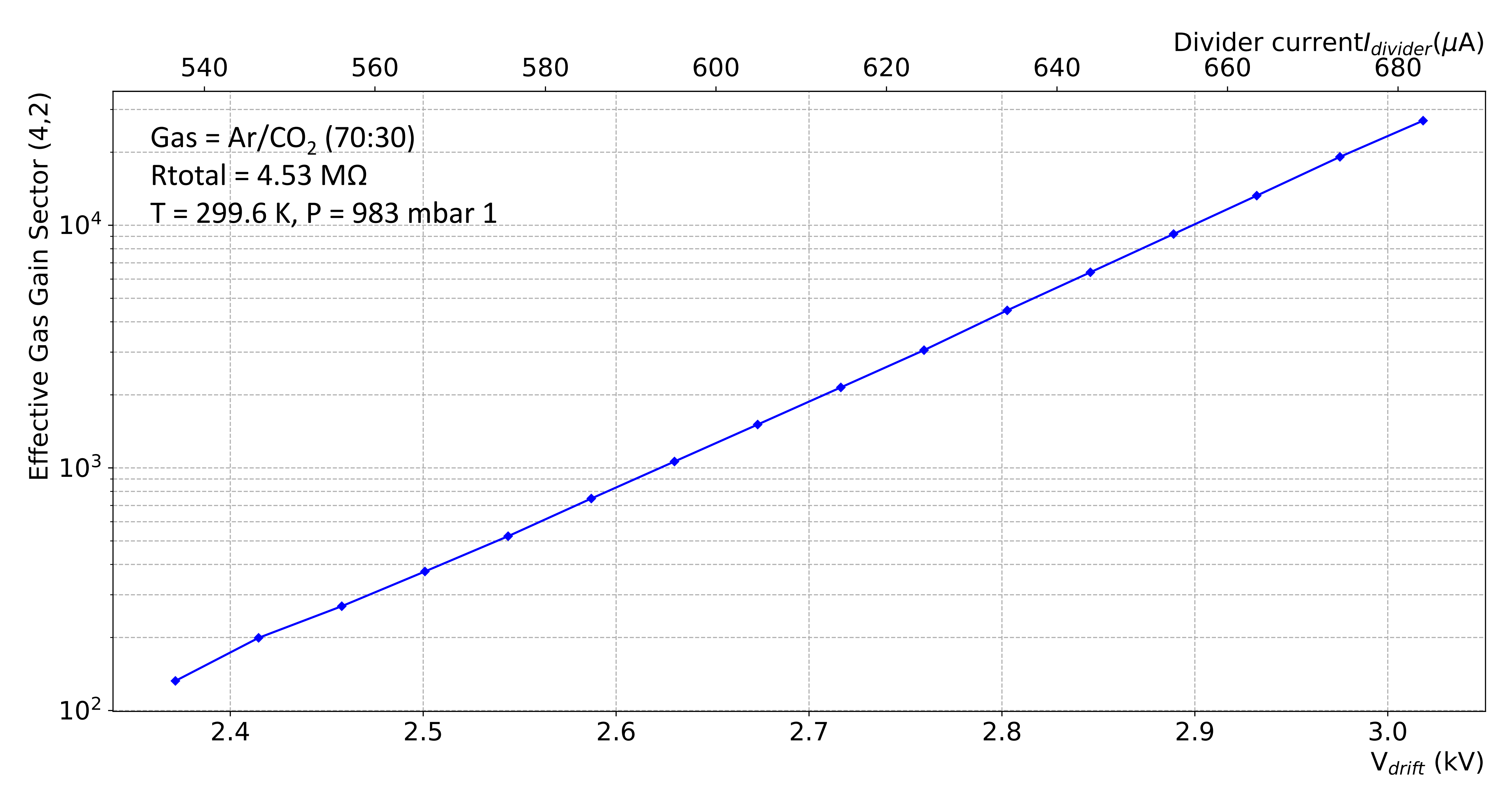

QC5a results for FIT0001

GEMs: QC Step 5a

Summary of Results

- Measure the **gain** vs. **current in HV divider** (prop. to applied voltage) using **X-ray source** flushed under **Ar/CO_2**

- Comparing the **primary ionization charge** produced by the incoming charged particle in the drift gap to the final **amplified charge** on RO

- $G = \frac{I_{RO}}{R \cdot N_{primary} \cdot e}$

- Each chamber is required to have effective gain within $\pm 1.1\sigma \pm 37\,\%$ of the nominal effective gas gain value: 2×10^4

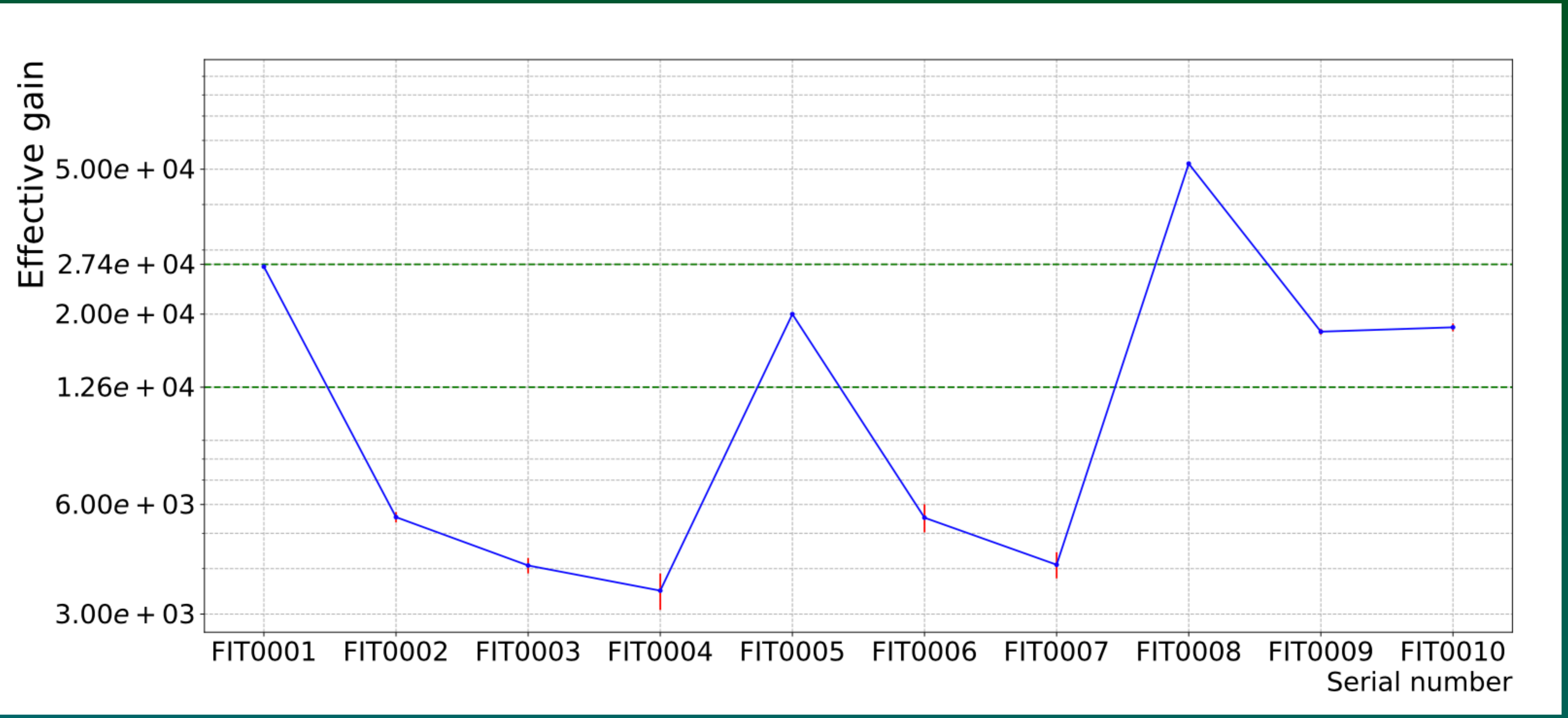

Summary of results for QC5a

GEMs: QC Step 5b

Response Uniformity Measurement

- Fix 24 analog pipeline voltage 25 (APV25) analog readout onto the readout Panasonic connectors according to the boss/sub mapping provided by the collaboration

- Performed by irradiating the entire chamber with the **X-ray** generator

- Operated at a reduced gas gain (typically between 500 and 600)

- the gain response across all readout strips must be below **37% of the standard deviation**

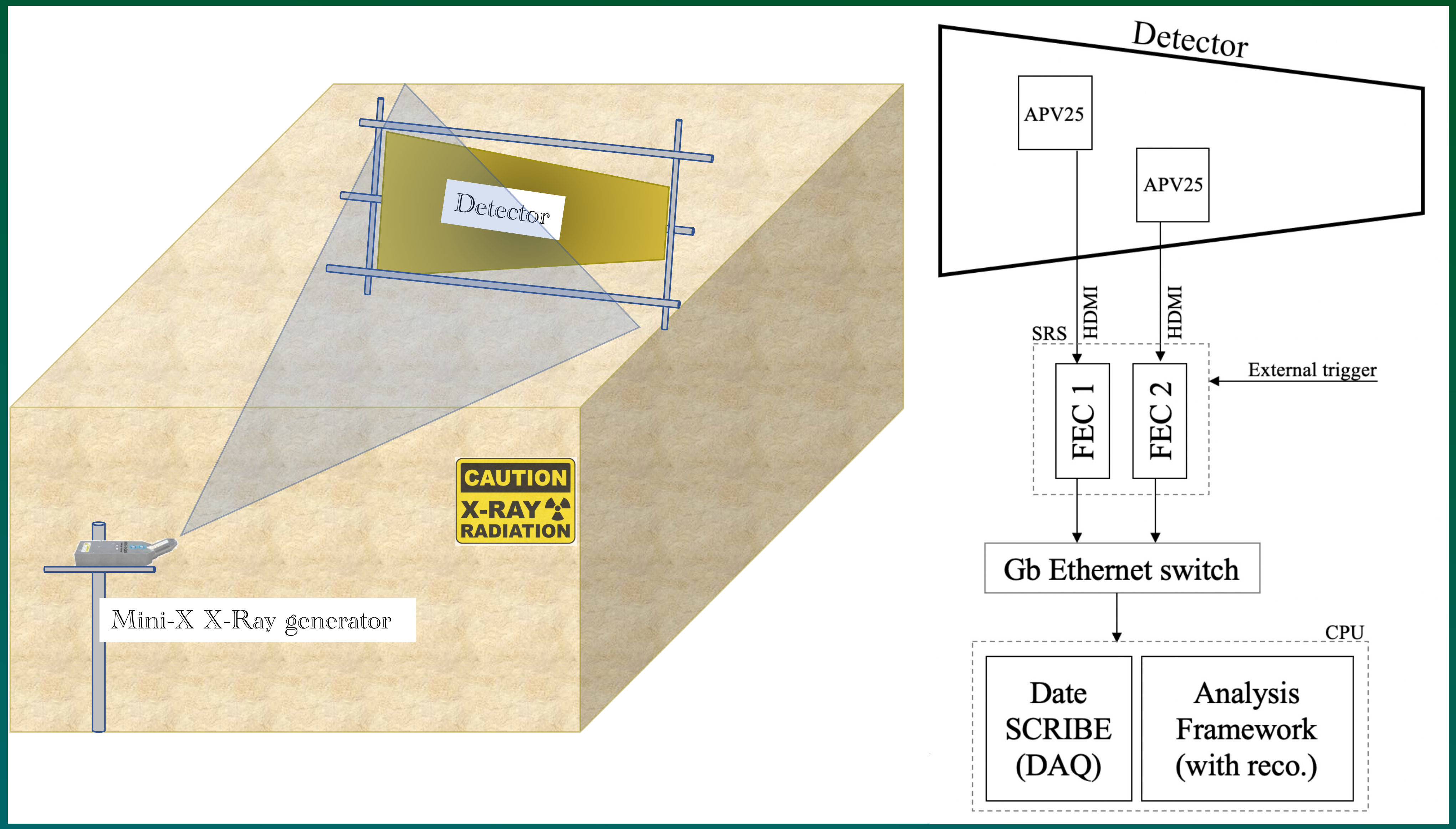

QC5b apparatus: The APV25 on each readout sector amplifies the induced charge on the readout strips and sends them to analog-to-digital converters (ADCs) to digitize the signal. The digitized signals are recorded by front-end concentrator cards (FECs), which are components of the larger RD51 Scalable Readout System (SRS)

GEMs: QC Step 5b

Response Uniformity Measurement

- Fix 24 analog pipeline voltage 25 (APV25) analog readout onto the readout Panasonic connectors according to the boss/sub mapping provided by the collaboration

- Performed by irradiating the entire chamber with the **X-ray** generator

- Operated at a reduced gas gain (typically between 500 and 600)

- the gain response across all readout strips must be below **37% of the standard deviation**

Uncertainty	Description	Contribution%
$\sigma_{thickness}$	Gap size between the GEM foils	1
$\sigma_{diameter}$	Diameter of holes in the GEM foil	4.2
$\sigma_{drift\ bending}$	Bending of the drift PCB	25
$\sigma_{RO\ bending}$	Bending of the RO PCB	7.5

The contributing parameters to the overall uncertainty in the gain uniformity response test

GEMs: QC Step 5b

Response Uniformity Measurement

- A GE1/1 readout board is divided into **768 regions** called **slices**
- Each **slice** containing **4 readout strips**.
- The **charge** collected from a **cluster of 4 readout strips** in a slice: **strip cluster charge**.
- The SRS system can produce an **ADC spectrum** for **each slice** or cluster.
- The prominent **peak** in an ADC spectrum for a cluster is the **X-ray fluorescence photopeak of Copper.**
- The fluorescence **photopeak** is located by fitting a **Cauchy distribution**
- The **photopeaks** of all cluster-strip charges are **histogramed**, and a **Gaussian** is fitted to it.

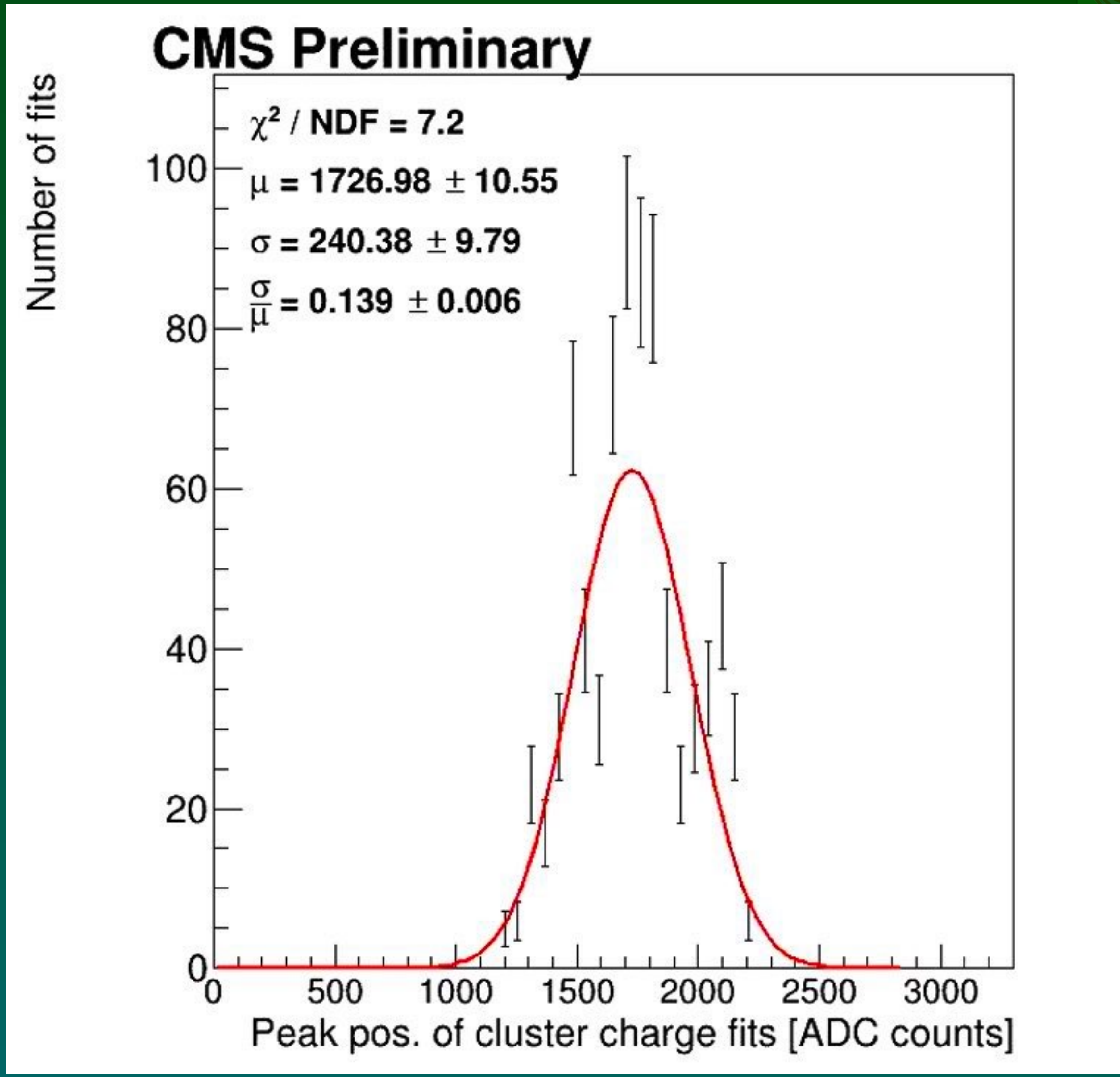

The means of the ADC spectra of the aggregate of strip-clusters is shown. The peak of the distribution is obtained through a Gaussian fit. The mean of the Gaussian represents the peak of the distribution. The ratio $\sigma/\mu \times 100 = 13\%$ represents the gain variation across the detector.

GEMs: QC Step 5b

Summary of Results

- Fix 24 analog pipeline voltage 25 (APV25) analog readout onto the readout Panasonic connectors according to the boss/sub mapping provided by the collaboration

- Performed by irradiating the entire chamber with the **X-ray** generator

- Operated at a reduced gas gain (typically between 500 and 600)

- the gain response across all readout strips must be below **37% of the standard deviation**

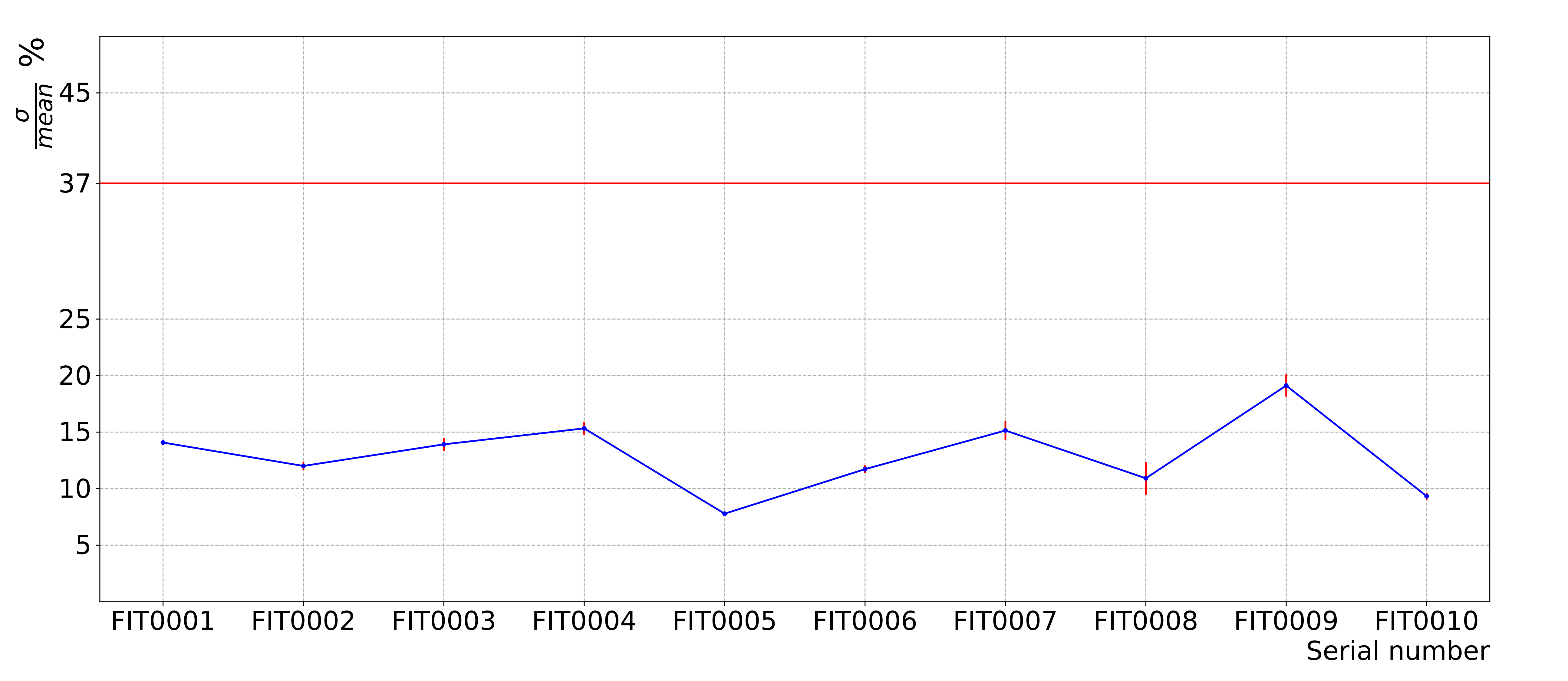

Summary of results for QC5b

Conclusion

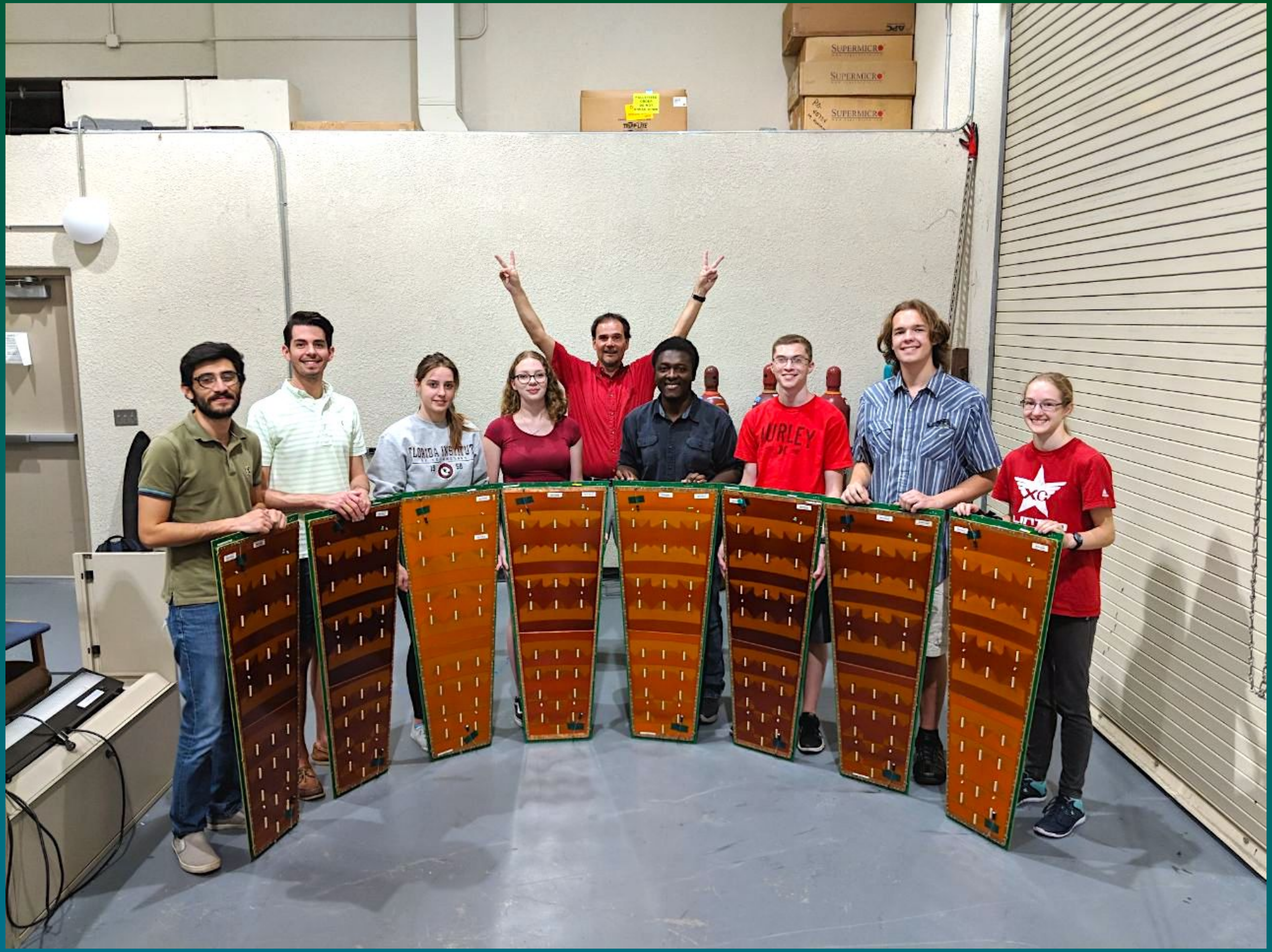

Layout

1. The Experimental Apparatus
2. Construction & Quality Control of GEM Detectors
3. The Dark Matter Problem

Introduction

The Dark Matter Problem

- The Standard Model of particle physics (SM) is a mathematically tight theory that describes fundamental physics and provides high-precision predictions consistent with decades of experimental studies.

- There are several important shortcomings that are of primary interest for current research in the field. Related to the research reported here is the fact that the **SM offers no explanation for the existence of dark matter** (DM), for which there is abundant astronomical evidence.

- Experimentally, DM has not yet been observed, and there is not yet any evidence for non-gravitational interactions between DM and Standard Model particles.

- The DM searches are perused in three major fronts:
  - Direct detection experiments
  - Indirect searches
  - **Collider searches** → {
    - Model-dependent searches
    - EFT model-independent searches
    - **Simplified model-independent searches** [1,2,3]

Introduction

The Dark Matter Problem

- The Standard Model of particle physics (SM) is a mathematically tight theory that describes fundamental physics and provides high-precision predictions consistent with decades of experimental studies.

- There are several important shortcomings that are of primary interest for current research in the field. Related to the research reported here is the fact that the **SM offers no explanation for the existence of dark matter** (DM), for which there is abundant astronomical evidence.

- Experimentally, DM has not yet been observed, and there is not yet any evidence for **non-gravitational interactions between DM and SM particles.**

- The DM searches are perused in three major fronts:
  - Direct detection experiments
  - Indirect searches
  - **Collider searches** → {
    - Model-dependent searches
    - EFT model-independent searches
    - **Simplified model-independent searches** [1,2,3]

Introduction

The Dark Matter Problem

- The Standard Model of particle physics (SM) is a mathematically tight theory that describes fundamental physics and provides high-precision predictions consistent with decades of experimental studies.

- There are several important shortcomings that are of primary interest for current research in the field. Related to the research reported here is the fact that the SM offers **no explanation for the existence of dark matter** (DM), for which there is abundant astronomical evidence.

- Experimentally, DM has not yet been observed, and there is not yet any evidence for **non-gravitational interactions between DM and SM particles.**

- The DM searches are perused in three major fronts:
  - Direct detection experiments
  - Indirect searches
  - **Collider searches** →
    - Model-dependent searches
    - EFT model-independent searches
    - **Simplified model-independent searches** [1,2,3]

Introduction

The Dark Sector

- The conventional approach in the search for new particles, including DM particles, has been to consider them to be **charged under at least some SM gauge symmetries.**

- While this approach has been the basis of 50 years of theoretical and experimental development in particle physics, the **experimental results have not been positively corroborated with this assumption.**

- To overcome these underwhelming results, attention has increasingly turned toward models wherein new particles are not charged under SM gauge symmetries.

- Collectively, these models are referred to as the ***dark sector*** or hidden-sector models [4,5].

- Under this assumption, if the DM does not seemingly interact with the SM sector, the implication is that it resides in a *dark sector* (charged under a *dark* symmetry group).

- If this new sector communicates with SM sector through a weak portal, then detection is possible at the LHC.

Introduction

The Dark Sector

- The conventional approach in the search for new particles, including DM particles, has been to consider them to be **charged under at least some SM gauge symmetries.**

- While this approach has been the basis of 50 years of theoretical and experimental development in particle physics, the **experimental results have not been positively corroborated with this assumption**.

- To overcome these underwhelming results, attention has increasingly turned toward models wherein new particles are **not charged under SM gauge symmetries.**

- Collectively, these models are referred to as the ***dark sector*** or hidden-sector models [4,5].

- Under this assumption, if the DM does not seemingly interact with the SM sector, the implication is that it resides in a *dark sector* (charged under a *dark* symmetry group).

- If this new sector communicates with SM sector through a weak portal, then detection is possible at the LHC.

Introduction

The Dark Sector

- The conventional approach in the search for new particles, including DM particles, has been to consider them to be **charged under at least some SM gauge symmetries.**

- While this approach has been the basis of 50 years of theoretical and experimental development in particle physics, the **experimental results have not been positively corroborated with this assumption**.

- To overcome these underwhelming results, attention has increasingly turned toward models wherein new particles are **not charged under SM gauge symmetries.**

- Collectively, these models are referred to as the ***dark sector*** or hidden-sector models [4,5].

- Under this assumption, if the DM does not seemingly interact with the SM sector, the implication is that it resides in a ***dark sector* (charged under a *dark* symmetry group).**

- If this new sector **communicates** with SM sector through a **weak portal**, then **detection is possible** at the LHC.

Introduction

The Dark Sector - Continued

- The portal may assume different forms based on the spin of the portal operator: **Spin 1-Vector**, Spin-1/2 Neutrinos, Spin0-Higgs (scalar), or Axions (pseudo-scalar).

- The focus of my research is the **Spin 1-Vector portal** where a dark gauge boson interacts with an SM gauge boson through ***kinetic mixing*** between one dark and one visible Abelian gauge boson. This gauge boson is called the the dark Z (Z_D) [6].

$$\mathscr{L} = -\frac{1}{4}B^{\mu\nu}B_{\mu\nu} - \frac{1}{4}B'^{\mu\nu}B'_{\mu\nu} - \varepsilon B^{\mu\nu}B'_{\mu\nu}$$

Introduction

The Dark Sector - Continued

- The portal may assume different forms based on the spin of the portal operator: **Spin 1-Vector**, Spin-1/2 Neutrinos, Spin0-Higgs (scalar), or Axions (pseudo-scalar).

- The focus of my research is the **Spin 1-Vector portal** where a dark gauge boson interacts with an SM gauge boson through ***kinetic mixing*** between one dark and one visible Abelian gauge boson. This gauge boson is called the **the dark Z (Z_D)** [6].

$$\mathscr{L} = -\frac{1}{4}B^{\mu\nu}B_{\mu\nu} - \frac{1}{4}B'^{\mu\nu}B'_{\mu\nu} - \varepsilon B^{\mu\nu}B'_{\mu\nu}$$

- $B^{\mu\nu}$ is the SM electromagnetic field tensor
- $B'^{\mu\nu}$ The field tensor in the dark sector
- ε is the kinetic mixing parameter

Layout

1. Experimental Apparatus
2. Construction & Quality Control of GEM Detectors
3. Dark Matter Problem
4. Model-independent Search

Model-Independent Search

The 2018 Analysis

- We explored the **pair production of new bosons** at the LHC in collaboration with research groups from Texas A&M, Rice University, and University of Sonora.
- Our analysis presents a search for **new light bosons** decaying into **muon pairs**, corresponding to an integrated luminosity of $59.7\ fb^{-1}$ at the center-of-mass energy $\sqrt{s} = 13\ TeV$, recorded during **2018** at the CMS.
- The **parameter space** probed is $0.25 < m < 60\ GeV$ for the **mass** of the **mediator** [7].

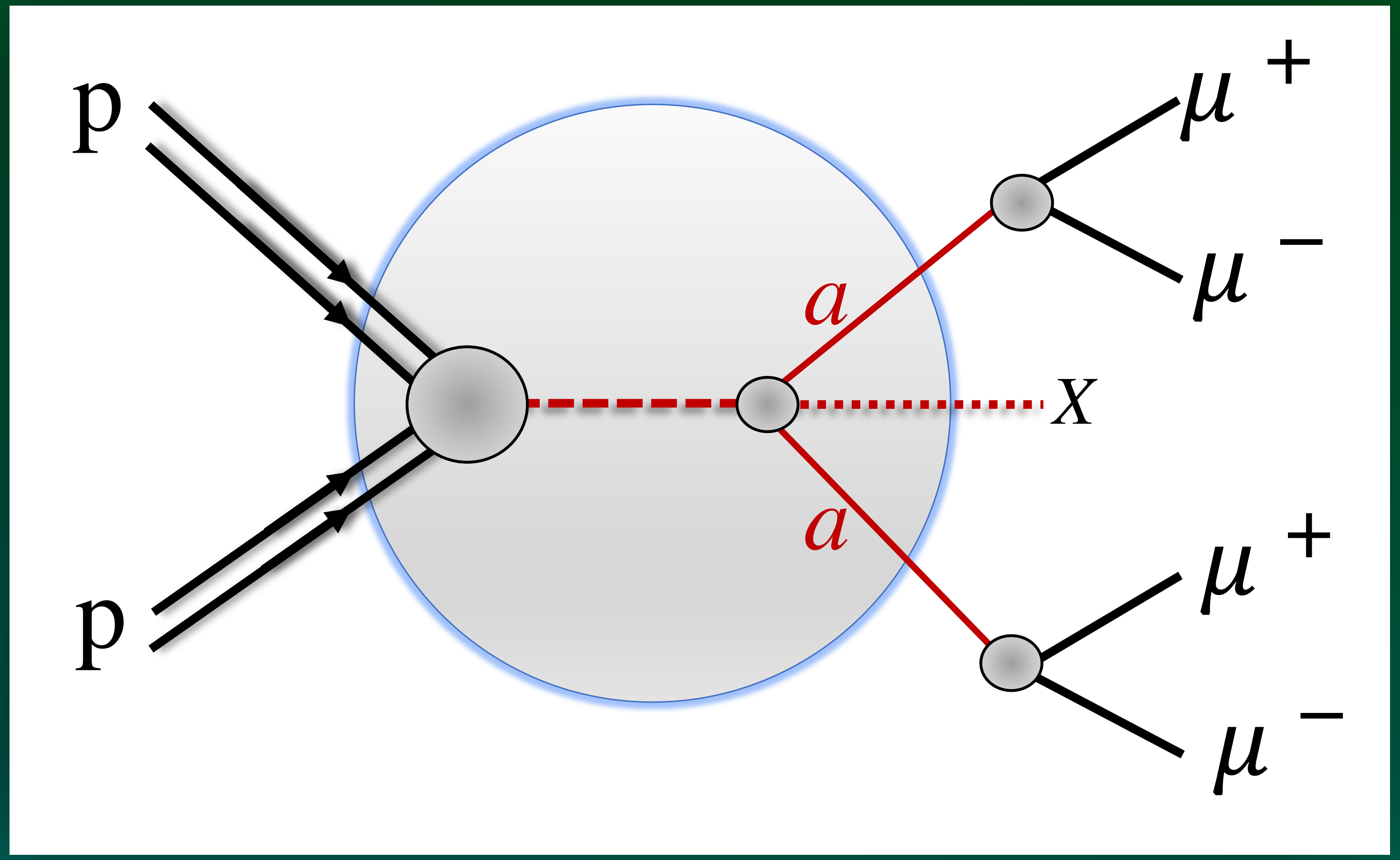

Figure1: *Schematic example of the pp interaction that produces a pair of new bosons of which each decays into a muon pair. The grey circle indicate the dark sector inter- actions. The X particle is to signify any excess processes other than the four lepton final state.*

Model-Independent Search

The 2018 Analysis

We have a CADI line with AN and draft paper based on Run II 2018 data with dimuon trigger w/o VTX constraints:

- CADI: HIG-21-004
- Pre-approval talk: Feb 16 , 2021
- Unblinded results: Apr 28 , 2021
- Twiki: HIG21004Run2
-

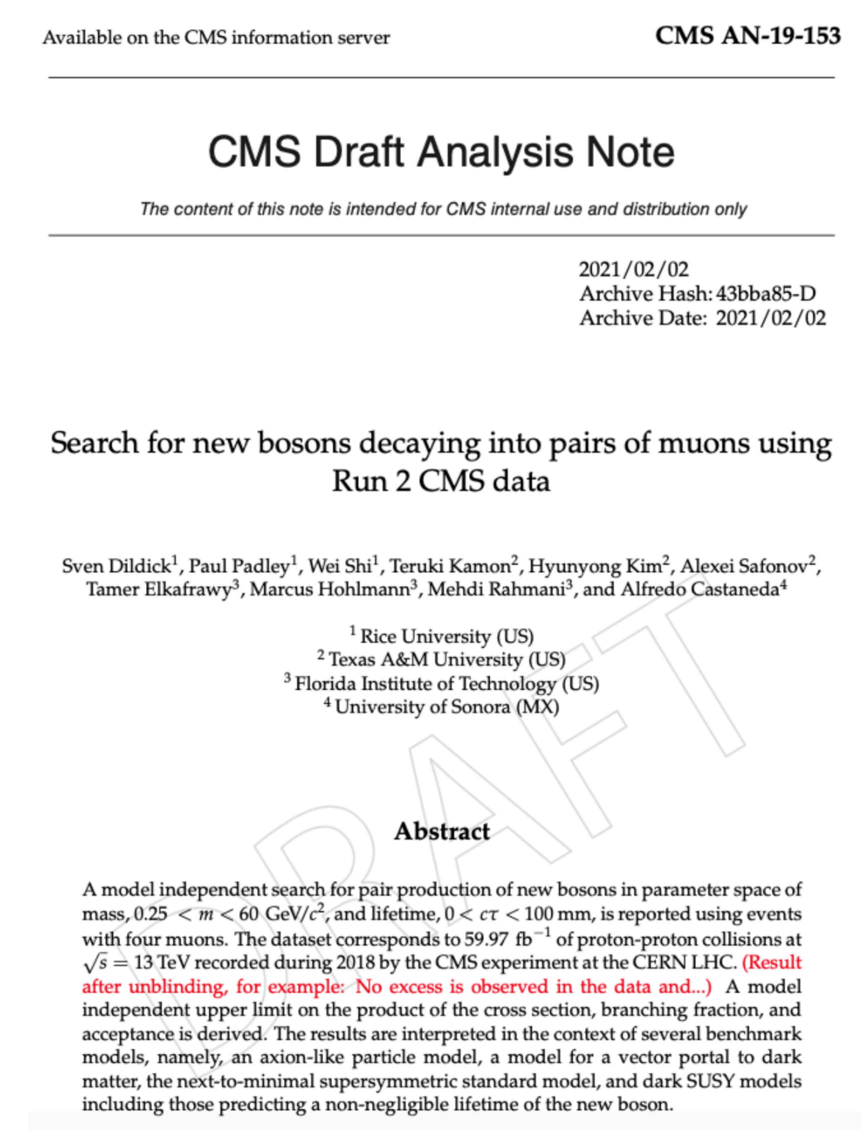
Available on the CMS information server

CMS AN-19-153

CMS Draft Analysis Note

The content of this note is intended for CMS internal use and distribution only

2021/02/02
Archive Hash: 43bba85-D
Archive Date: 2021/02/02

Search for new bosons decaying into pairs of muons using Run 2 CMS data

Sven Dildick[1], Paul Padley[1], Wei Shi[1], Teruki Kamon[2], Hyunyong Kim[2], Alexei Safonov[2], Tamer Elkafrawy[3], Marcus Hohlmann[3], Mehdi Rahmani[3], and Alfredo Castaneda[4]

[1] Rice University (US)
[2] Texas A&M University (US)
[3] Florida Institute of Technology (US)
[4] University of Sonora (MX)

Abstract

A model independent search for pair production of new bosons in parameter space of mass, $0.25 < m < 60$ GeV/c^2, and lifetime, $0 < c\tau < 100$ mm, is reported using events with four muons. The dataset corresponds to 59.97 fb^{-1} of proton-proton collisions at $\sqrt{s} = 13$ TeV recorded during 2018 by the CMS experiment at the CERN LHC. (Result after unblinding, for example: No excess is observed in the data and...) A model independent upper limit on the product of the cross section, branching fraction, and acceptance is derived. The results are interpreted in the context of several benchmark models, namely, an axion-like particle model, a model for a vector portal to dark matter, the next-to-minimal supersymmetric standard model, and dark SUSY models including those predicting a non-negligible lifetime of the new boson.

Thank conveners:

Keti Kaadze
Stephane Cooperstein

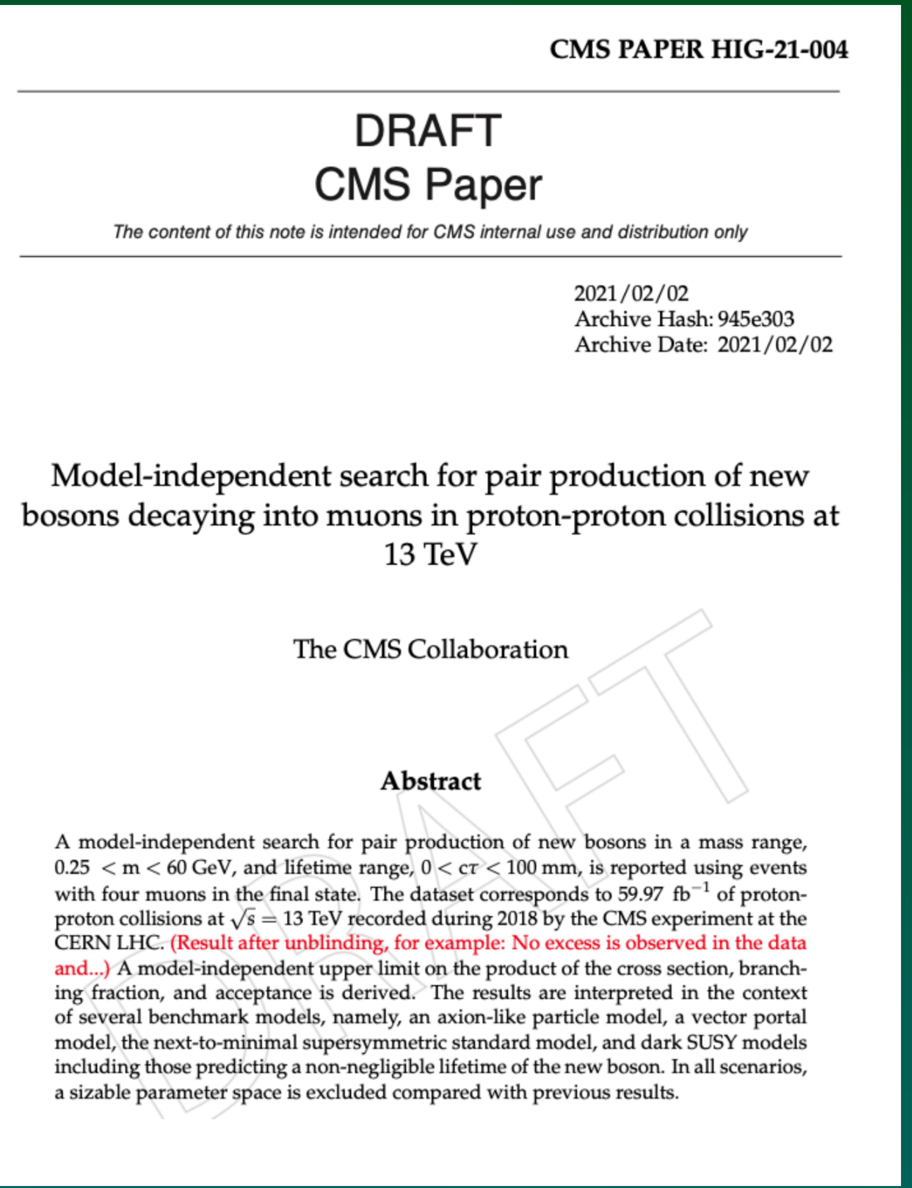
CMS PAPER HIG-21-004

DRAFT
CMS Paper

The content of this note is intended for CMS internal use and distribution only

2021/02/02
Archive Hash: 945e303
Archive Date: 2021/02/02

Model-independent search for pair production of new bosons decaying into muons in proton-proton collisions at 13 TeV

The CMS Collaboration

Abstract

A model-independent search for pair production of new bosons in a mass range, $0.25 < m < 60$ GeV, and lifetime range, $0 < c\tau < 100$ mm, is reported using events with four muons in the final state. The dataset corresponds to 59.97 fb^{-1} of proton-proton collisions at $\sqrt{s} = 13$ TeV recorded during 2018 by the CMS experiment at the CERN LHC. (Result after unblinding, for example: No excess is observed in the data and...) A model-independent upper limit on the product of the cross section, branching fraction, and acceptance is derived. The results are interpreted in the context of several benchmark models, namely, an axion-like particle model, a vector portal model, the next-to-minimal supersymmetric standard model, and dark SUSY models including those predicting a non-negligible lifetime of the new boson. In all scenarios, a sizable parameter space is excluded compared with previous results.

Layout

1. Experimental Apparatus
2. Construction & Quality Control of GEM Detectors
3. Dark Matter Problem
4. Model-independent Search
5. Vector-portal Model

Bench-Mark Models

The Dark Scalar Model

- In this model, the Z_D particle is produced via kinetic mixing mechanism between the SM Z and the dark boson Z_D (gauge boson of a new $U(1)_D$ symmetry group.)
- The mixing parameter: ε
- The dark scalar s_D, a complex scalar field, is assumed to be *not* self-conjugate (Bose symmetry)
- For the purposes of simplicity the branching fraction $\mathscr{B}$ of s_D to muons is considered to be 100%. The
- Feynman diagram for this process is shown in Fig. 2 [8, 9].(Other models in **App. A**)

$$pp \rightarrow Z_D \rightarrow s_D \overline{s_D} \rightarrow \mu^+\mu^-\mu^+\mu^-$$

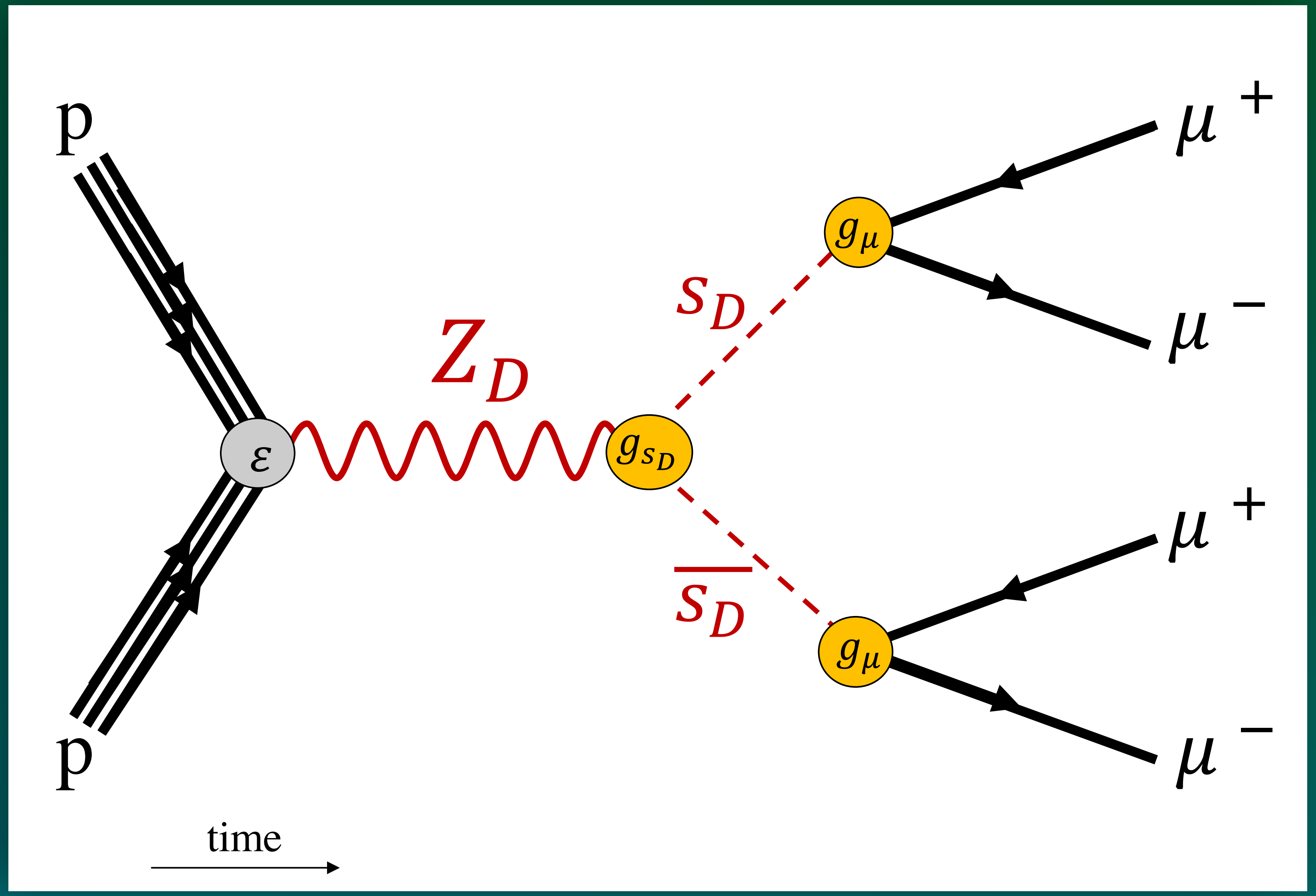

Figure2: Z_D decays into a pair of scalar dark matter particles which then each subsequently decay into two oppositely charged muons.

Bench-Mark Models

The Dark Scalar Model

- In this model, the Z_D particle is produced via kinetic mixing mechanism between the SM Z and the dark boson Z_D (gauge boson of a new $U(1)_D$ symmetry group.)
- The mixing parameter: ε
- The dark scalar s_D, a **complex scalar field**, is assumed to be ***not* self-conjugate** (Bose symmetry)
- For the purposes of simplicity the branching fraction $\mathscr{B}$ of s_D to muons is considered to be 100%. The

- Feynman diagram for this process is shown in Fig. 2 [8, 9].(Other models in **App. A**)

$$pp \to Z_D \to s_D\overline{s_D} \to \mu^+\mu^-\mu^+\mu^-$$

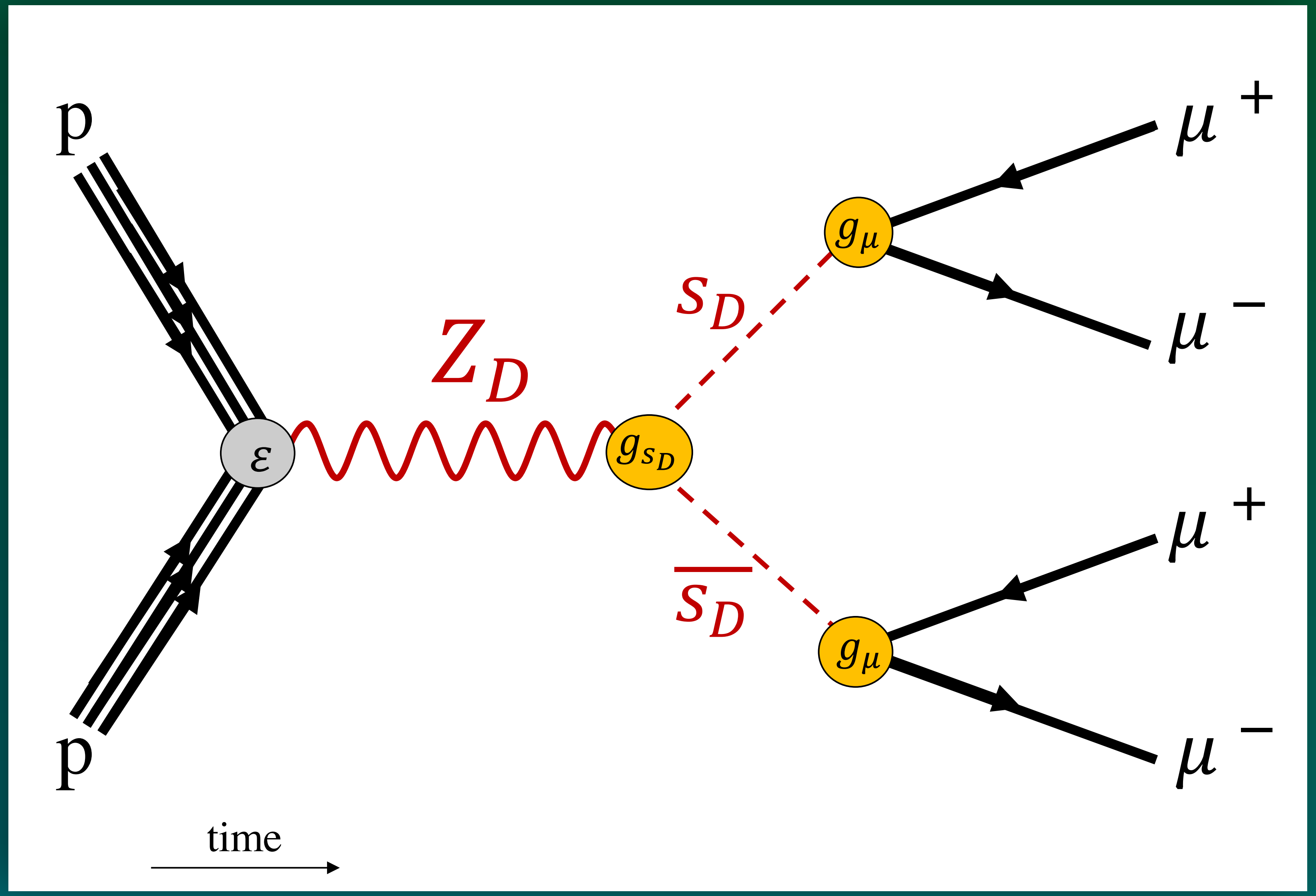

Figure2: Z_D decays into a pair of scalar dark matter particles which then each subsequently decay into two oppositely charged muons.

Bench-Mark Models

The Dark Scalar Model

- In this model, the Z_D particle is produced via kinetic mixing mechanism between the SM Z and the dark boson Z_D (gauge boson of a new $U(1)_D$ symmetry group.)

- The mixing parameter: ε

- The dark scalar s_D, a **complex scalar field**, is assumed to be ***not* self-conjugate** (Bose symmetry)

- For the purposes of simplicity the branching fraction $\mathscr{B}$ of s_D to muons is considered to be 100%. The

- Feynman diagram for this process is shown in Fig. 2 [8, 9].(Other models in **App. A**)

$$pp \to Z_D \to s_D\overline{s_D} \to \mu^+\mu^-\mu^+\mu^-$$

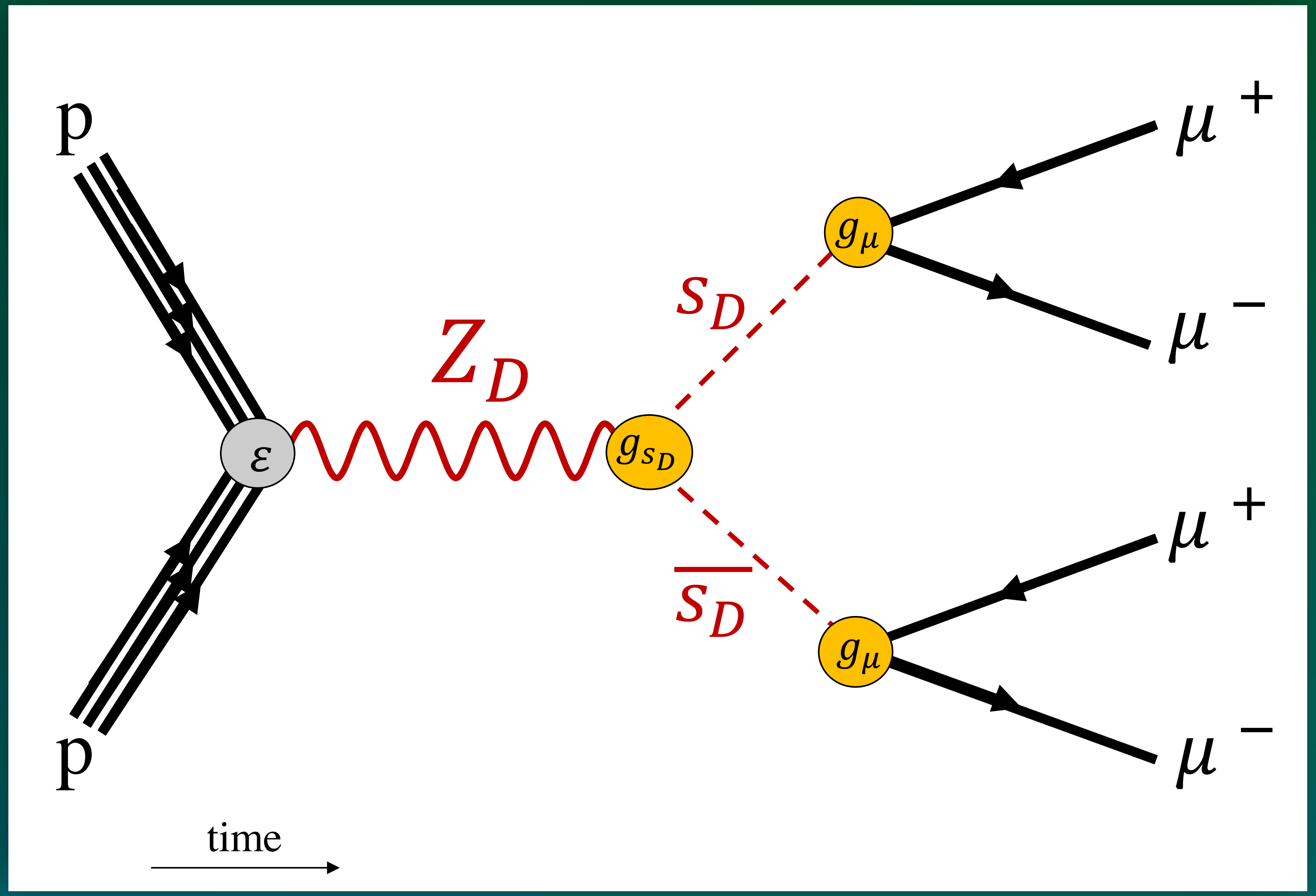

Figure2: Z_D decays into a pair of scalar dark matter particles which then each subsequently decay into two oppositely charged muons.

Hard Process

Kinematics of the Model

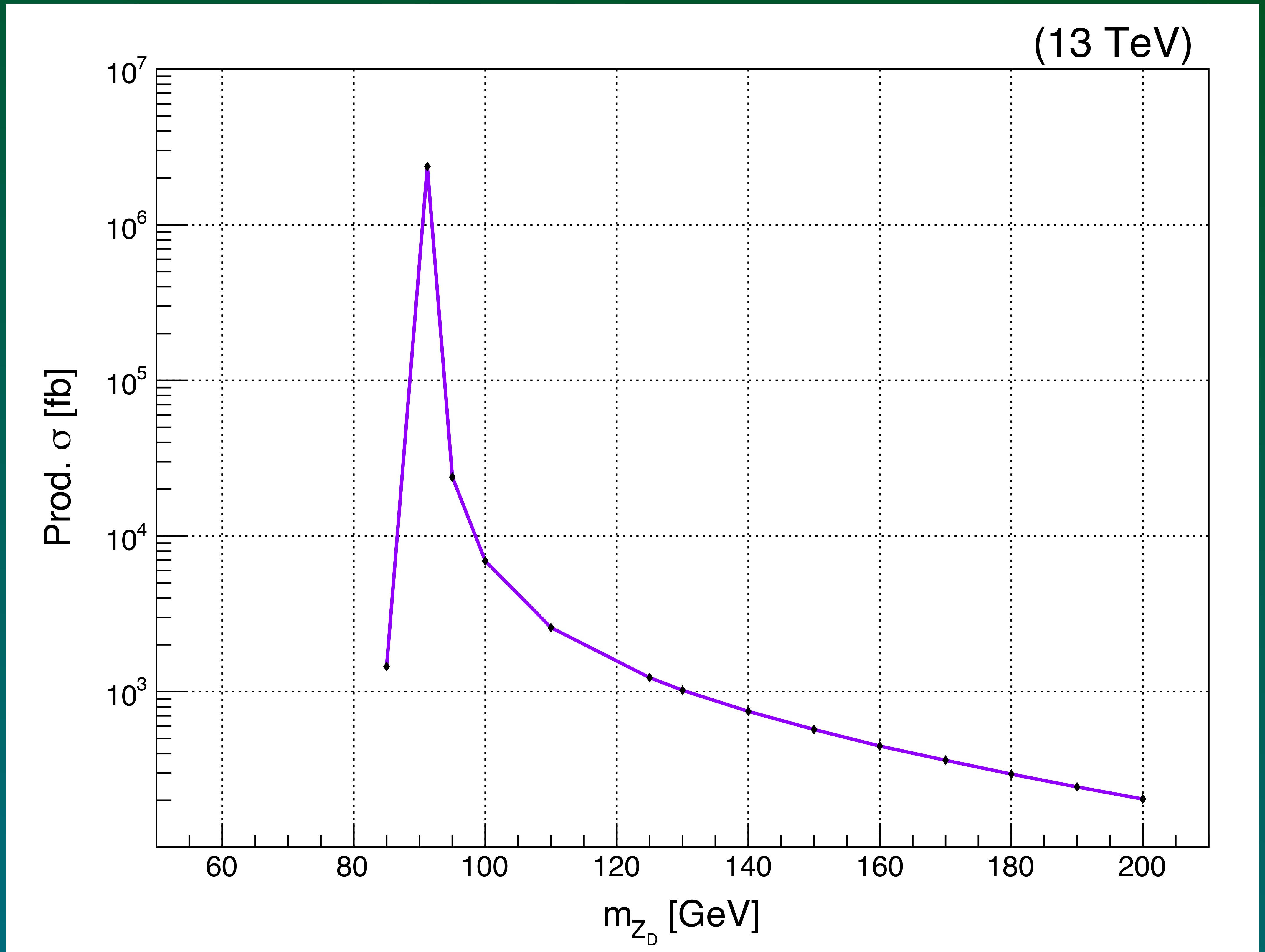

Figure3: A scan of production cross-section for varying mass of Z_D

Hard Process

Kinematics of the Model

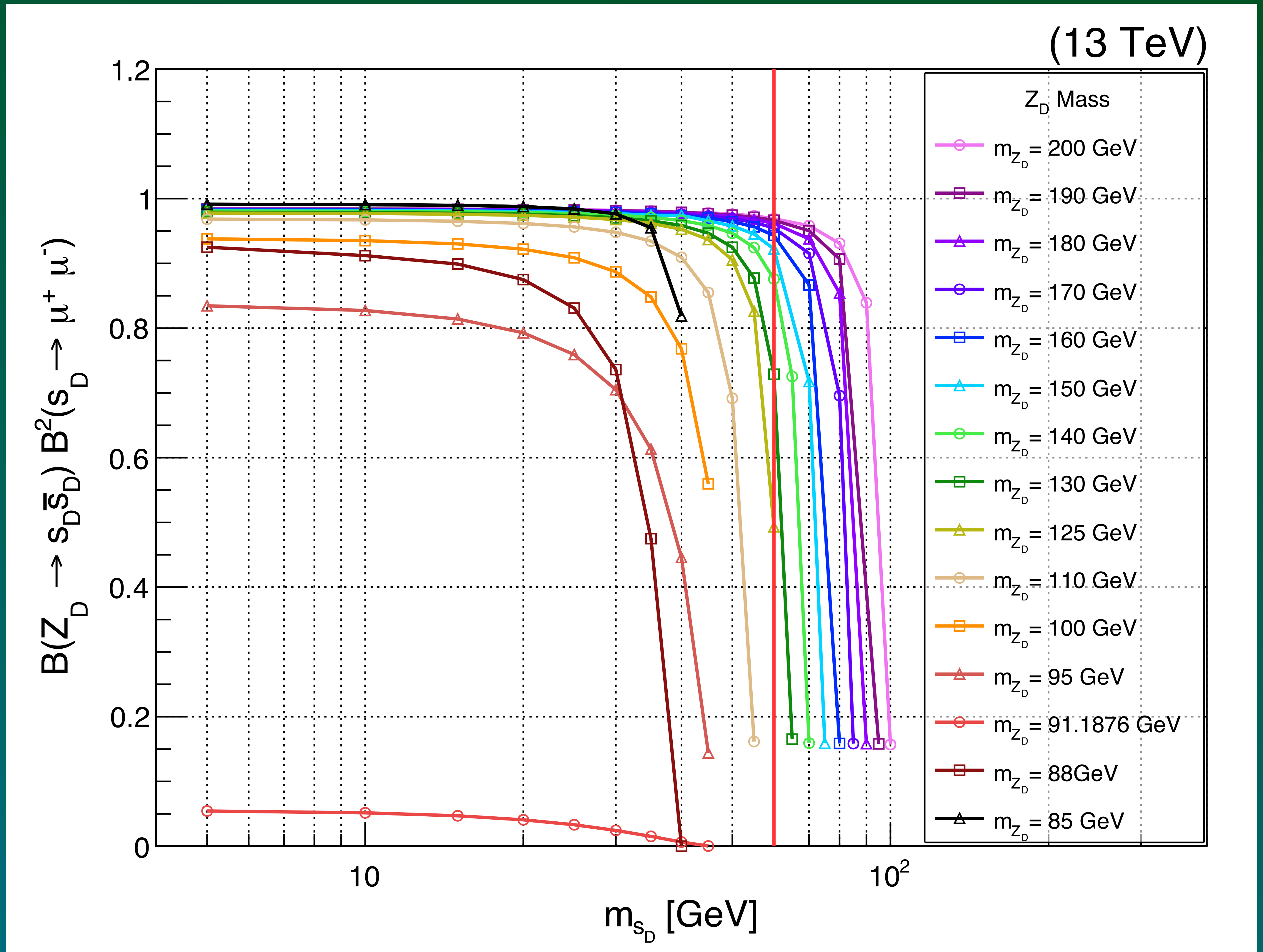

Figure4: A scan of branching fraction for varying mass of Z_D and s_D

Hard Process

Kinematics of the Model

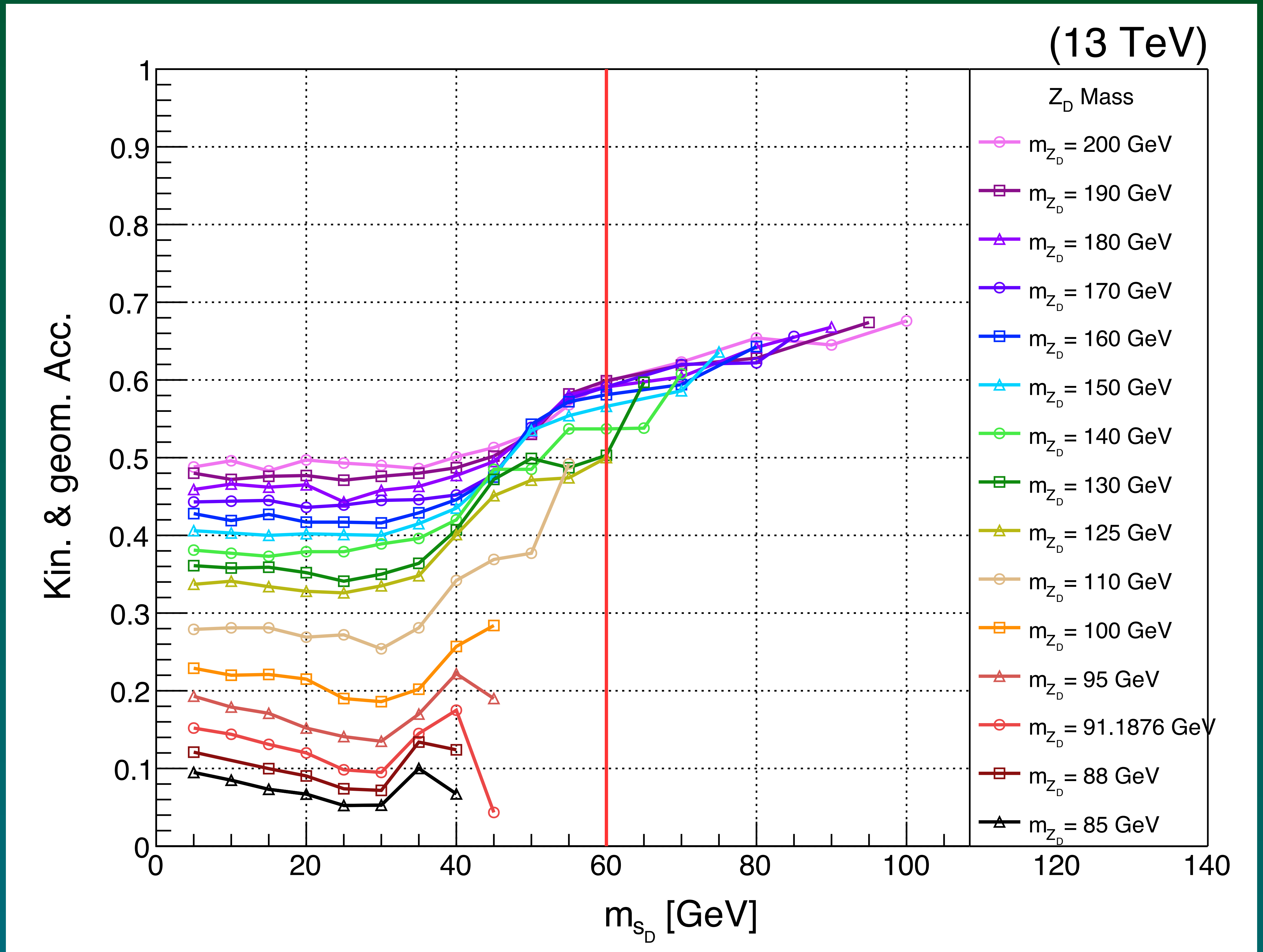

Figure5: A scan of geometrical and kinematic acceptance of the muon selection for varying mass of Z_D and s_D

Hard Process

Kinematics of the Model

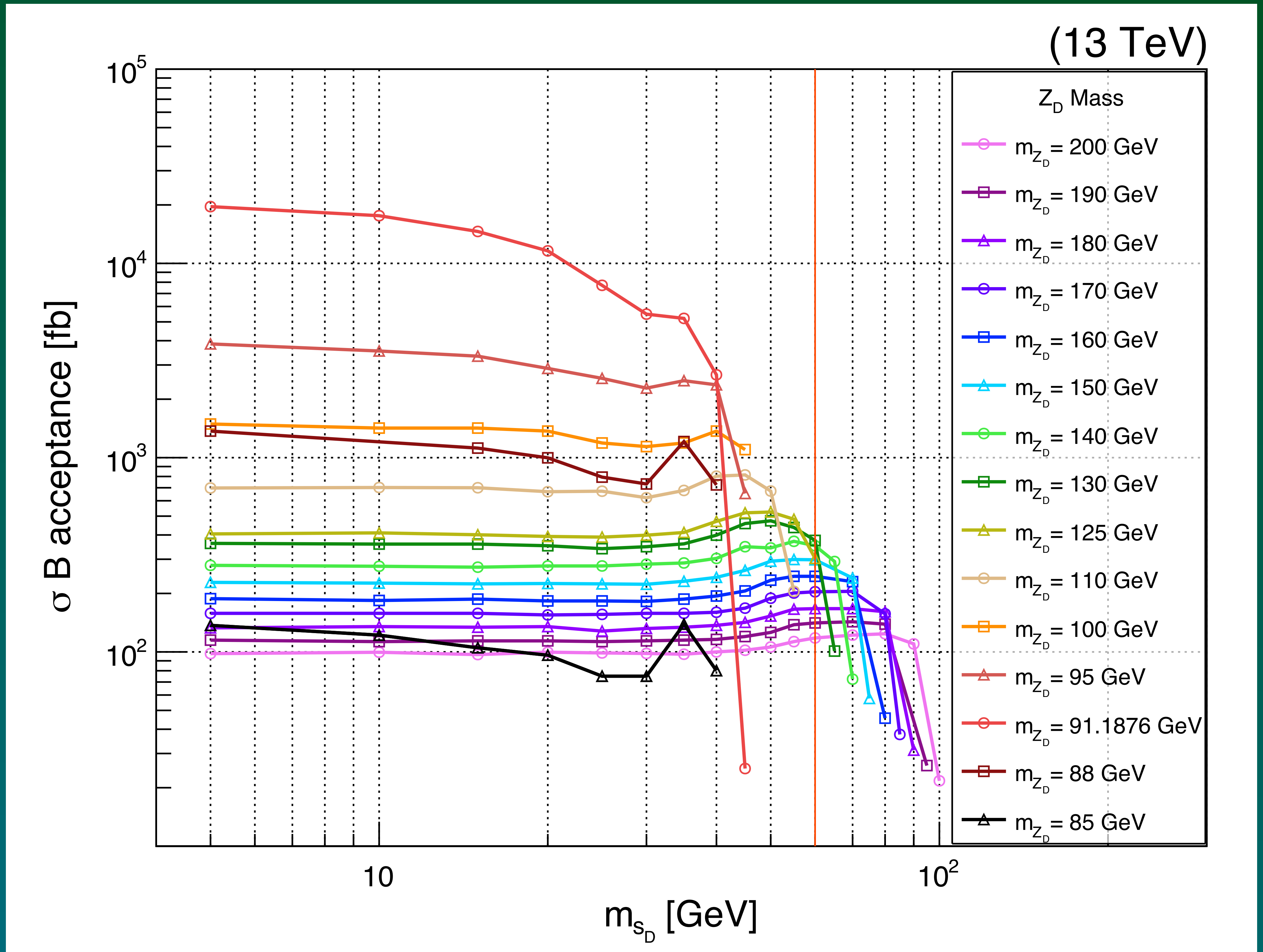

Figure6: Multiplication production cross-section, branching fraction, and acceptance as an indication of sensitivity for varying mass of ZD and sD

Layout

1. Experimental Apparatus
2. Construction & Quality Control of GEM Detectors
3. Dark Matter Problem
4. Model-independent Search
5. Samples & Selection

Samples

Monte-Carlo Simulation & Data

MC Simulation

Simulation Process	Description
Model Implementation	Feynrules
Hard Scattering Simulation	amc@nlo v2.6.5
Parton showering	PYTHIA 8
Hadronization, detector response, &	CMSSW 10 2 X

2018 Data

Dataset Labels	Number of
/DoubleMuon/Run2018A-17Sep2018-v2/	75 499 908
/DoubleMuon/Run2018B-17Sep2018-v1/	35 057 758
/DoubleMuon/Run2018C-17Sep2018-v1/	34 565 869
/DoubleMuon/Run2018D-PromptReco-v2/	169 225 355
Total	314 348 890

Analysis

Trigger and Muon Selection

Trigger Paths
HLT_DoubleL2Mu23NoVtx_2Cha
HLT_Mu18_Mu9_SameSign
HLT_TrkMu12_DoubleTrkMu5NoFiltersNoVtx,
HLT_TripleMu_12_10_5

For more on triggers see App. D

Muon selection
slimmedMuons in MiniAOD
PF Loose muon (>=3) + standalone-only (SA) muon
Two muons: p_T >24 GeV, |eta| < 2
Four muons: p_T >8 GeV, |eta| < 2.4

Analysis

Muon Pairing

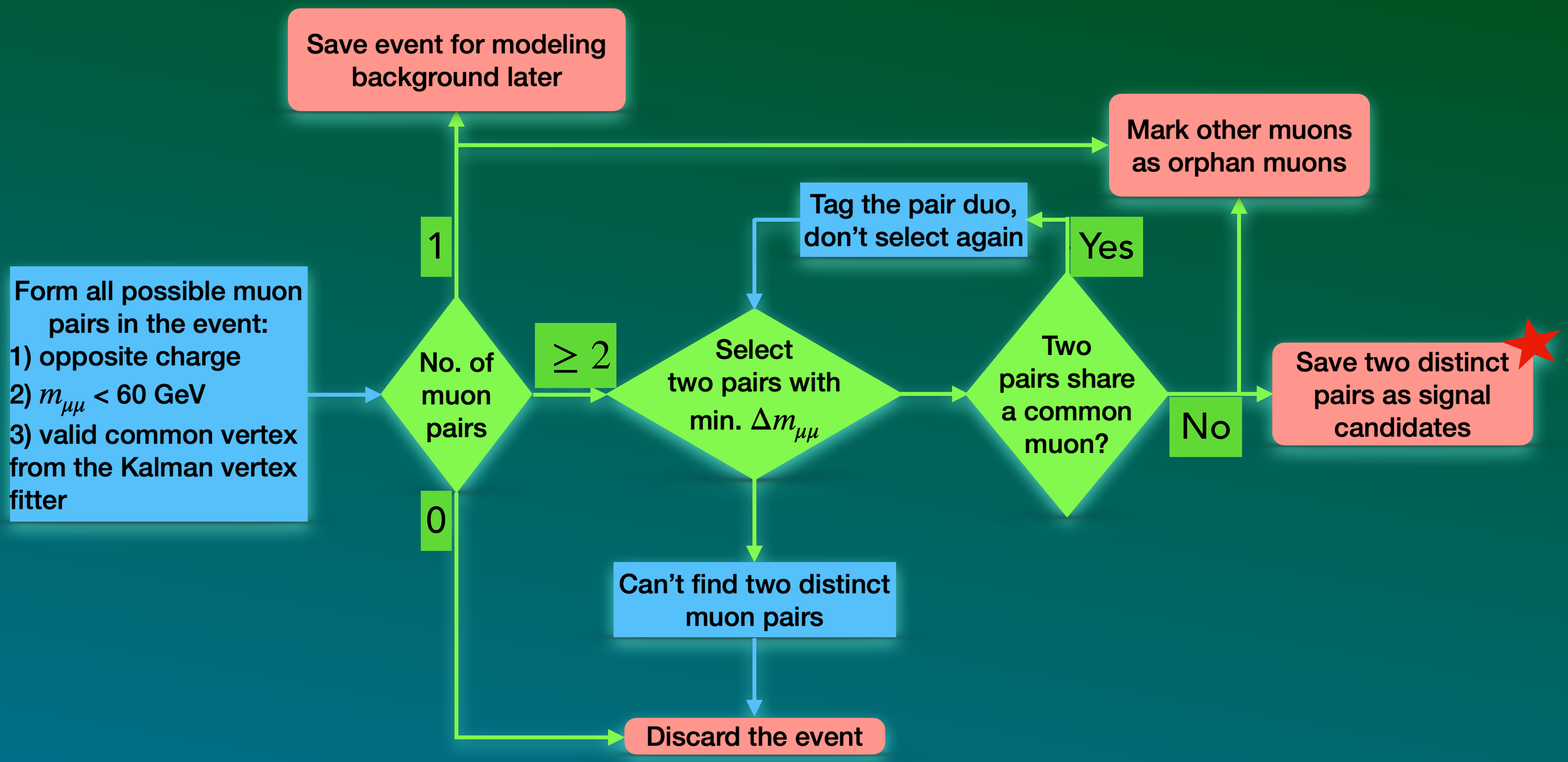

Analysis

High-Level Selection

Selection	Description
Pixel Hit	Valid pixel hit for at least one muon in the muon pair: $L_{xy} < 16$ cm, $L_Z < 51.6$ cm (See App. E)
Dimuon Vertex	Fit dimuon vertex of each muon pair using KalmanVertexFitter, $P_{\mu\mu} > P(L_{xy}, f(\Delta R), N_{SA-\mu})$ (See App. E)
Mass Window	Two signal dimuon required to have consistent invariant mass (See App. E)

Mass Window

Defining Control and Signal Regions

- Since the moun pairs are produced from supposedly the **same scalars** with **consistent masses**, the invariant mass of muon pairs should be consistent as well
- Conventional way of defining a mass consistency window:
  - The **width** of the SR window is adjusted by the **di-muon mass reconstruction resolution** eg., a Gaussian fit to the di-muon mass and the standard deviation 3σ would result in ~99% signal efficiency
  - This method **does not** work for **higher masses** ($\gtrsim 10$ GeV)
  - Higher mass: radiative **non-gaussian tails**
- Instead we define the **window width** by the **efficiencies** that we desire: 90%

$$m_1 - m_2 = f(\frac{m_1 + m_2}{2})$$

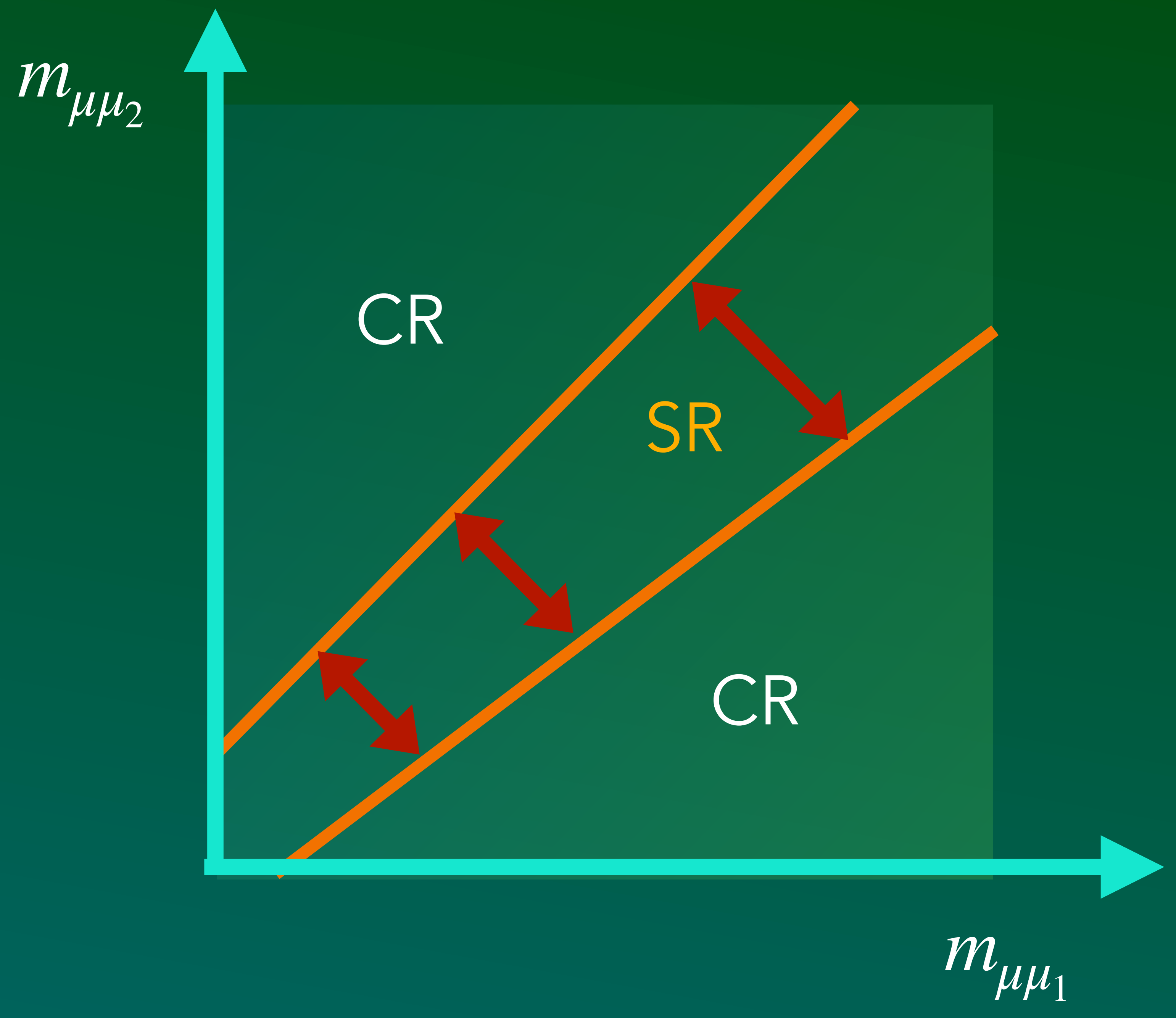

For more on mass window cut see App. E

Mass Window

Defining Control and Signal Regions

- Since the moun pairs are produced from supposedly the **same scalars** with **consistent masses**, the invariant mass of muon pairs should be consistent as well
- Conventional way of defining a mass consistency window:
  - The **width** of the SR window is adjusted by the **di-muon mass reconstruction resolution** eg., a Gaussian fit to the di-muon mass and the standard deviation 3σ would result in ~99% signal efficiency
  - This method **does not** work for **higher masses** ($\gtrsim 10$ GeV)
  - Higher mass: radiative **non-gaussian tails**
- Instead we define the **window width** by the **efficiencies** that we desire: 90%

$$m_1 - m_2 = f(\frac{m_1 + m_2}{2})$$

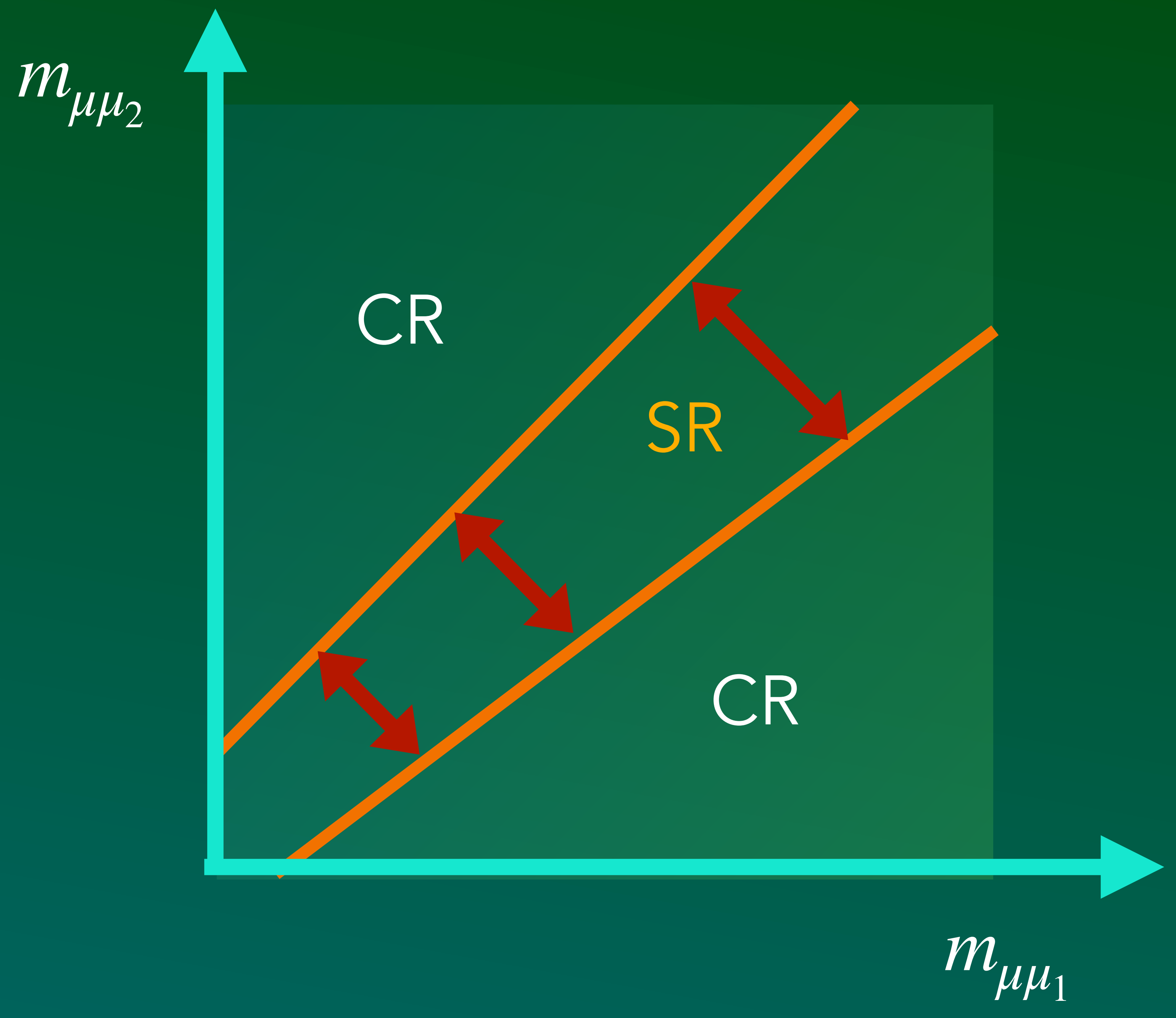

For more on mass window cut see App. E

Mass Window

Defining Control and Signal Regions

- Since the moun pairs are produced from supposedly the **same scalars** with **consistent masses**, the invariant mass of muon pairs should be consistent as well
- Conventional way of defining a mass consistency window:
  - The **width** of the SR window is adjusted by the **di-muon mass reconstruction resolution** eg., a Gaussian fit to the di-muon mass and the standard deviation 3σ would result in ~99% signal efficiency
  - This method **does not** work for **higher masses** ($\gtrsim 10$ GeV)
  - Higher mass: radiative **non-gaussian tails**
- Instead we define the **window width** by the **efficiencies** that we desire: 90%

$$m_1 - m_2 = f(\frac{m_1 + m_2}{2})$$

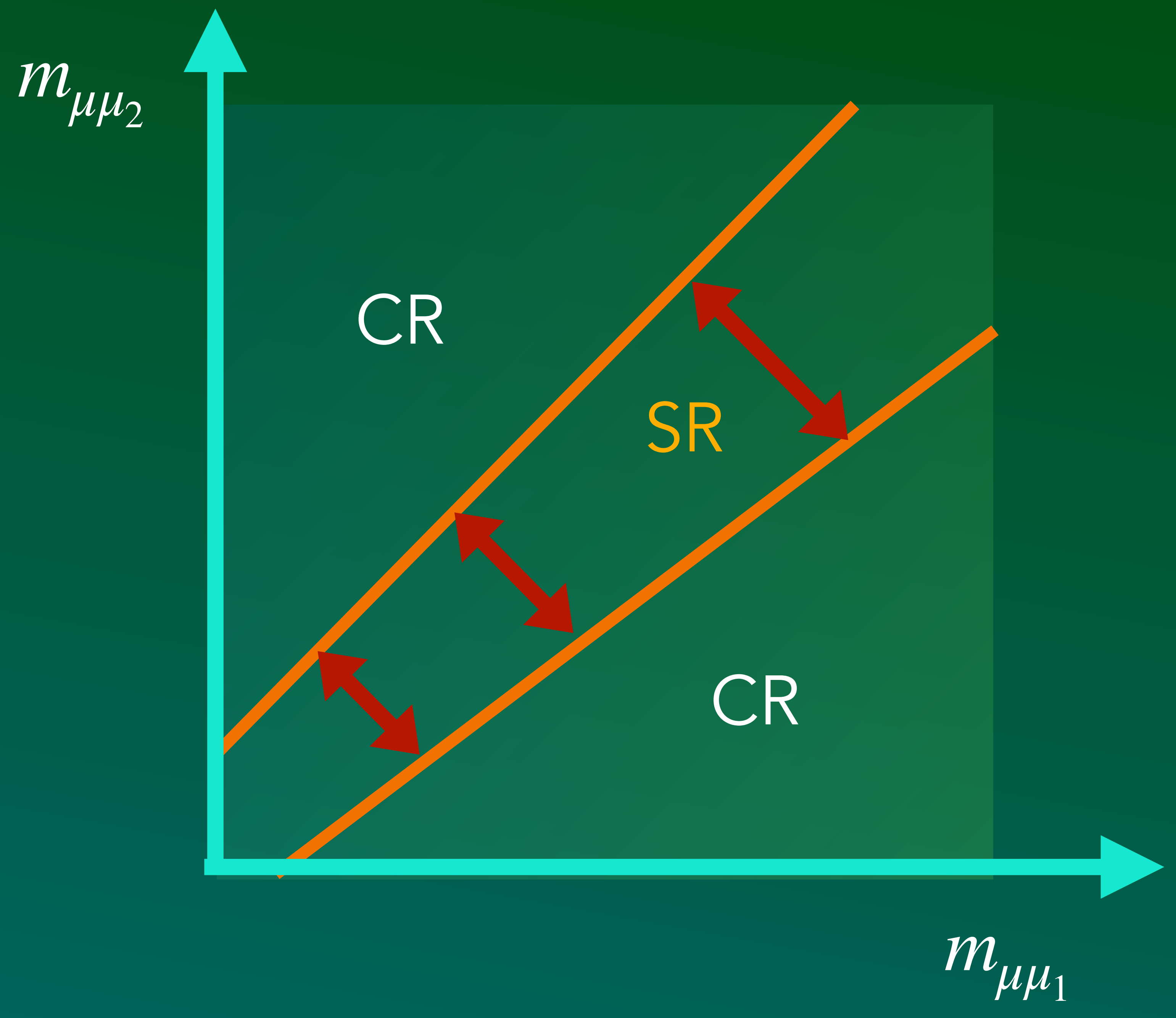

For more on mass window cut see App. E

Model-Indepence Performance

Generator v.s. Reco Efficiency

- Model independent ratio: $\epsilon_{Full}/\alpha_{Gen}$
  - α_{Gen} : generator level acceptance
    - 4 gen-muons p_T and η selection + fiducial cuts
  - ϵ_{Full}: full analysis efficiency
    - 4 reco-muons p_T and η selection + fiducial cuts+ full selection
- Constant $\epsilon_{Full}/\alpha_{Gen}$ indicates that the model performance is independent of its parameters
- Average $\epsilon_{Full}/\alpha_{Gen}$ = 0.418, is consistent with other benchmark models in the analysis

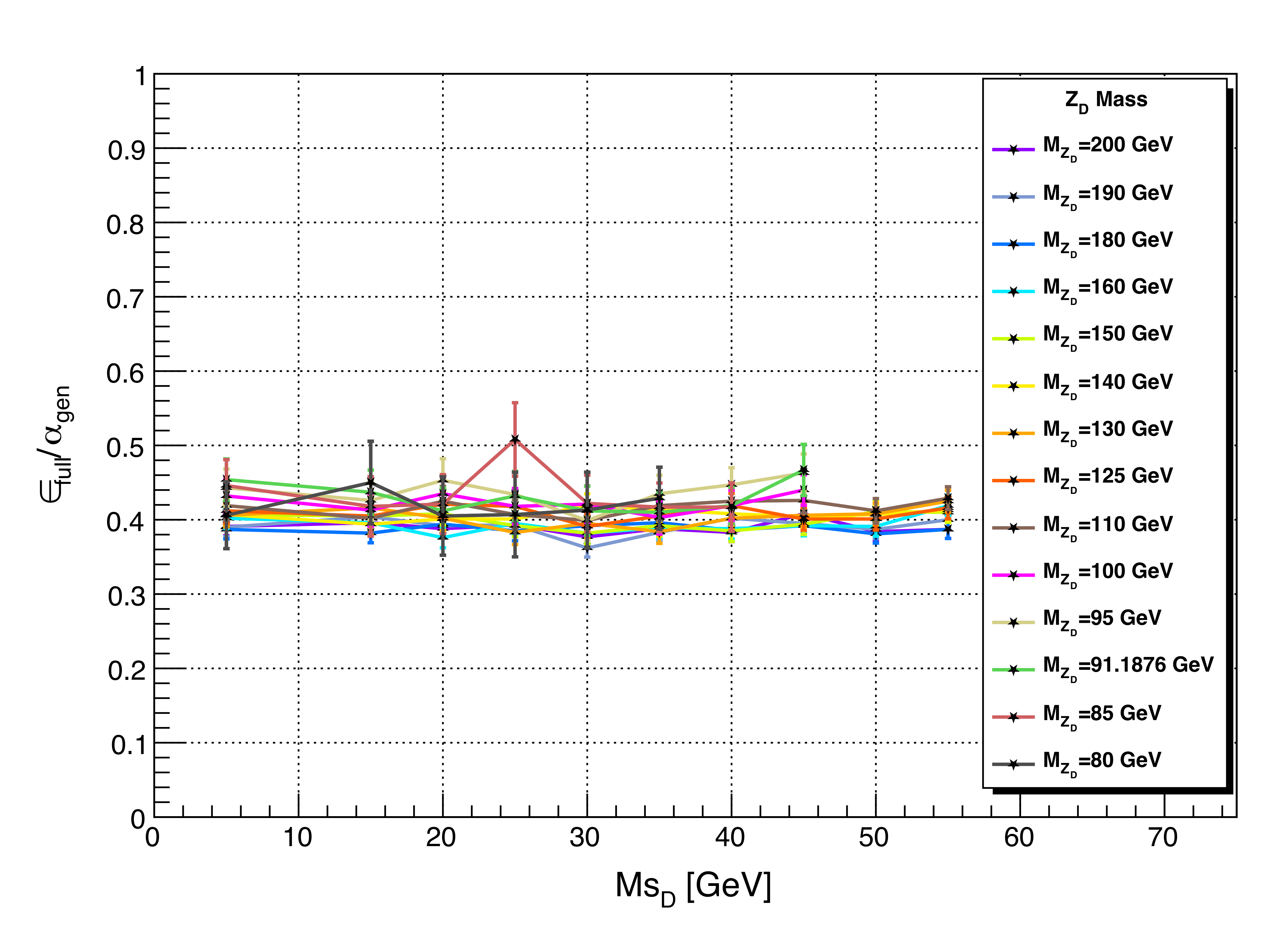

Figure4: Total selection efficiency over generator level selection acceptance, $\epsilon_{Full}/\alpha_{gen}$ as a function of the s_D mass for various Z_D masses in the vector portal model. The KM parameter, ε, is 10^{-2}.

Layout

1. Experimental Apparatus
2. Construction & Quality Control of GEM Detectors
3. Dark Matter Problem
4. Model-independent Search
5. Samples & Selection
6. Background Estimation

Background Estimation

Below Upsilon (Υ) Resonances (0.25-9 GeV)

- Dominated by QCD multi-jet processes, especially contributions from $b\bar{b}$
- Double semi-leptonic decay or decay via resonances ($\eta, \omega, \phi, J/\psi(1S), \psi(2S)$)
- Data driven (2018 DoubleMuon): because, MC for QCD processes are limited
- Construct 2D background templates, based on 1D MC distributions and fitting them -> $f(m_{\mu\mu_1}) \otimes f(m_{\mu\mu_2})$. (See **App. B**)
- Estimate the number of background events in the signal region

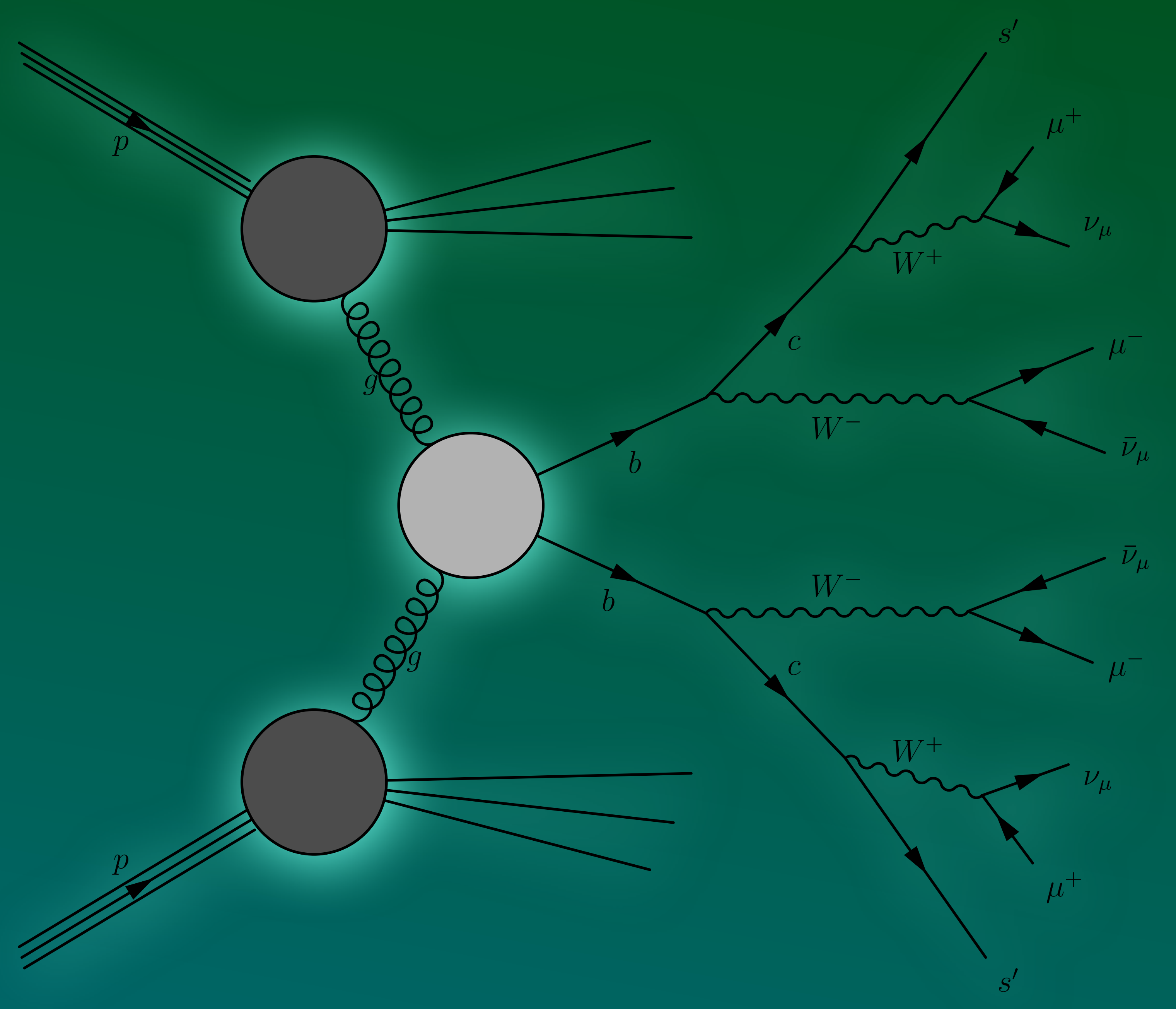

Figure5: Double semi-leptonic $b\bar{b}$ decays

Background Estimation

Below Upsilon (ϒ) Resonances (0.25-9 GeV)

- Dominated by QCD multi-jet processes, especially contributions from $b\bar{b}$

- Double semi-leptonic decay or decay via resonances $(\eta, \omega, \phi, J/\psi(1S), \psi(2S))$

- Data driven (2018 DoubleMuon): because, MC for QCD processes are limited

- Construct 2D background templates, based on 1D MC distributions and fitting them -> $f(m_{\mu\mu_1}) \otimes f(m_{\mu\mu_2})$. (See **App. B**)

- Estimate the number of background events in the signal region

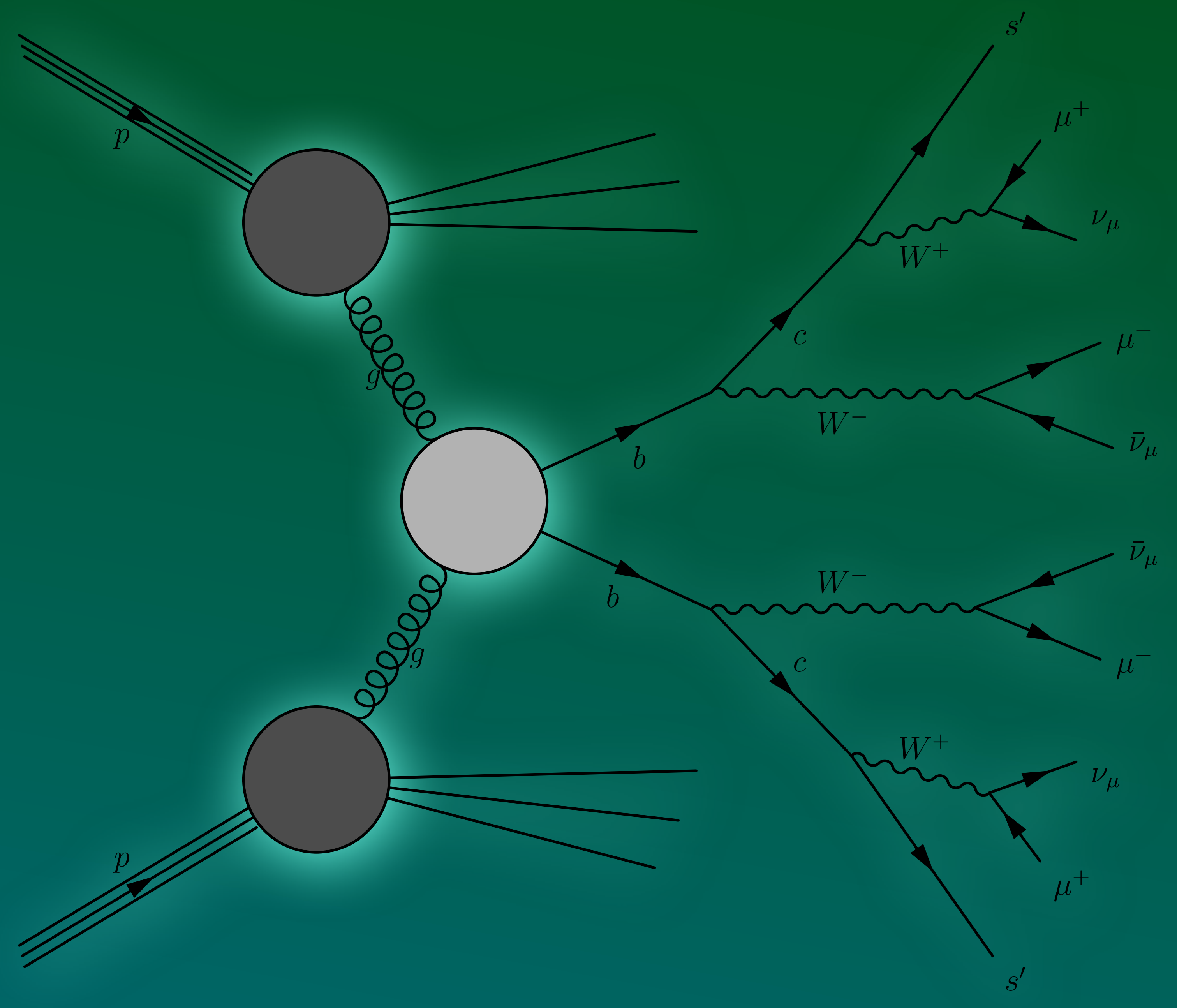

Figure5: Double semi-leptonic $b\bar{b}$ decays

Background Estimation

Below Upsilon (ϒ) Resonances (0.25-9 GeV)

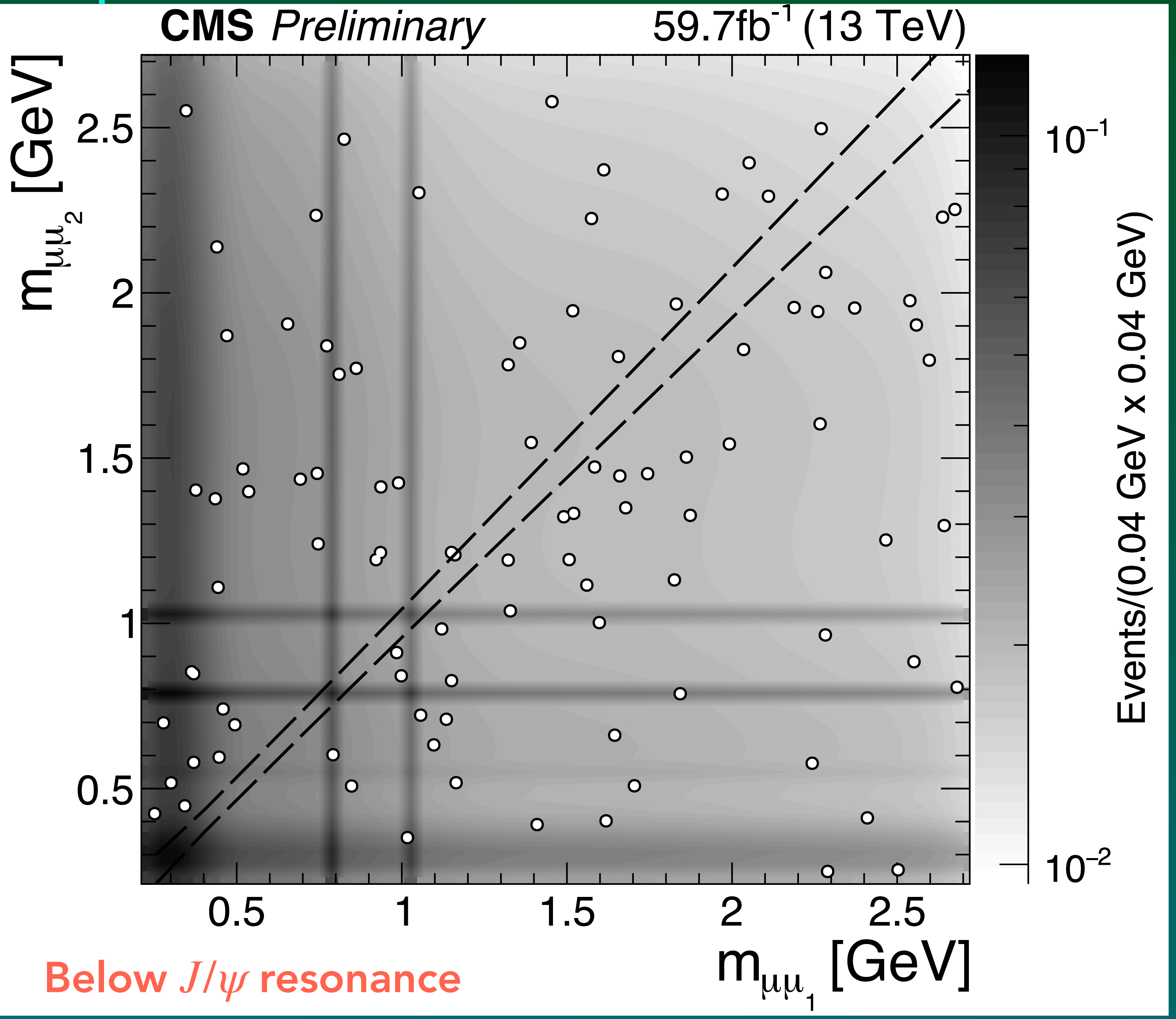

Figure6: 2D QCD background template + data at the CR

- 2D template integral SR/CR = 0.043/0.969
- 2-dimu events at CR: 98 (**SR remain blinded**)
- Estimated BKG events at SR: **4.34 +/- 0.44** (stat.)

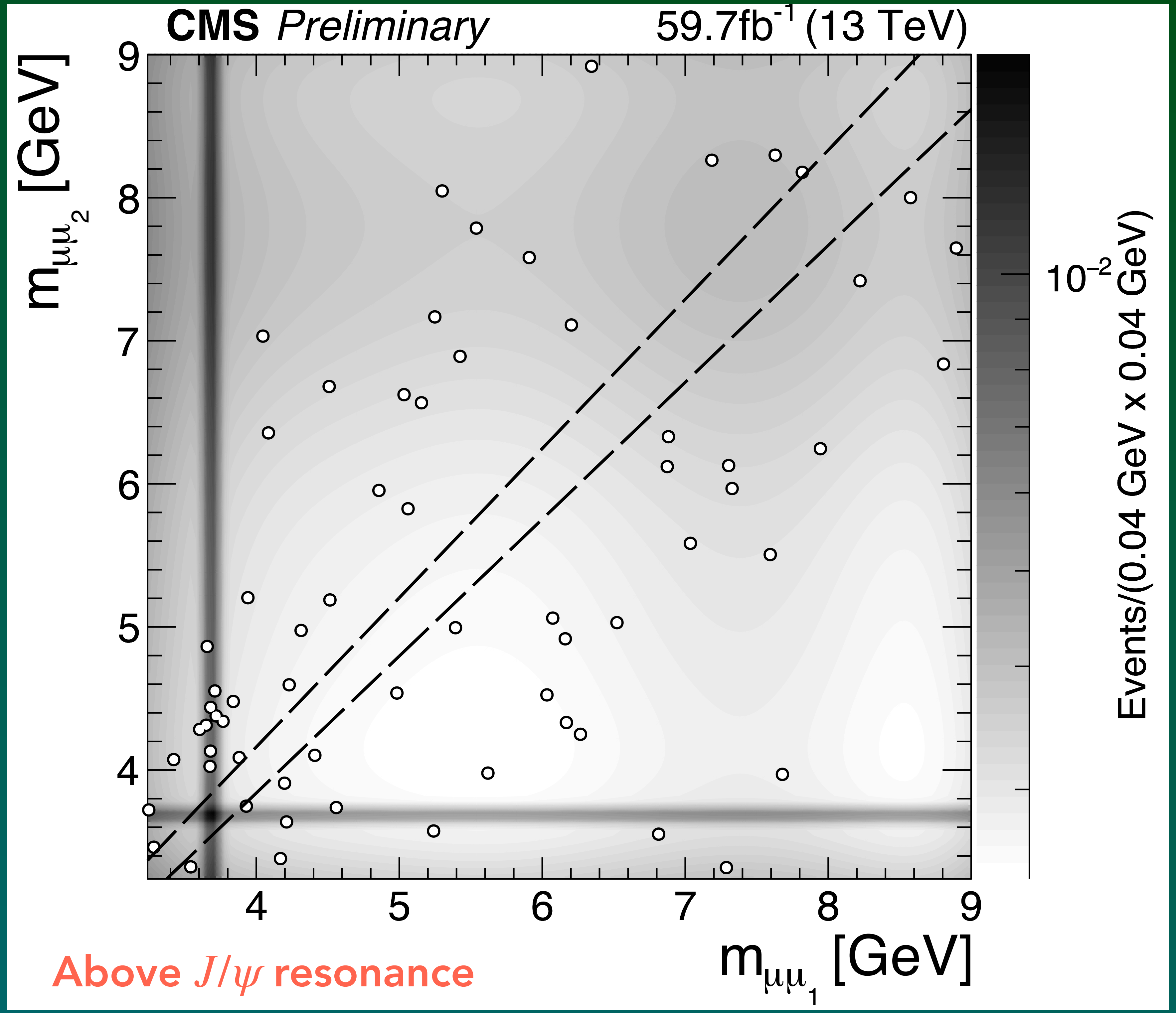

Figure7: 2D QCD background template + data at the CR

- 2D template integral SR/CR = 0.035/0.965
- 2-dimu events at CR: 66 (**SR remain blinded**)
- Estimated BKG events at SR: **6.16 +/- 0.76** (stat.)

Background Estimation

Above Upsilon (ϒ) Resonances (11-60 GeV)

- QED radiated high-energy photons produces muon pairs, each muon is then paired with Drell-Yan (DY) single muons which mimics our di-muon signal
- Reject the events with QED background
- Alternative pairing: pair the QED radiated muon with the DY muon
- Reject the event if:
  - Alternative pairing trailing mass < 3 GeV
  - Alternative pairing trailing $\Delta R < 0.2$

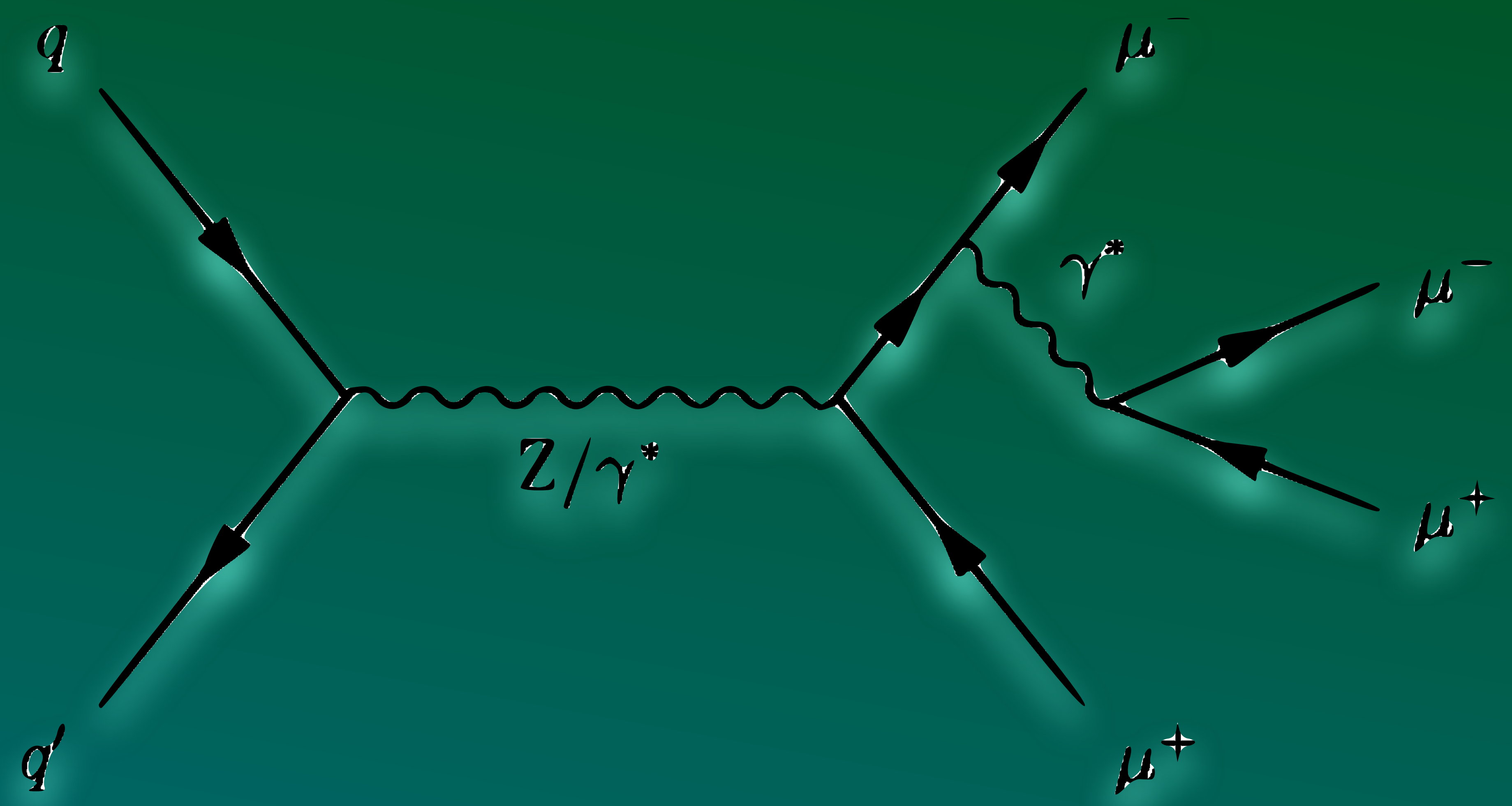

Figure8: The Feynman diagram for QED radiation in DY process. The pairing of the muon decaying in the DY with muon decaying from the QED radiation mimics our signal

Background Estimation

Above Upsilon (ϒ) Resonances (11-60 GeV)

- QED radiated high-energy photons produces muon pairs, each muon is then paired with Drell-Yan (DY) single muons which mimics our di-muon signal
- Reject the events with QED background
- Alternative pairing: pair the QED radiated muon with the DY muon
- Reject the event if:
    - Alternative pairing trailing mass < 3 GeV
    - Alternative pairing trailing $\Delta R < 0.2$

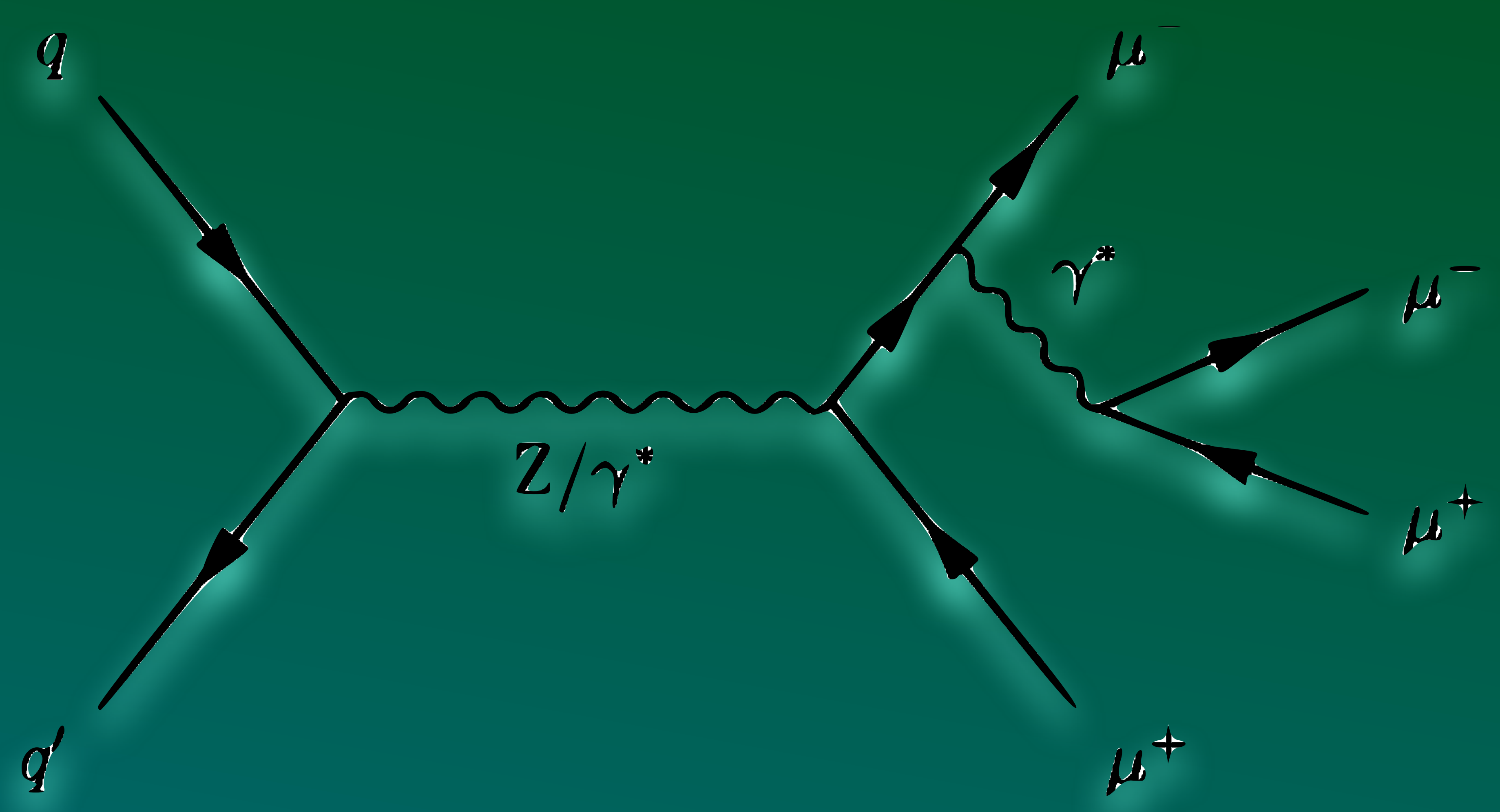

Figure8: The Feynman diagram for QED radiation in DY process. The pairing of the muon decaying in the DY with muon decaying from the QED radiation mimics our signal

Background Estimation

Above Upsilon (ϒ) Resonances (11-60 GeV) - Control Region

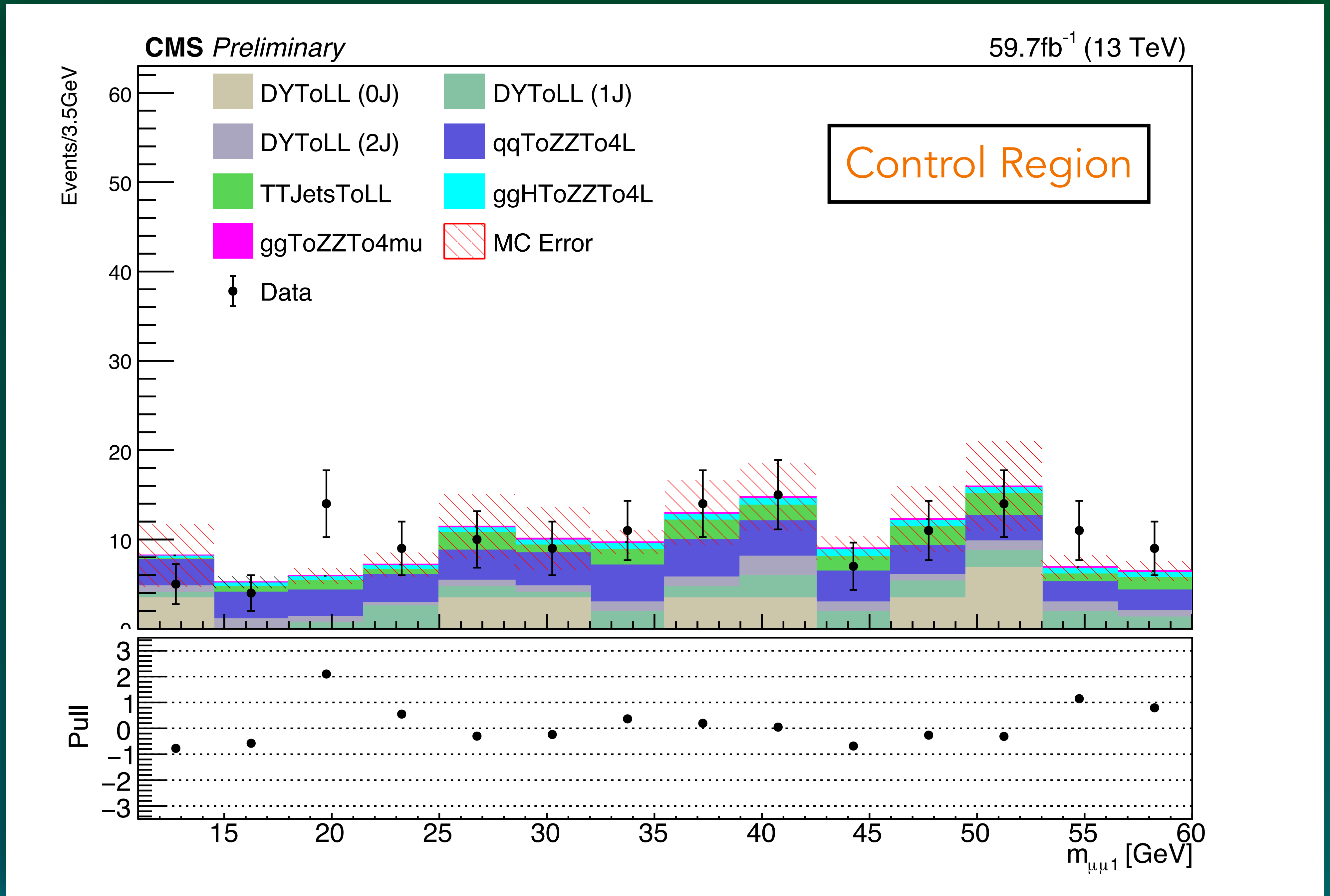

Figure9: MC simulation compared with the data in control region for muon pair 1.

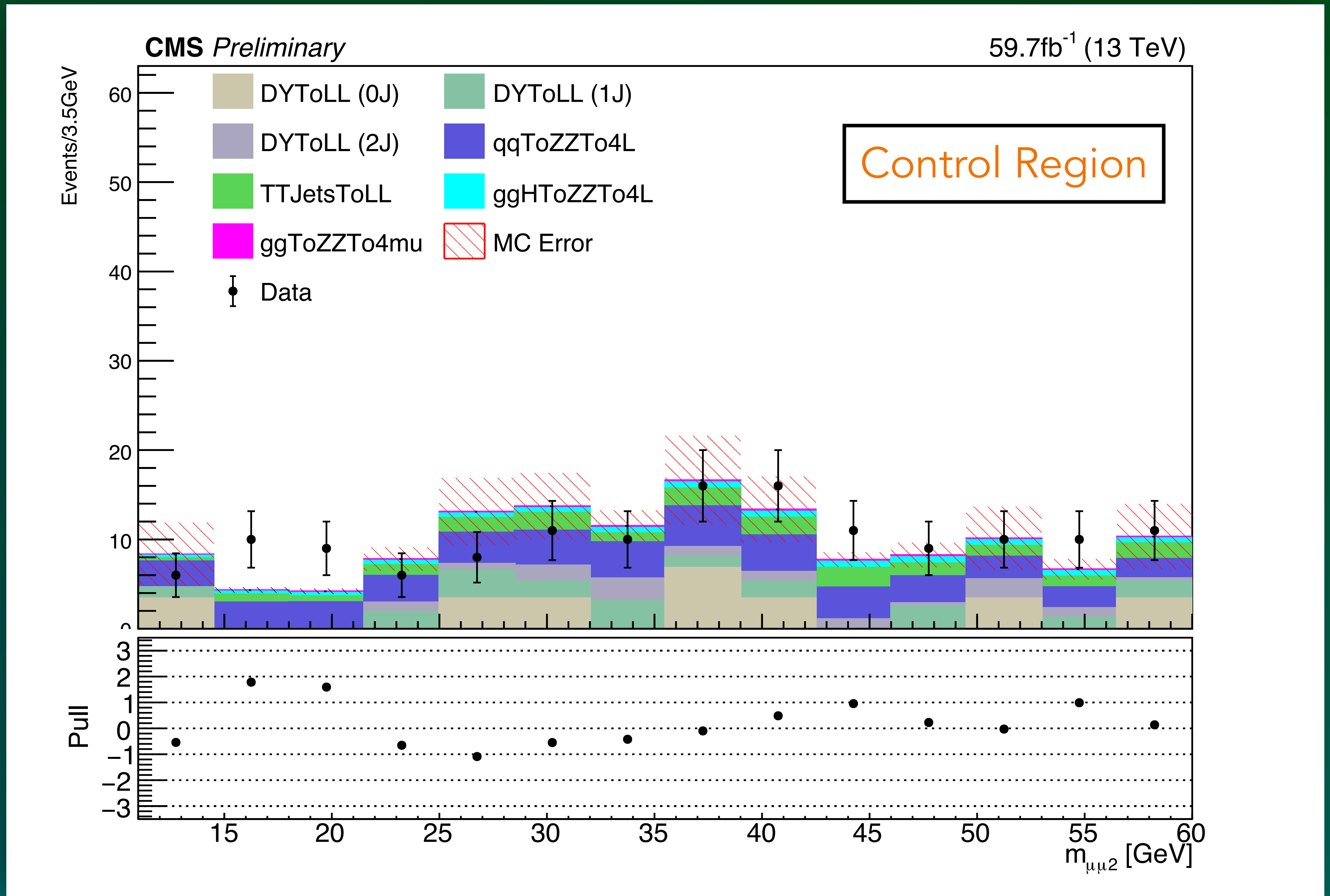

Figure10: MC simulation compared with the data in control region for muon pair 2.

Background Estimation

Above Upsilon (ϒ) Resonances (11-60 GeV) - Control Region

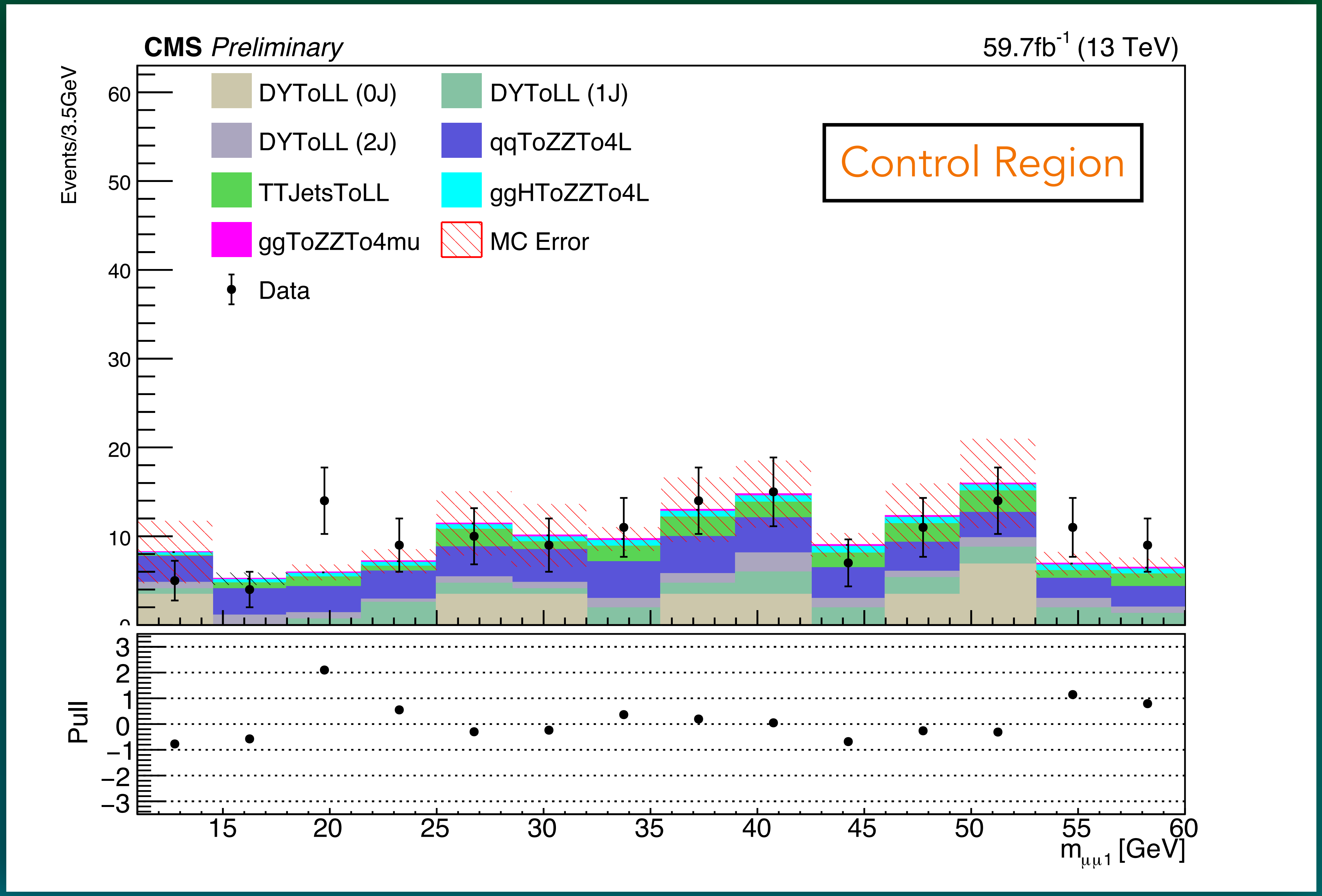

Figure9: MC simulation compared with the data in control region for muon pair 1.

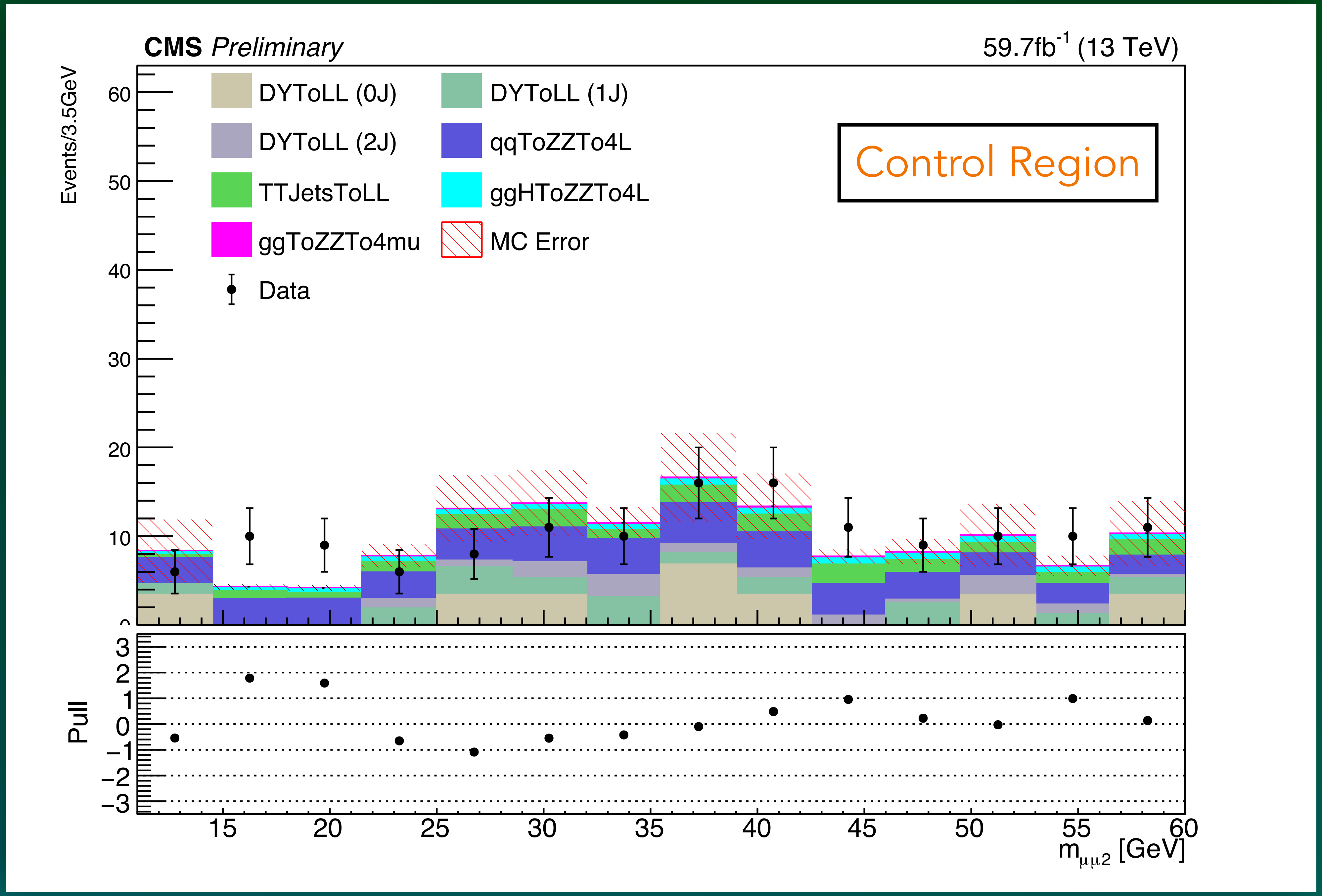

Figure10: MC simulation compared with the data in control region for muon pair 2.

Good agreement between data and MC in control region

$$\frac{data}{MC} = 1.05 \pm 0.12$$

Background Estimation

Above Upsilon (ϒ) Resonances (11-60 GeV) - Signal Region

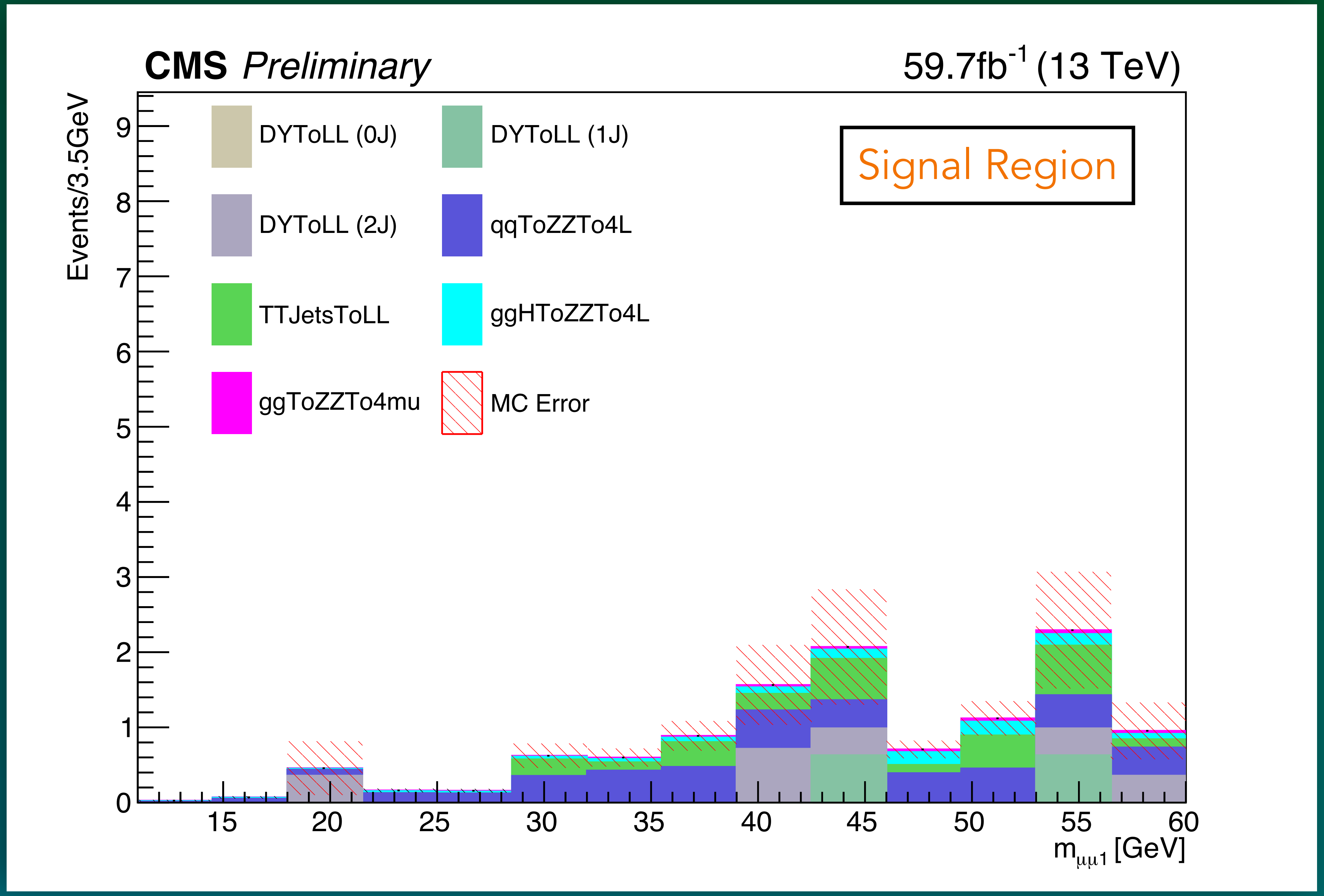

Fig11: MC simulation in signal region for muon pair 1.

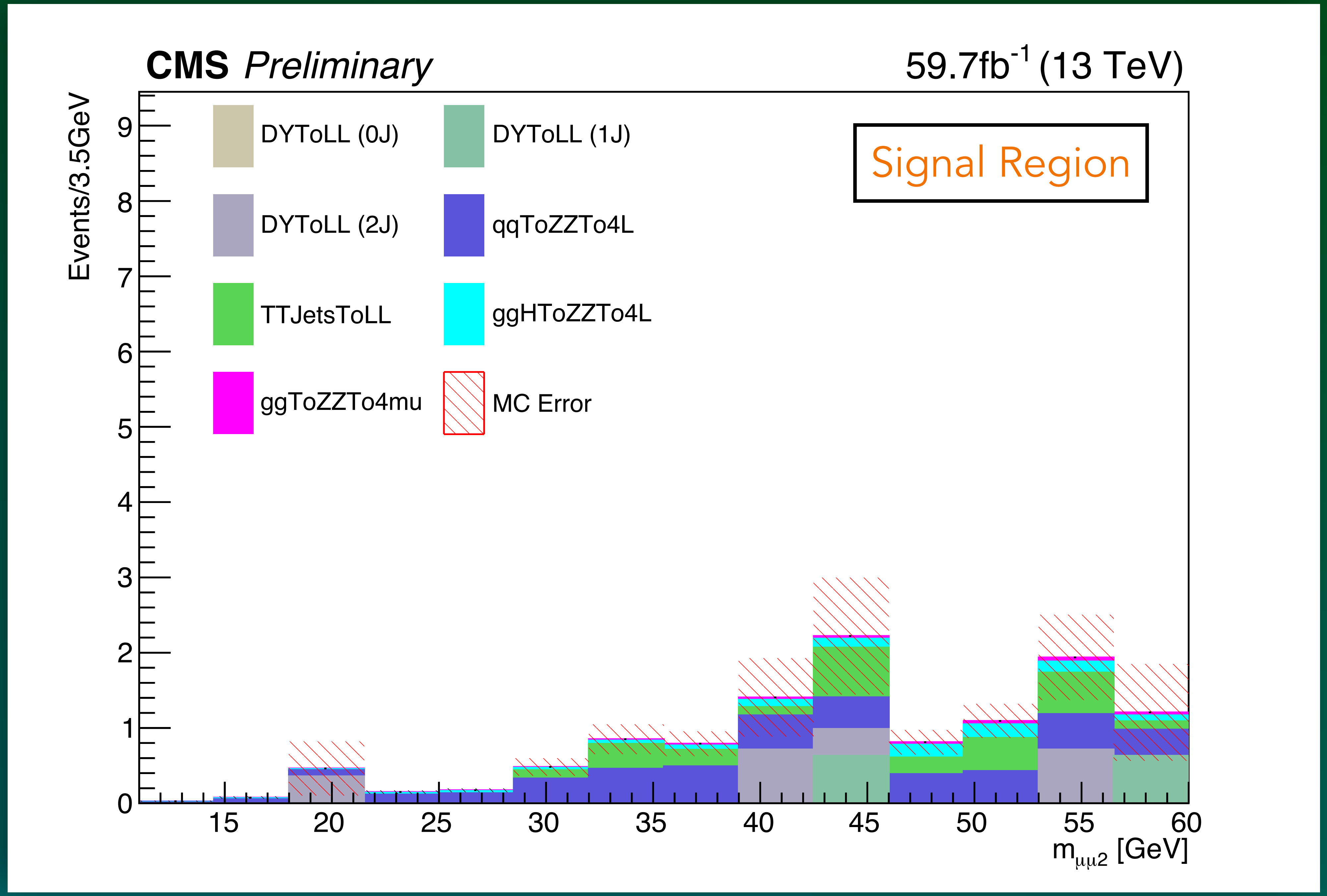

Fig12: MC simulation in signal region for muon pair 2.

Background Estimation

Above Upsilon (ϒ) Resonances (11-60 GeV) - Signal Region

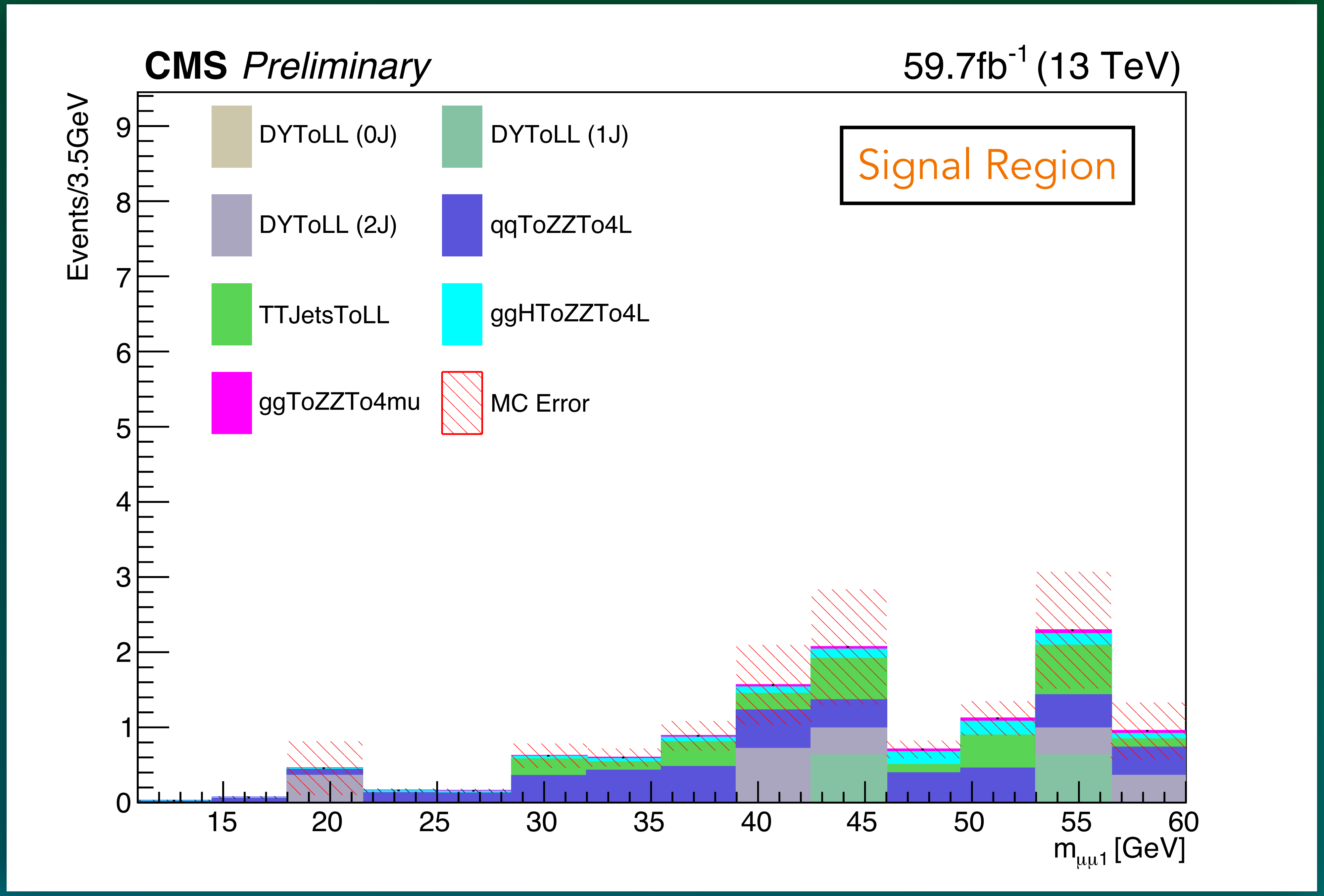

Fig11: MC simulation in signal region for muon pair 1.

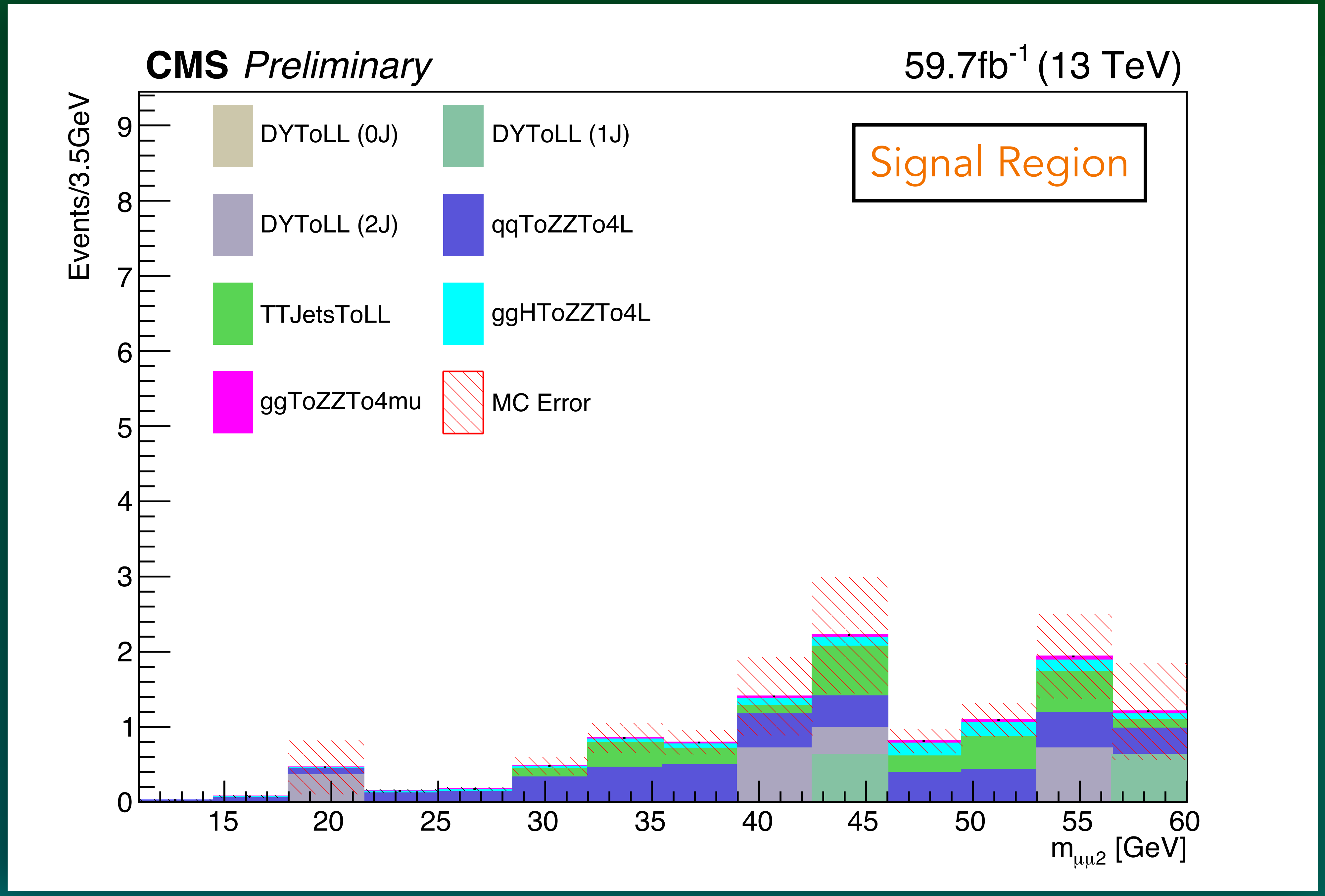

Fig12: MC simulation in signal region for muon pair 2.

Smooth background shape in the SR is obtained via adaptive Kernel Density Estimation (KDE). See **App. C**

Estimated number of background events in the SR

$$SR : 12.28 \pm 2.01$$

Layout

1. Experimental Apparatus
2. Construction & Quality Control of GEM Detectors
3. Dark Matter Problem
4. Model-independent Search
5. Samples & Selection
6. Background Estimation
7. Expected Limits

Expected Limits

Expected Limit on Kinetic Mixing parameter

- Close to zero background analysis: expected 95% CL upper limit is ~3 events at each mass point
  - $\sigma(pp \to Z_D)\mathscr{B}(Z_D \to s_D\overline{s_D})\mathscr{B}^2(s_D \to \mu^+\mu^-) \times \alpha_{gen} \leq \dfrac{N_{\mu\mu}}{L \times r}$
  - $N_{\mu\mu}$: 95% CL upper limit on the number of events
  - $\mathscr{L} = 59.7\ fb^{-1},\ \ r = SF_{\epsilon_{Full}} \times \epsilon^{MC}_{Full}/\alpha_{Gen}$

HLT SF calculation: **App.F**

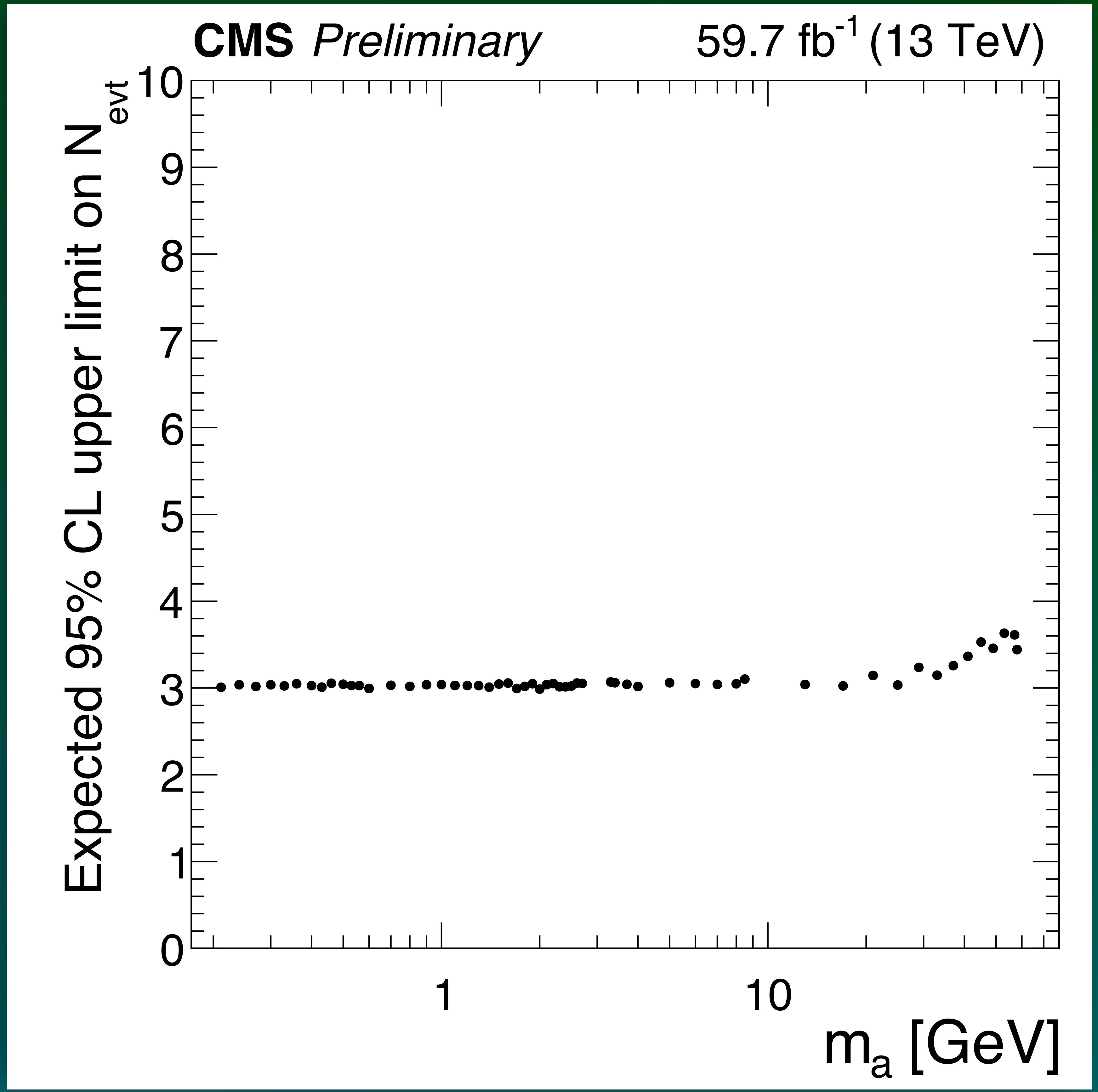

Figure13A: 95% upper limit on expected number of events

Expected Limits

Expected Limit on Kinetic Mixing parameter

- Close to zero background analysis: expected 95% CL upper limit is ~3 events at each mass point
  - $\sigma(pp \to Z_D)\mathscr{B}(Z_D \to s_D\overline{s_D})\mathscr{B}^2(s_D \to \mu^+\mu^-) \times \alpha_{gen} \leq \frac{N_{\mu\mu}}{L \times r}$
  - $N_{\mu\mu}$: 95% CL upper limit on the number of events
  - $\mathscr{L} = 59.7\ fb^{-1}$, $r = SF_{\epsilon_{Full}} \times \epsilon^{MC}_{Full}/\alpha_{Gen}$

HLT SF calculation: **App.F**

- By translating the production cross-section to ϵ^2, we set 95% CL limit on

$$\varepsilon^2\mathscr{B}(Z_D \to s_D\overline{s_D})\mathscr{B}^2(s_D \to \mu^+\mu^-)$$

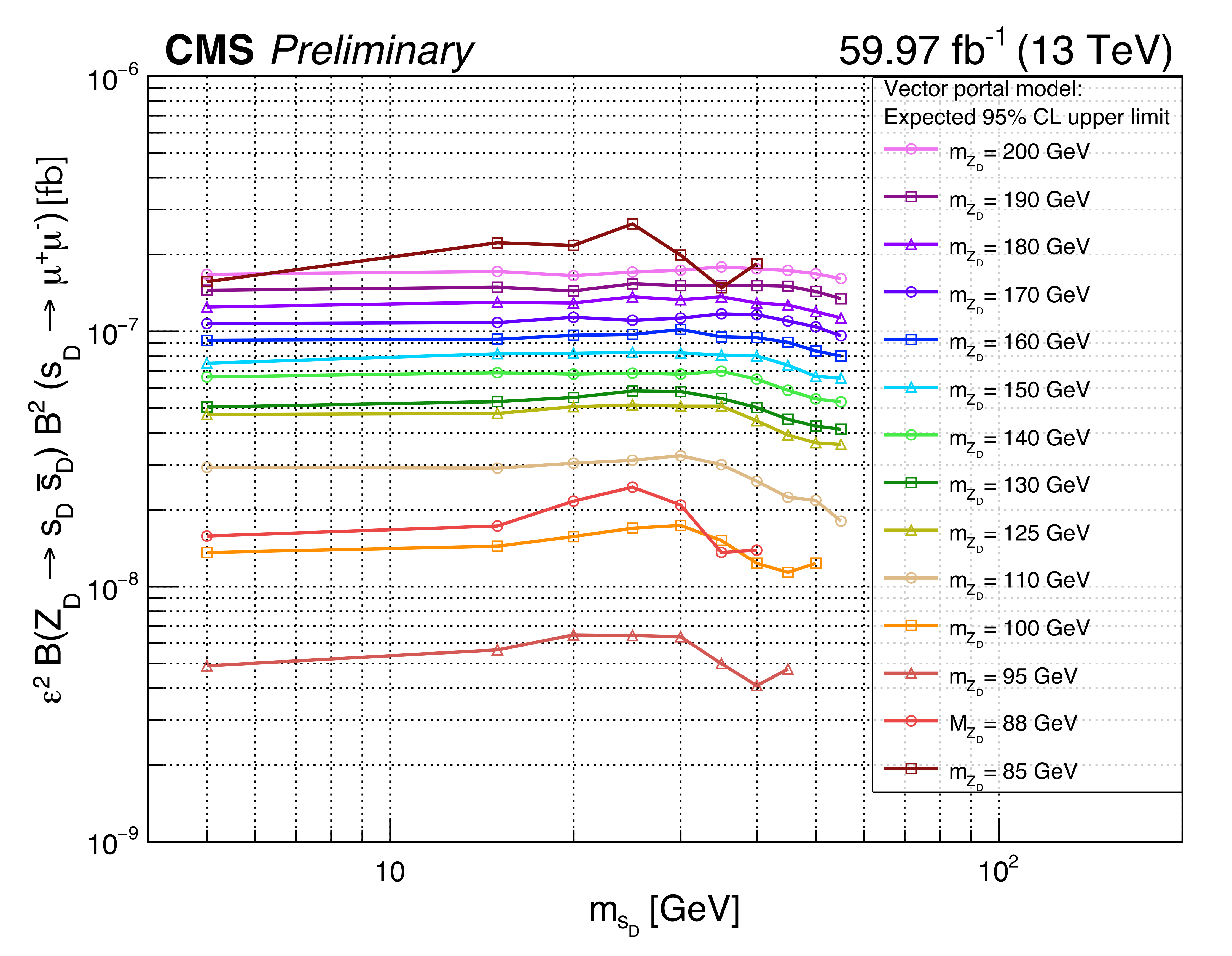

Figure13B: The expected 95% CL upper limits function of the dark scalar mass m_{s_D} and the dark vector boson mass m_{Z_D}

Expected Limits

Expected Limit on Kinetic Mixing parameter

- Close to zero background analysis: expected 95% CL upper limit is ~3 events at each mass point
  - $\sigma(pp \to Z_D)\mathscr{B}(Z_D \to s_D\overline{s_D})\mathscr{B}^2(s_D \to \mu^+\mu^-) \times \alpha_{gen} \leq \frac{N_{\mu\mu}}{L \times r}$
  - $N_{\mu\mu}$: 95% CL upper limit on the number of events
  - $\mathscr{L} = 59.7\ fb^{-1},\ r = SF_{\epsilon_{Full}} \times \epsilon^{MC}_{Full}/\alpha_{Gen}$ HLT SF calculation: **App.F**
- By translating the production cross-section to ϵ^2, we set 95% CL limit on

$$\varepsilon^2\mathscr{B}(Z_D \to s_D\overline{s_D})\mathscr{B}^2(s_D \to \mu^+\mu^-)$$

- The limit curves exhibit a structure with an increase and a dip as the s_D mass approaches the kinematic limit of $m_{Z_D}/2$.

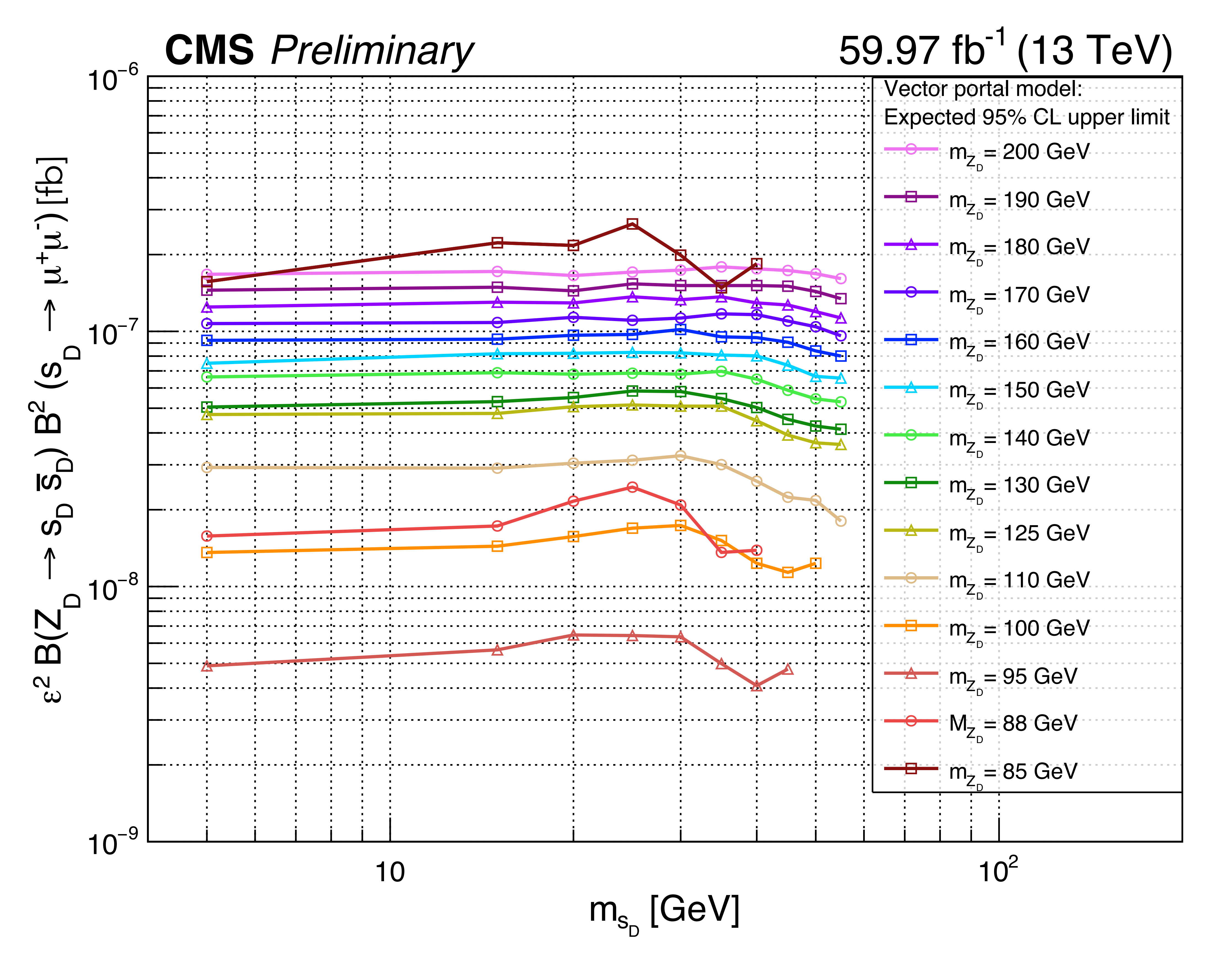

Figure13B: The expected 95% CL upper limits function of the dark scalar mass m_{s_D} and the dark vector boson mass m_{Z_D}

Layout

1. Experimental Apparatus
2. Construction & Quality Control of GEM Detectors
3. Dark Matter Problem
4. Model-independent Search
5. Samples & Selection
6. Background Estimation
7. Expected Limits
8. Results

Unbinding The Signal Region

Below Below Upsilon (ϒ) Background

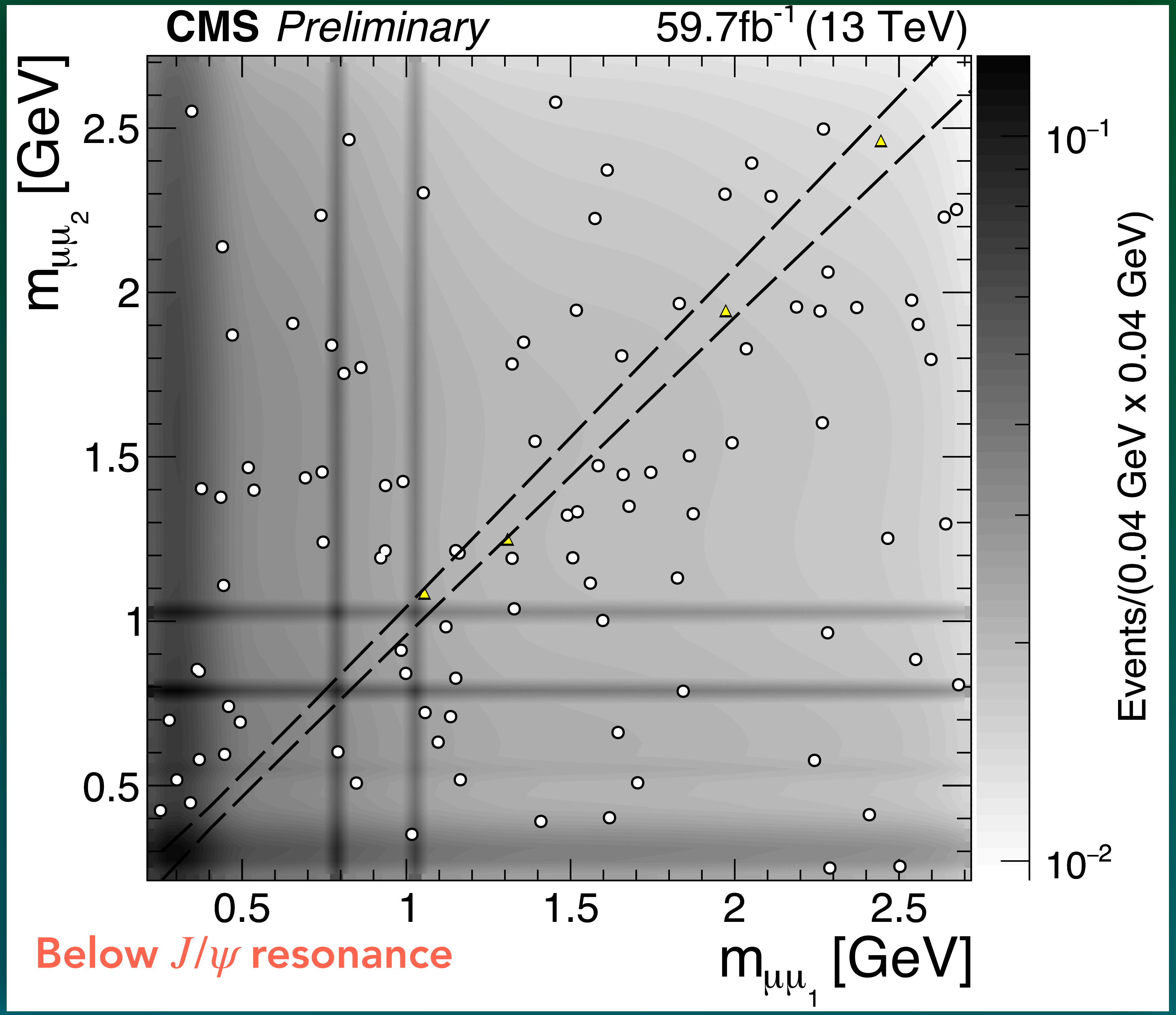

Figure14: 2D QCD background at SR

- Estimated Background events at SR:

$$4.34 \pm 0.44(stat.) \pm 0.18(sys.)$$

- Observed: 4 events

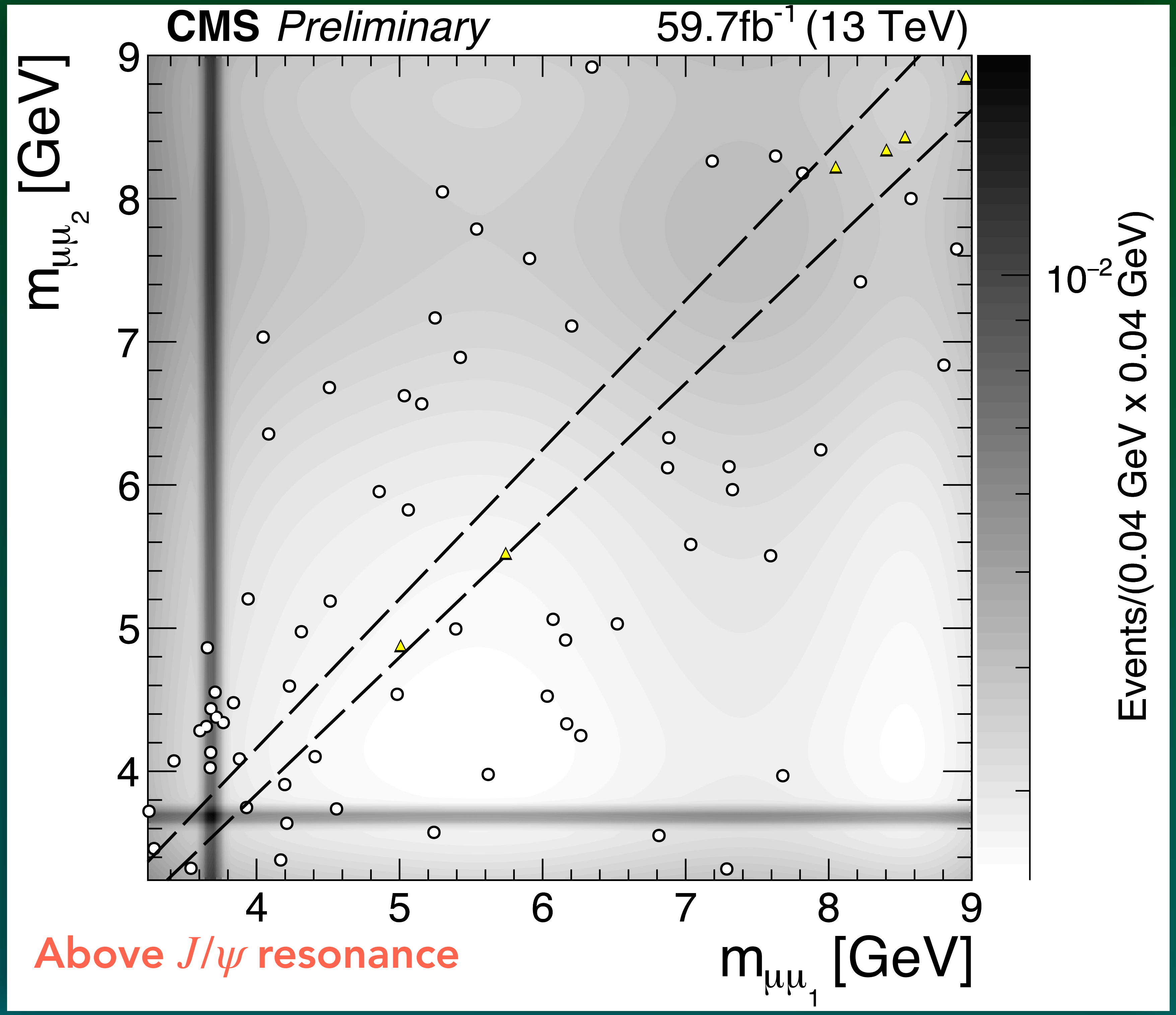

Figure15: 2D QCD background at SR

- Estimated Background events at SR:

$$6.16 \pm 0.76(stat.) \pm 0.09(sys.)$$

- Observed: 6 events

Unblinding The Signal Region

Above Upsilon (ϒ) Background

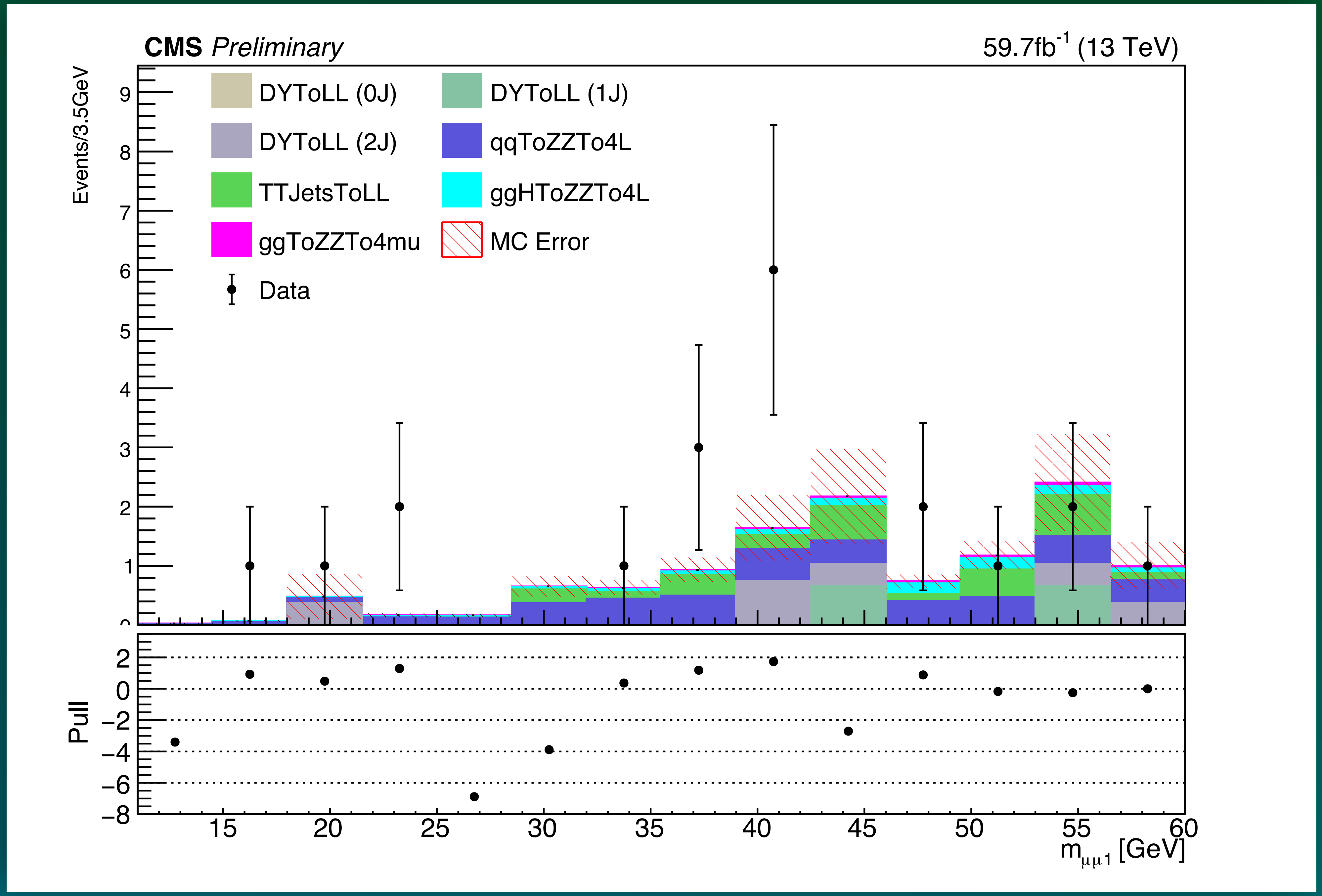

Figure16: MC simulation compared with observed data at SR

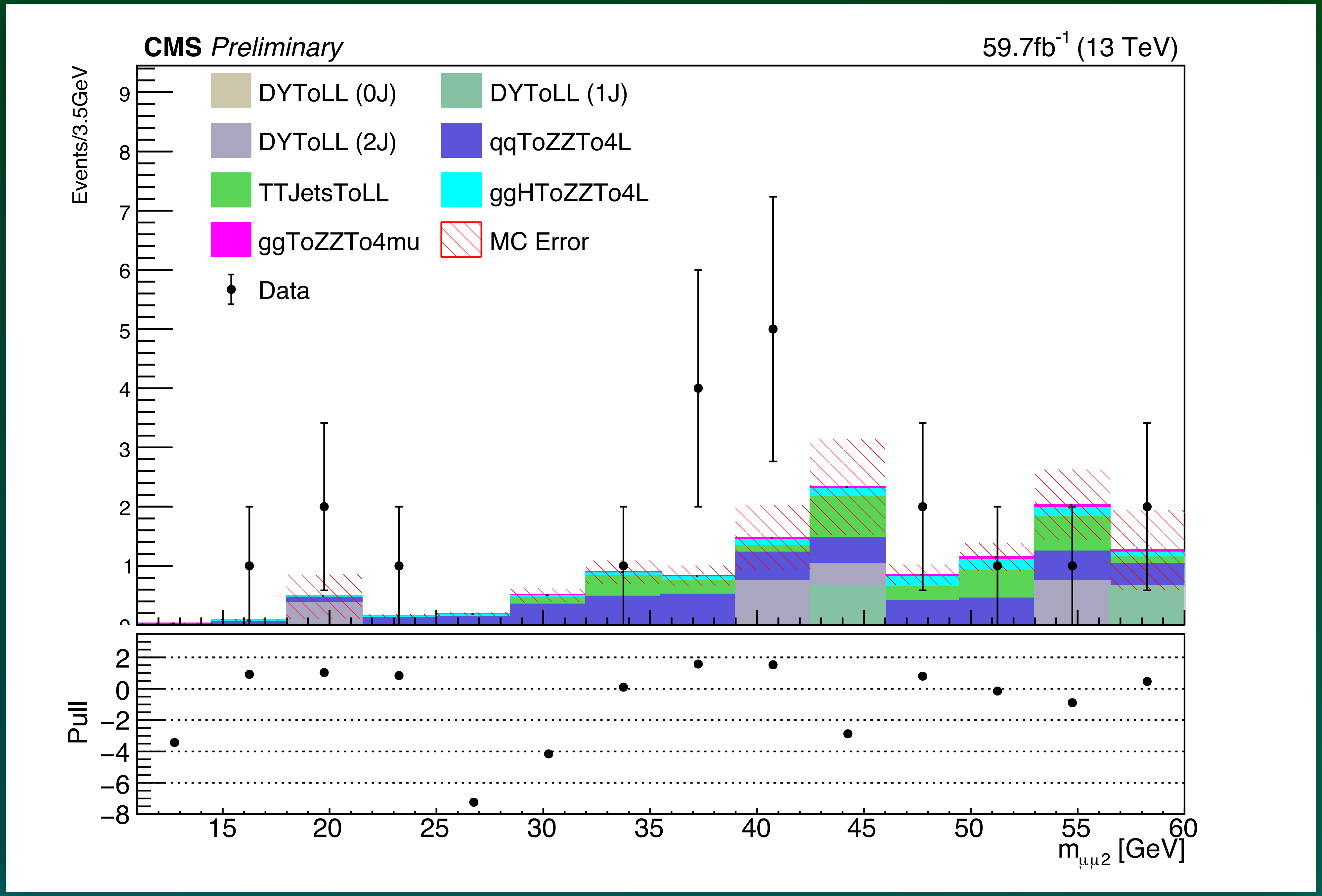

Figure17: MC simulation compared with observed data at SR

Estimated number of background events in the SR

$SR : 12.28 \pm 2.01$

Observed: 20 events

Unblinding The Signal Region

Below Upsilon (Υ) Background

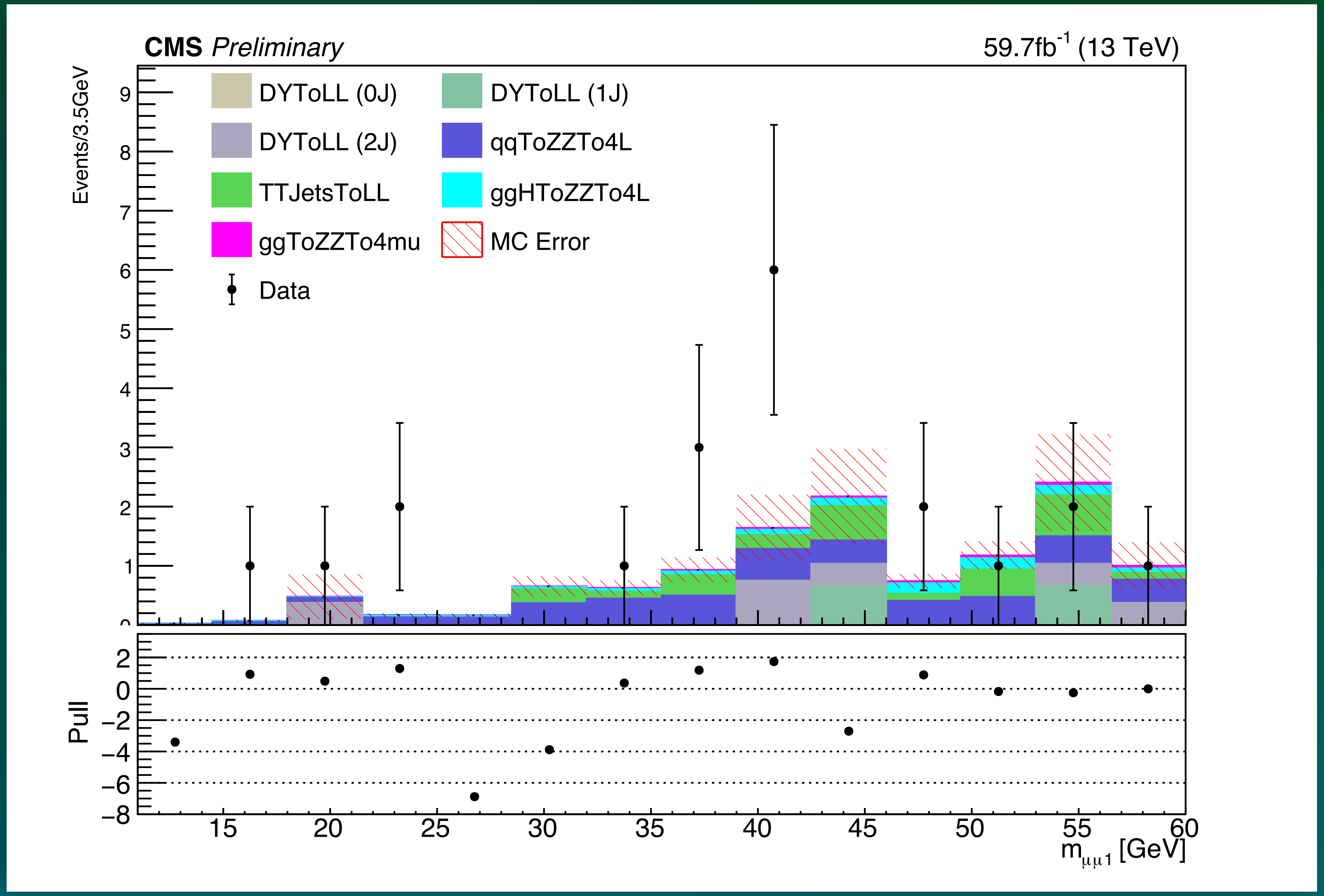

Figure16: MC simulation compared with observed data at SR

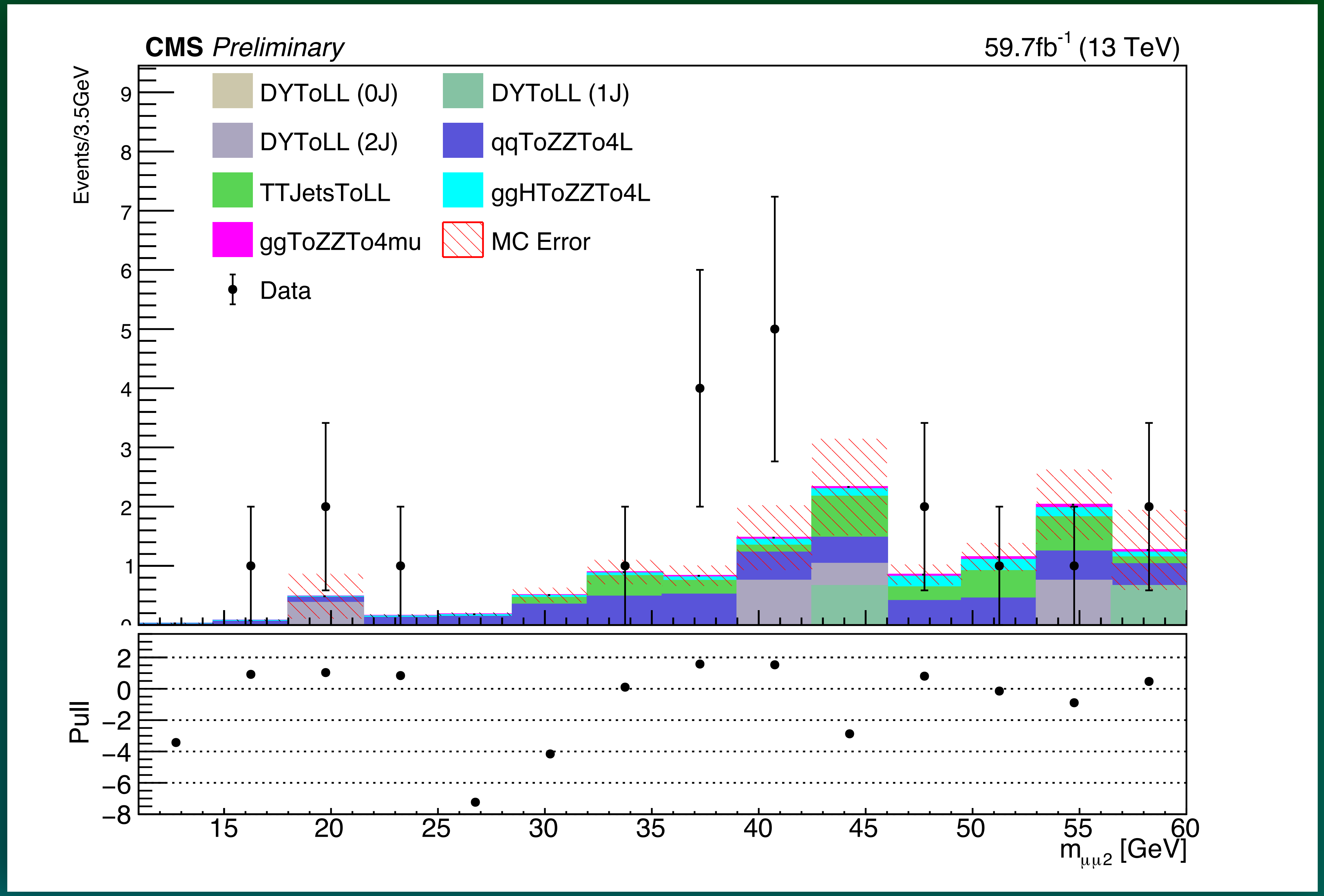

Figure17: MC simulation compared with observed data at SR

Estimated number of background events in the SR

$SR : 12.28 \pm 2.01$

Observed: 20 events

→ consistent with predicted background events, pulls within 2σ (only statistical errors considered)

Unblinding the Signal Region

Observed Limits

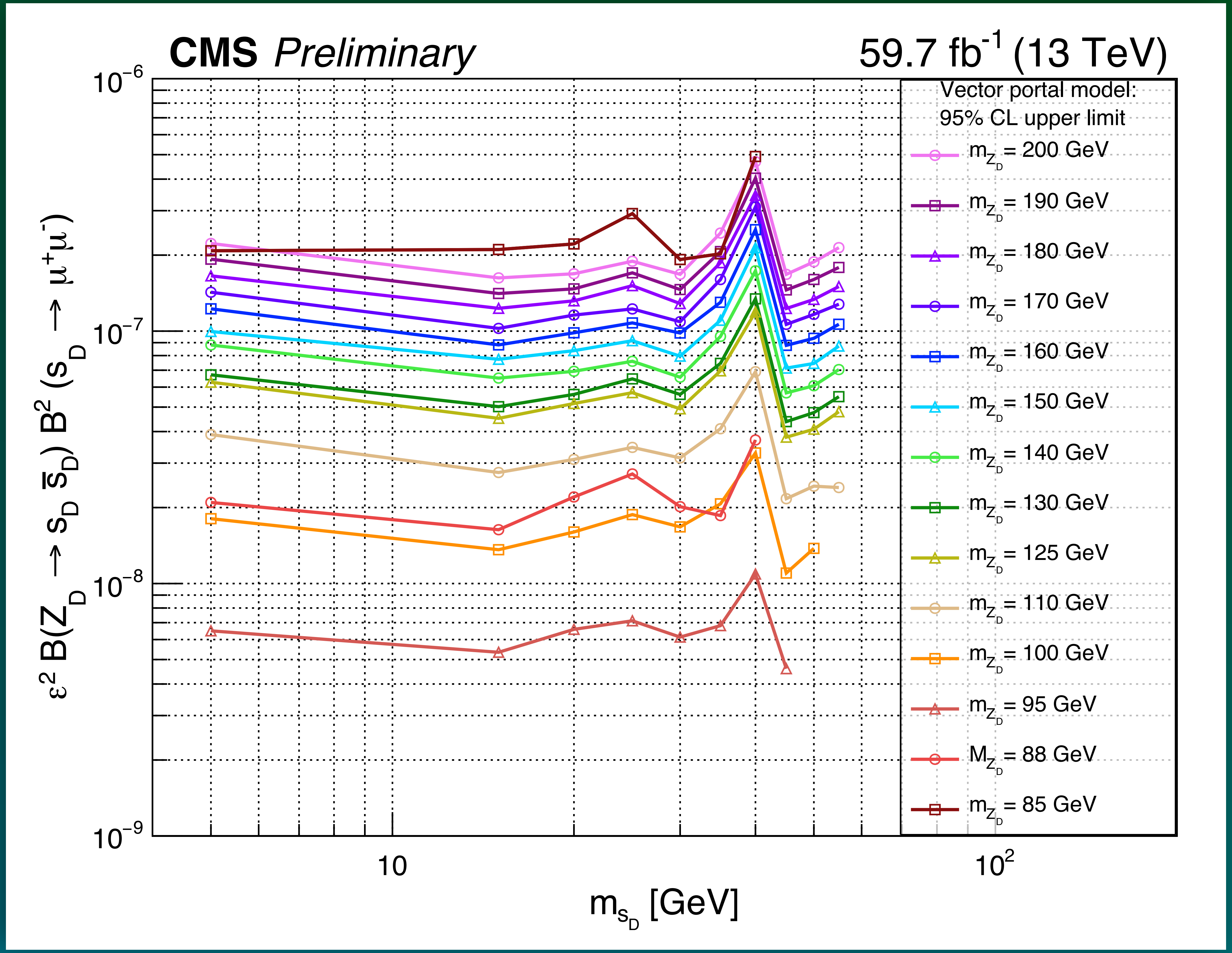

Figure18: Figure13: The observed 95% CL upper limits function of the dark scalar mass m_{s_D} and the dark vector boson mass m_{Z_D}

Unblinding the Signal Region

2018 Conclusion

- In 20-25 GeV region we observe 3 events
- The expected number of events in the said region is ~0.31
- Poisson probability for 0.31 fluctuating to 3 is 0.00364
- This could mean the background may not have been well modeled in this region
- This observation lead our research to explore the addition of **2017** CMS data to the our analysis

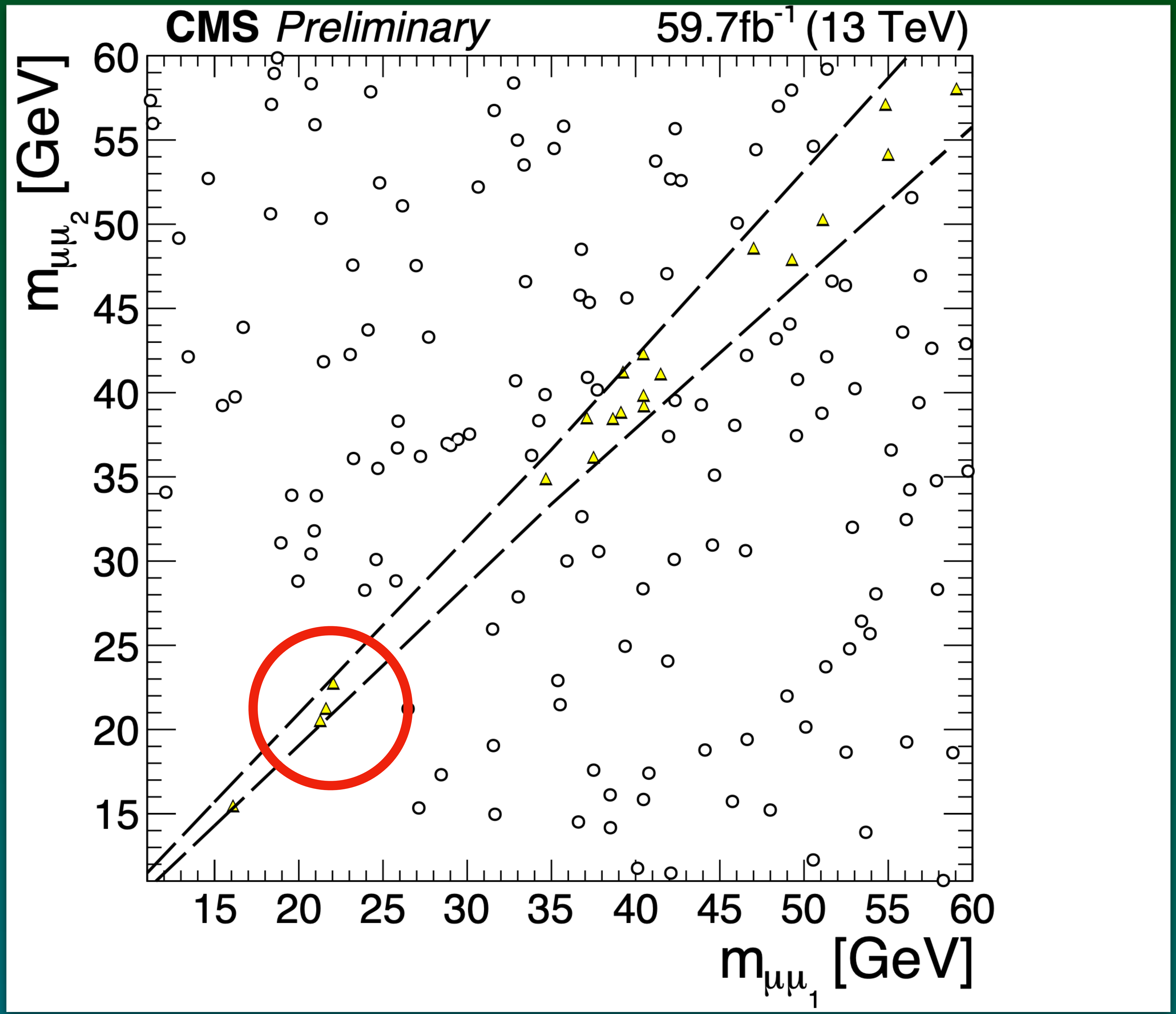

Figure32: Unblinded Signal Region above ϒ resonances

Unblinding the Signal Region

2018 Conclusion

- In 20-25 GeV region we observe 3 events
- The expected number of events in the said region is ~0.31
- Poisson probability for 0.31 fluctuating to 3 is 0.00364
- This could mean the background may not have been well modeled in this region
- This observation lead our research to explore the addition of **2017** CMS data to the our analysis

Brazilian plots: **App.G**

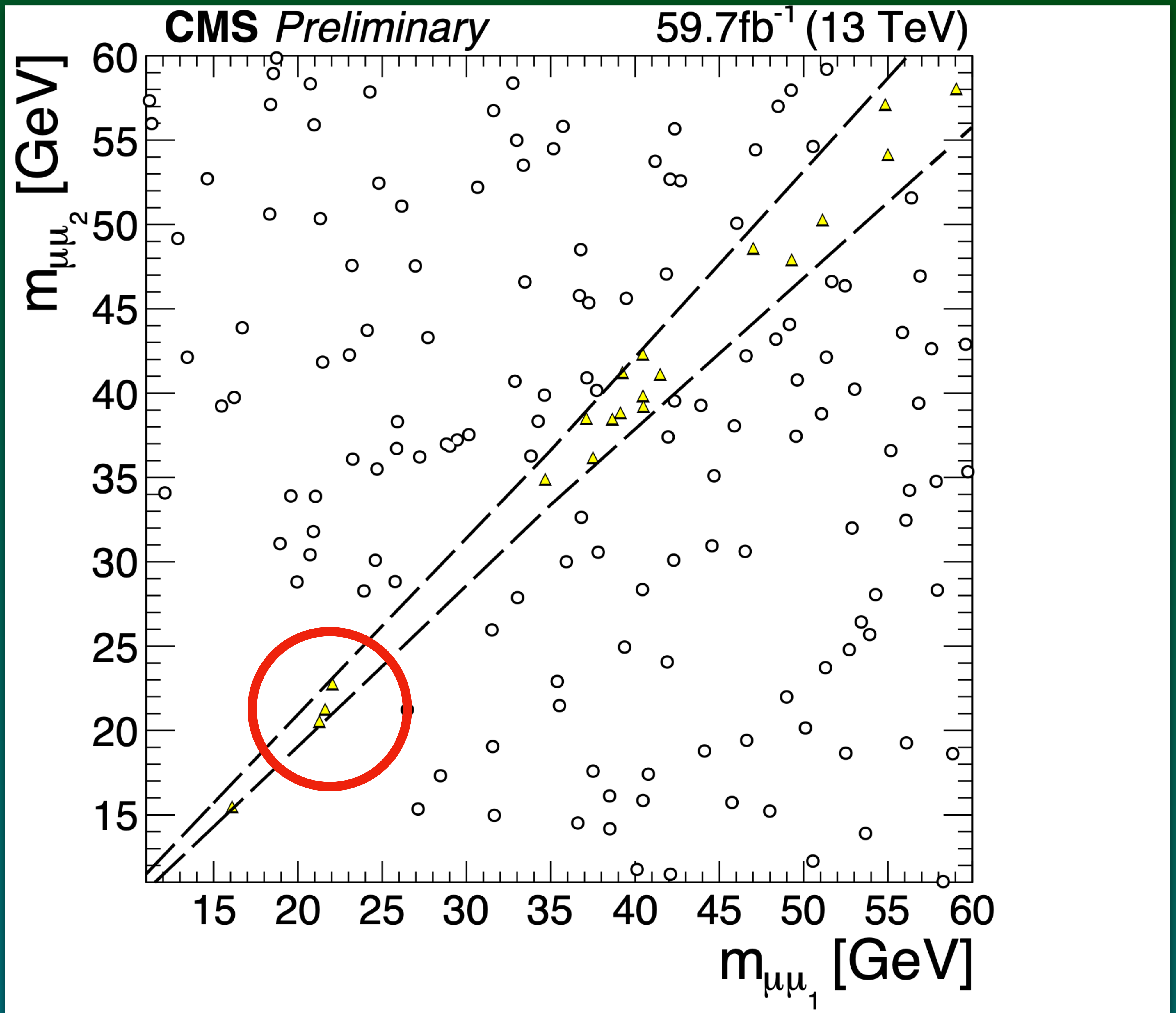

Figure32: Unblinded Signal Region above Υ resonances

Layout

1. Experimental Apparatus
2. Construction & Quality Control of GEM Detectors
3. Dark Matter Problem
4. Model-independent Search
5. Samples & Selection
6. Background Estimation
7. Expected Limits
8. Results
9. 2017 Analysis

2017 Analysis

Tigger Paths and Selections

Trigger Paths
HLT_Mu23_Mu12 **(HLT_DoubleL2Mu23NoVtx_2Cha in 2018)**
HLT_Mu18_Mu9_SameSign
HLT_TrkMu12_DoubleTrkMu5NoFiltersNoVtx
HLT_TripleMu_12_10_5

Muon selection
slimmedMuons in MiniAOD
4 PF Loose muon
Two muons: p_T >13 GeV, $|\eta|$ < 2
Four muons: p_T >8 GeV, $|\eta|$ < 2.4

2017 Data

Dataset Labels	Number of
/DoubleMuon/Run2017B-31Mar2018-v1/	14 501 767
/DoubleMuon/Run2017C-31Mar2018-v1/	49 636 525
/DoubleMuon/Run2017D-31Mar2018-v1/	23 075 733
/DoubleMuon/Run2017E-31Mar2018-v1/	51 589 091
/DoubleMuon/Run2017F-31Mar2018-v1/	79 756 560
Total	218 559 676

2017 Analysis

Model-Independance Performance

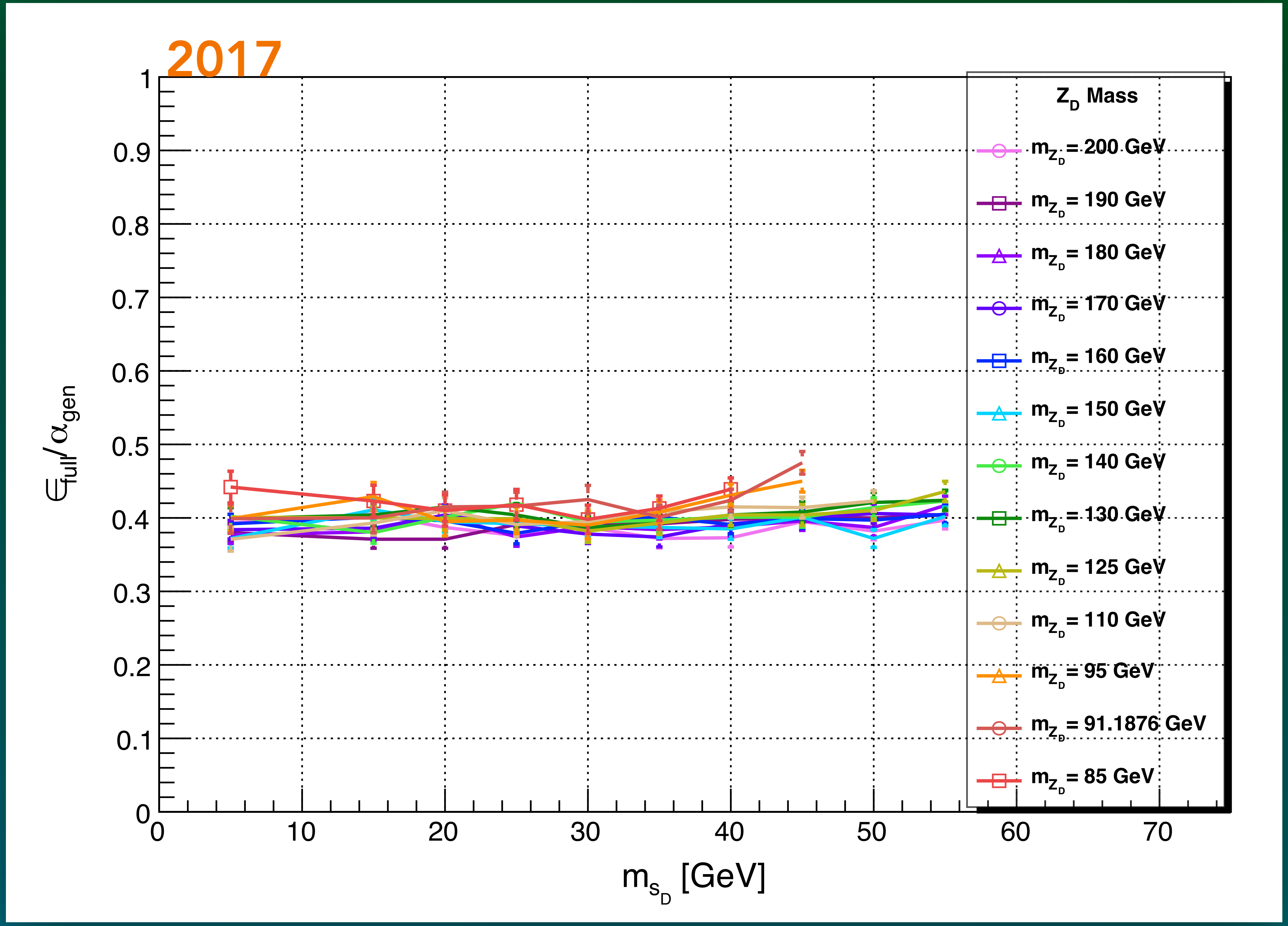

Figure33: Total selection efficiency over generator level selection acceptance, $\epsilon_{Full}/\alpha_{gen}$ as a function of the s_D mass for various Z_D masses in the vector portal model. The KM parameter, ε, is 10^{-2}

FLORIDA TECH

2017 Analysis

Background: Below ϒ Resonances

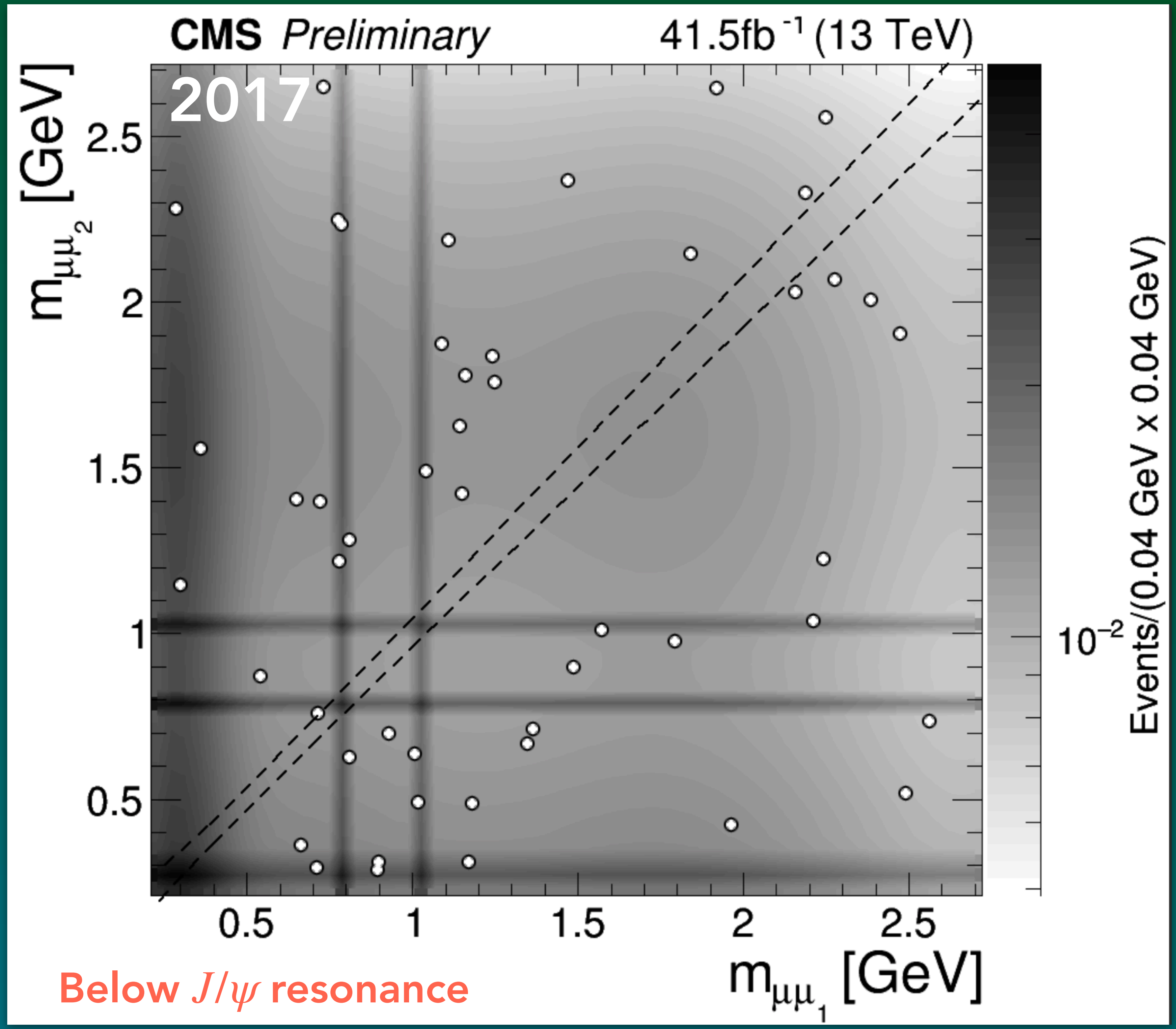

Figure34: 2D QCD background template + data at the CR

- 2D template integral SR/CR = 0.044/0.964
- 2-dimu events at CR: 49 (**SR remain blinded**)
- Estimated BKG events at SR: **2.26 +/- 0.32** (stat.)

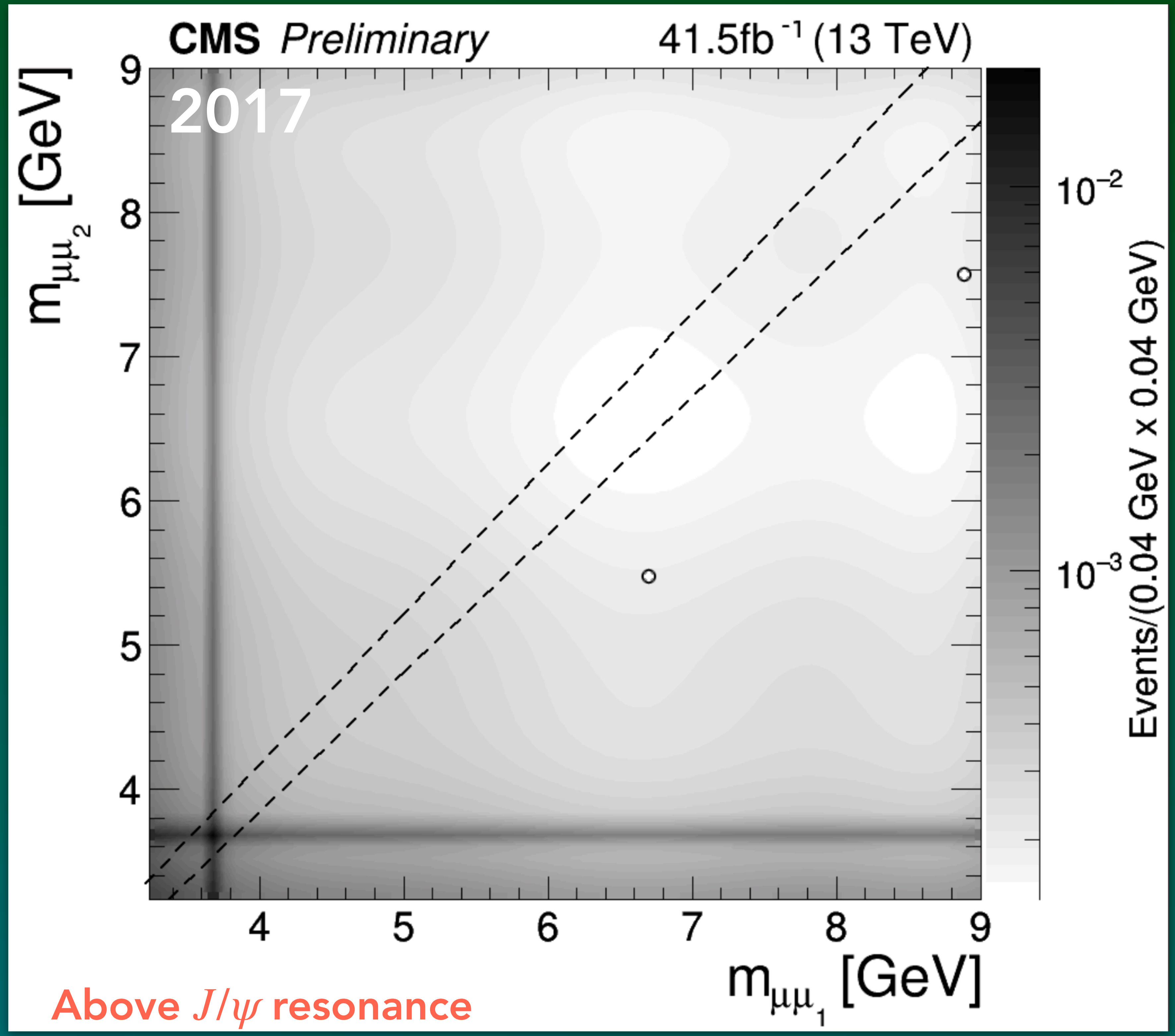

Figure35: 2D QCD background template + data at the CR

- 2D template integral SR/CR = 0.087/0.918
- 2-dimu events at CR: 2 (**SR remain blinded**)
- Estimated BKG events at SR: **0.19 +/- 0.13** (stat.)

2017 Analysis

Background: Above ϒ Resonances

- For 2017 analysis we used QED MC simulated samples in CR for $\mu\mu_1$ and $\mu\mu_2$ similar to the 2018 analysis
- Used Kernel Density Estimation (KDE) to fit the distributions
- Constructed 2D KDE templates
- The signal region in the corridor is still blinded

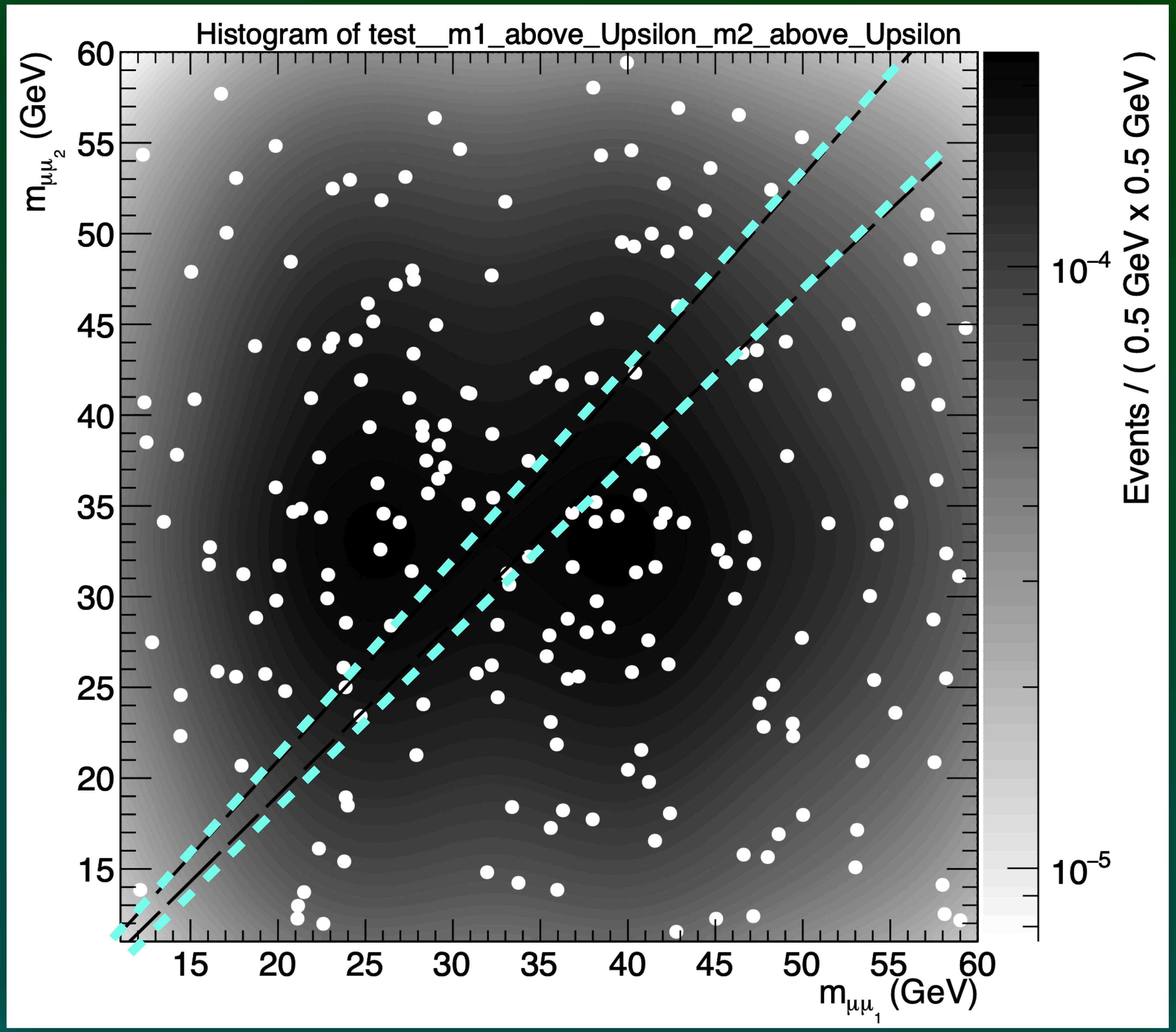

Figure36: 2D KDE background template for above ϒ resonance masses

- 2D template integral SR/CR = 0.082/0.918
- 2-dimu events at CR: 212 (**SR remain blinded**)
- Estimated BKG events at SR: **18.97 +/- 1.3** (stat.)

2017 Analysis

2017 Summary

- The expected limit is to be set after scale factor calculations, such as: HLT, NNLO, and reconstruction scale factors
- The results to be combined with 2018 and 2016 results using the Higgs combine tool
- Unblind 2017 analysis and produce final limit
- The analysis remains approximately near zero background analysis

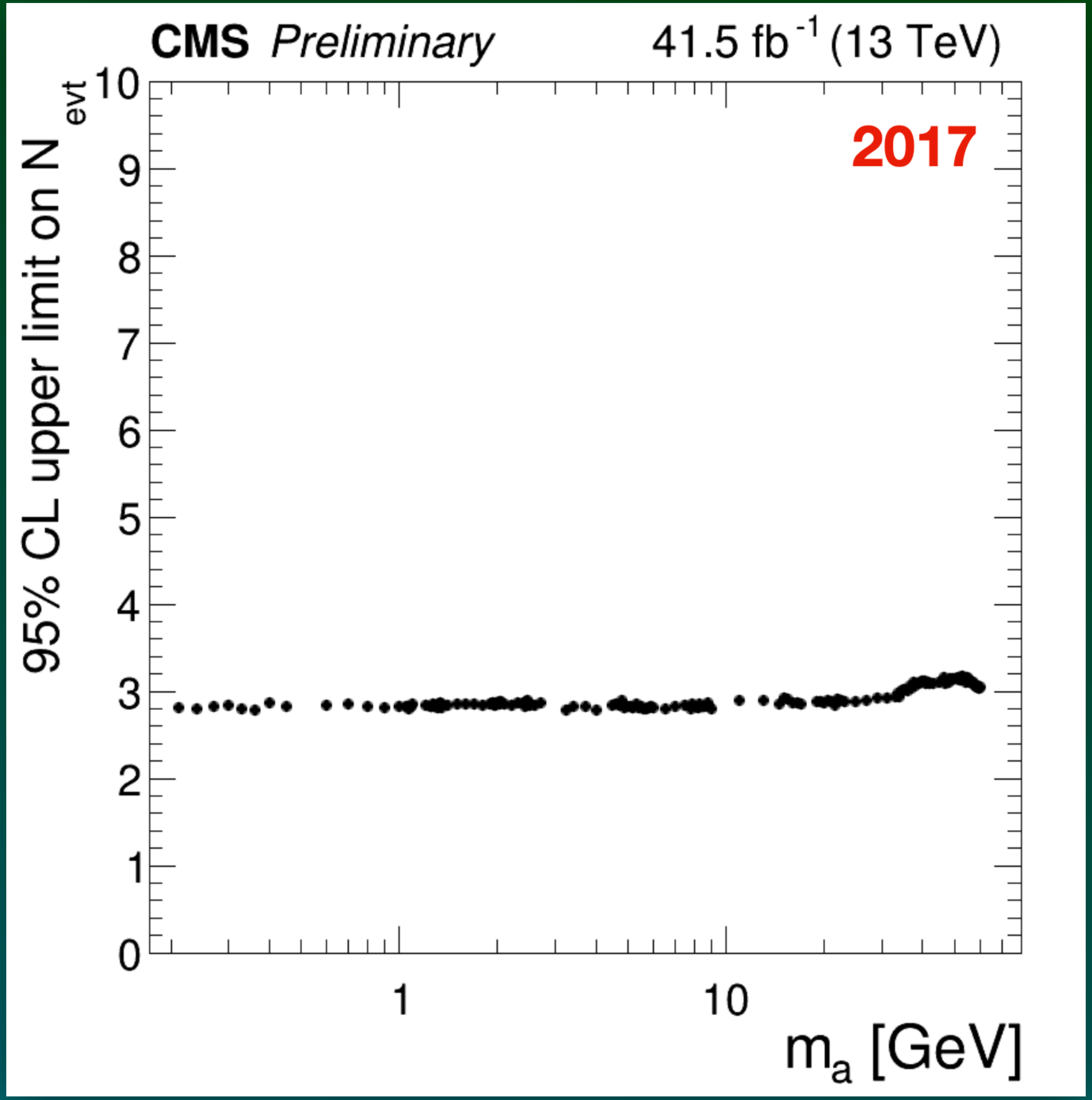

Figure37: Expected model independent 95% CL upper limit on the number of events

Summary

- A model independent analysis for $pp \rightarrow 2a \rightarrow 4\mu$ is represented

- A vector-portal model is introduced as a benchmark dark matter model: $pp \rightarrow Z_D \rightarrow s_D\overline{s_D} \rightarrow 4\mu$

- Model independent upper limits on kinetic mixing parameter, cross-section branching ratio, and acceptance is set

- The 2018 data from CMS is analyzed

- We are adding 2017 data to the analysis to improve the background modeling

Conferences and Awards

- Winter 2022: First place award for International ML4SCI Machine-Learning Hackathon.
- Summer 2021: DPF July Virtual Meeting.
- Spring 2020: APS April Virtual Meeting.
- Fall 2018: The 85th annual meeting of the APS Southeastern Section.
- pring 2018: Outstanding student of the year award at Florida Institute of Technology.
- Winter 2018: Awarded the CMS Authorship.
- Fall 2017: IEEE Nuclear Science Symposium and Medical Imaging Conference (NSS/MIC).
- Spring 2017: APS April Meeting.
- Spring 2017: Florida Academy of Sciences- 81 st Annual Meeting: Has recognized as an Honorable Mention by the Physics and Space Sciences Section of the Academy.

Publications

- Conferences
  - “Vector-Portal Search for Dark Matter Particles", Aug 2020 (Snowmass LOI)
  - "Low-mass GEM detector with radial zigzag readout strips for forward tracking at the EIC", Nov 2017 [Operational involvement]
- Papers
  - "Quality Control of Mass-Produced GEM Detectors for the CMS GE1/1 Muon Upgrade", March 2022
  - "Illuminating long-lived dark vector bosons via exotic Higgs decays at s√=13TeV", Nov 2021 (last revised 27 Feb 2022)
  - "Layout and Assembly Technique of the GEM Chambers for the Upgrade of the CMS First Muon Endcap Station", Dec 2018
  - "Study of lifetimes and cross-sections of a dark vector boson with a final state of muons and dark fermions at $\sqrt{s}$ = 13 TeV" Sept 2021 (AN)
  - "CMS Technical Design Report for the Phase-2 Upgrade of the CMS Muon Detectors," Sept 2017 (TDR)
- Currently active
  - HIG-21-004: 2018 analysis
  - AN-21-220: 2017 analysis

References

[1] E. Dudas, Y. Mambrini, S. Pokorski, and A. Romagnoni, "Invisible z′ and dark matter," Journal of High Energy Physics, vol. 2009, no. 08, p. 014, 2009

[2] J. Goodman and W. Shepherd, "Lhc bounds on uv-complete models of dark matter," arXiv preprint arXiv:1111.2359, 2011

[3] H. An, X. Ji, and L.-T. Wang, "Light dark matter and zprime dark force at colliders," Journal of High Energy Physics, vol. 2012, no. 7, pp. 1–25, 2012

[4] J. L. Feng, M. Kaplinghat, H. Tu, and H.-B. Yu, "Hidden charged dark matter," Journal of Cosmology and Astroparticle Physics, vol. 2009, no. 07, p. 004, 2009.

[5] J. D. Wells, "How to find a hidden world at the large hadron collider," arXiv preprint arXiv:0803.1243, 2008.

[6] D. Curtin, R. Essig, S. Gori, and J. Shelton, "Illuminating dark photons with high-energy colliders," Journal of High Energy Physics, vol. 2015, no. 2, pp. 1–45, 2015.

[7] A. M. Sirunyan et al., "A search for pair production of new light bosons decaying into muons in proton-proton collisions at 13 TeV," Physics Letters B, vol. 796, pp. 131–154, 2019.

[8] D. Abercrombie et al., "Dark Matter Benchmark Models for Early LHC Run-2 Searches: Report of the ATLAS/CMS Dark Matter Forum," Phys. Dark Univ., vol. 27, p. 100371, 2020.

[9] F. Bishara, R. Contino, and J. Rojo, "Higgs pair production in vector-boson fusion at the LHC and beyond," Eur. Phys. J. C, vol. 77, no. 7, p. 481, 2017.

Backups

The Experimental Apparatus

Offline Muon Reconstruction

- Offline reconstruction reconstruction process starts after the data taking
- The offline muon reconstruction benefits from similar algorithms as online: PF and Kelman fitter at the HLT level
- CMS PF algorithm then accepts the reconstructed muons and applies selection
- Selection: such as isolation & Single/DoubleMuon trigger types apply to SA, tracker, or global muons.
- CMS reconstruction software provides fits and charge weighting to form segments
- Muon IDs include loose, medium, tight, soft, and high momentum muons
- **Loose muons** are used for **prompt analysis** at the primary vertex, which is the focus of this thesis.
- Tune-P algorithm chooses a final p_t measurement from several refits of the muon tracks based on statistical goodness-of-fit and relative pt resolution.
- The fit that is used in my analysis is the **inner-tracker-fit**, where the p_t is determined solely based on tracker fit.

FLORIDA TECH

GEMs: QC Step 5b

Response Uniformity Measurement

- A GE1/1 readout board is divided into **768 regions** called **slices**

- Each **slice** containing **4 readout strips**.

- The **charge** collected from a **cluster of 4 readout strips** in a slice: **strip cluster charge**.

- The SRS system can produce an **ADC spectrum** for **each slice** or cluster.

- The prominent **peak** in an ADC spectrum for a cluster is the **X-ray fluorescence photopeak of Copper.**

- The fluorescence **photopeak** is located by fitting a **Cauchy distribution**

- The **photopeaks** of all cluster-strip charges are **histogramed**, and a **Gaussian** is fitted to it.

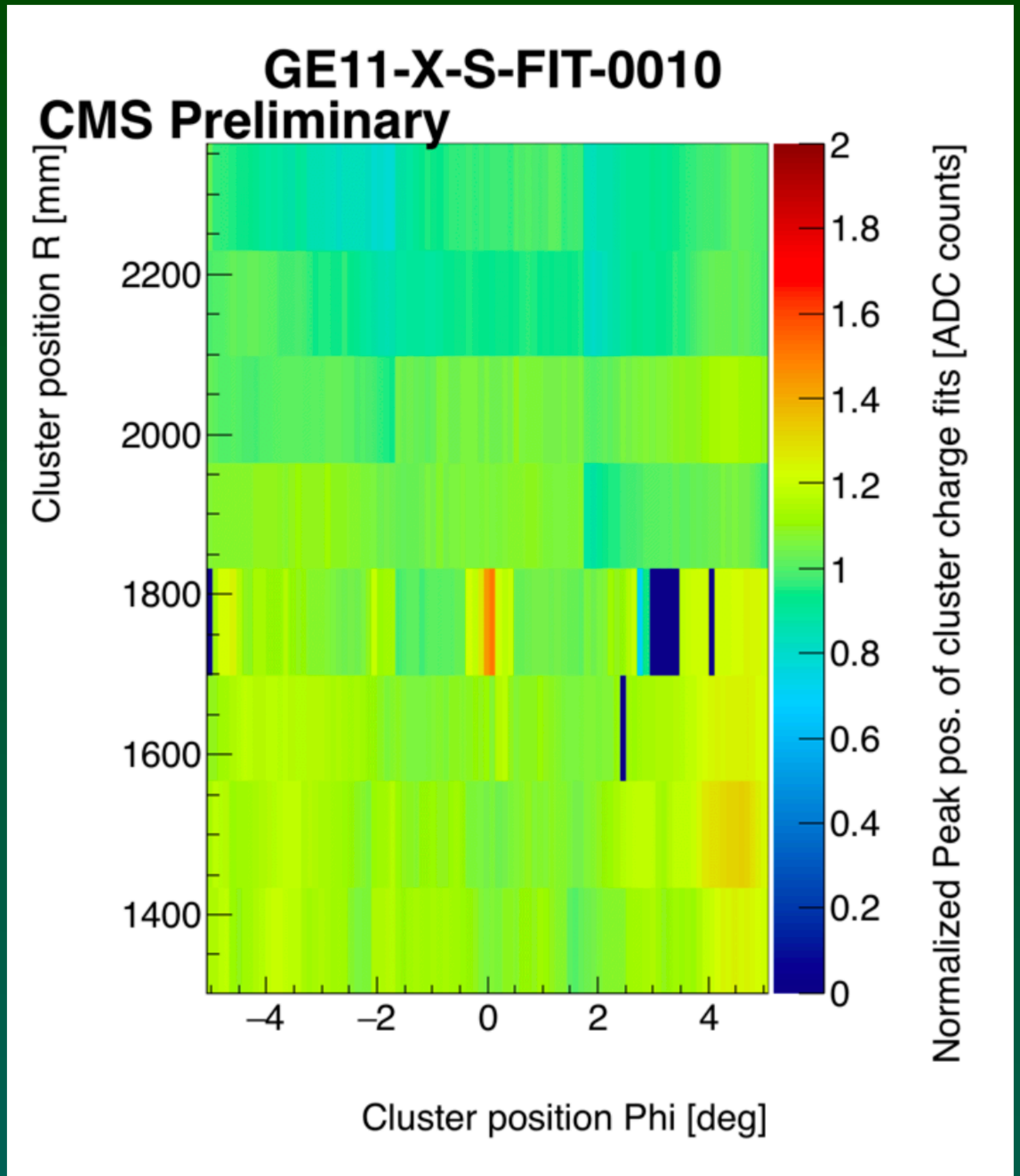

The relative gain variation across a FIT-assembled GE1/1 chamber is shown. The x-axis is plotted as the angular distance from the center of the chamber (iφ) while the y-axis is the radial distance from the beamline. The binning in the horizontal axis corresponds to four-strip slices, while the vertical binning corresponds to the eight iη sectors on the chamber. The color map is the normalized peak position of the cluster charges to the chamber average. The dark blue represents the strips with failed fits.

Appendix A

Benchmark Models

Dark SUSY

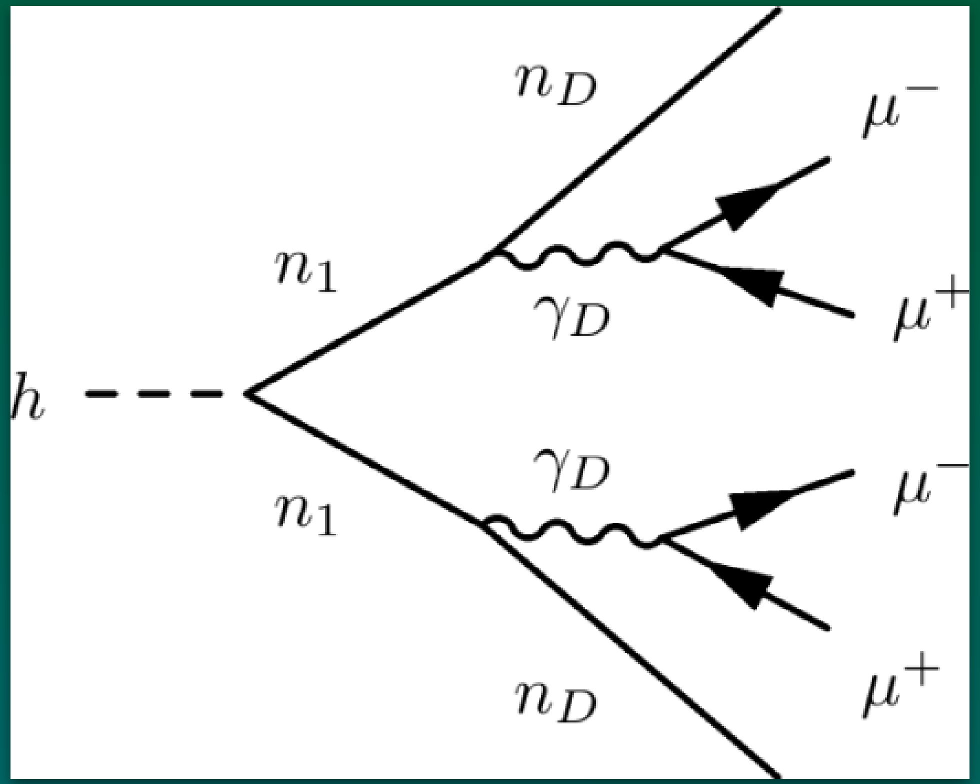

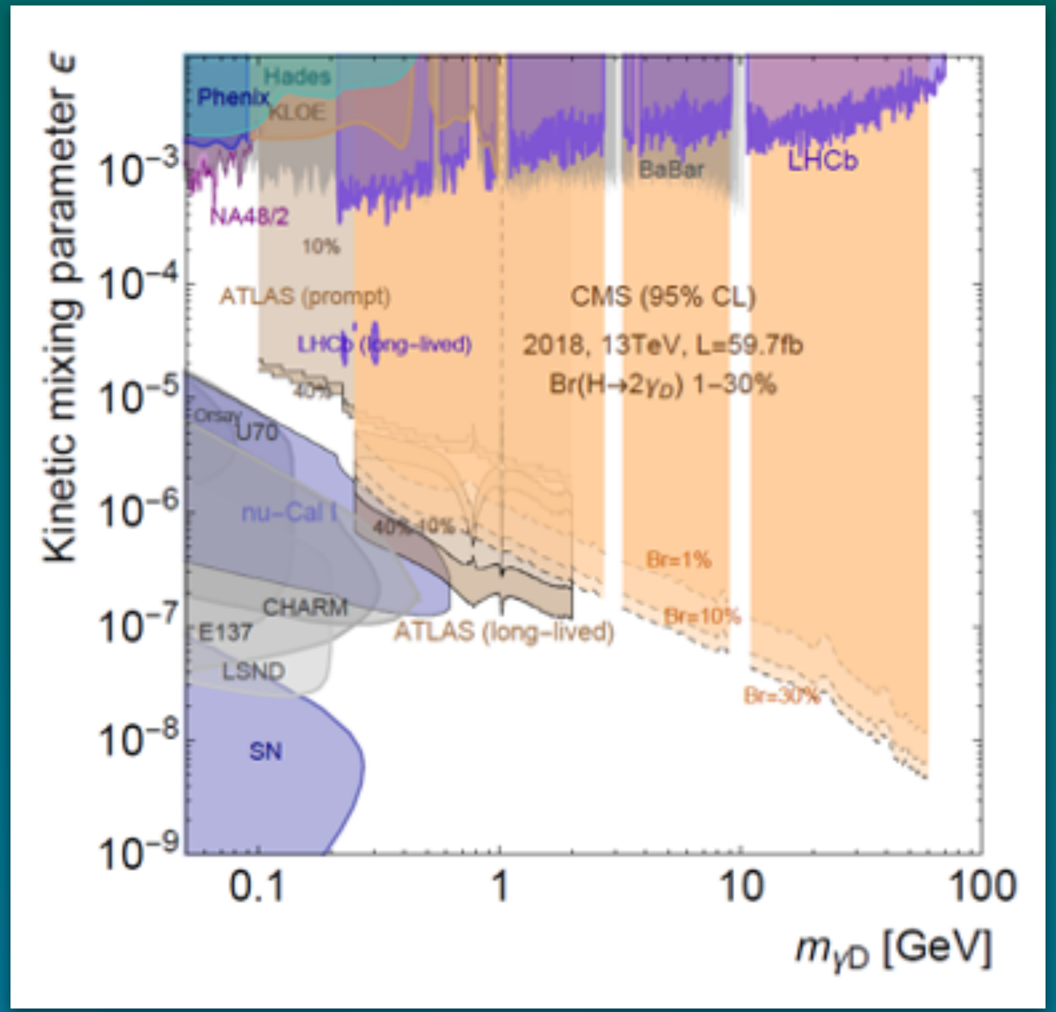

NMSSM

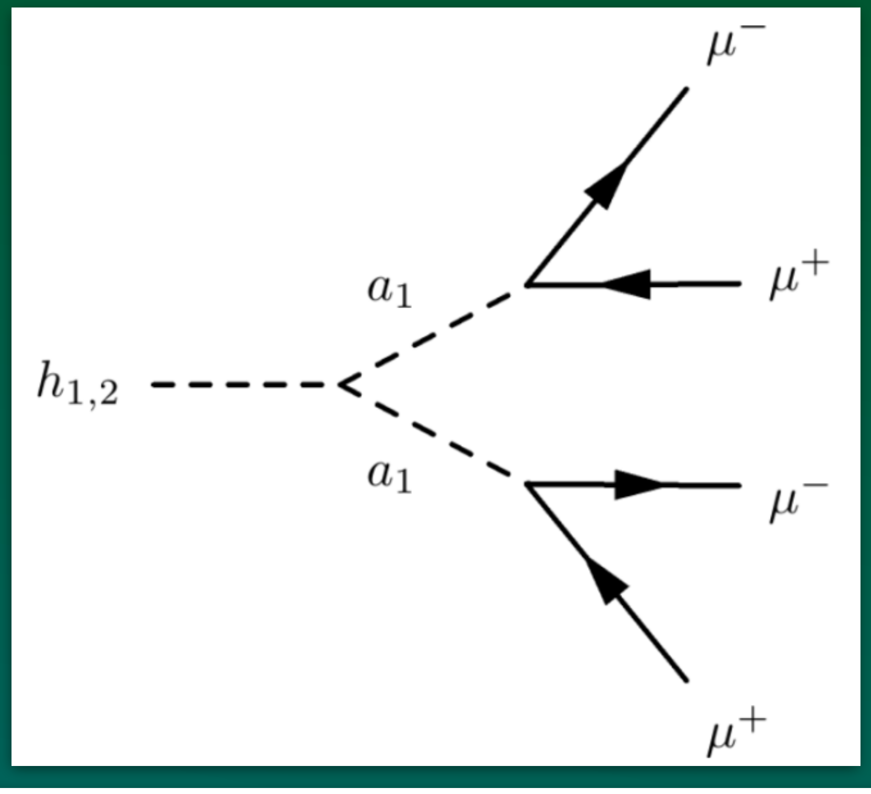

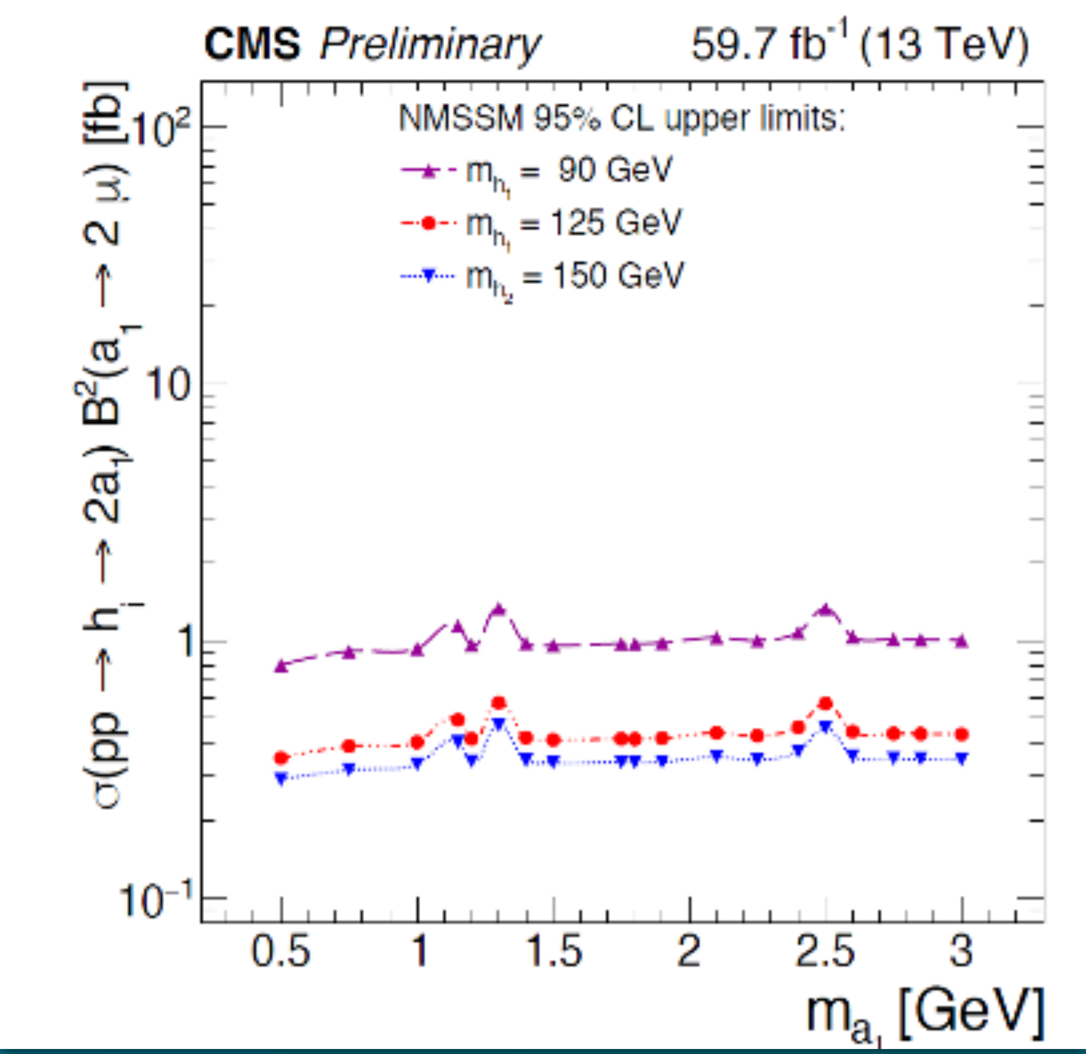

ALP

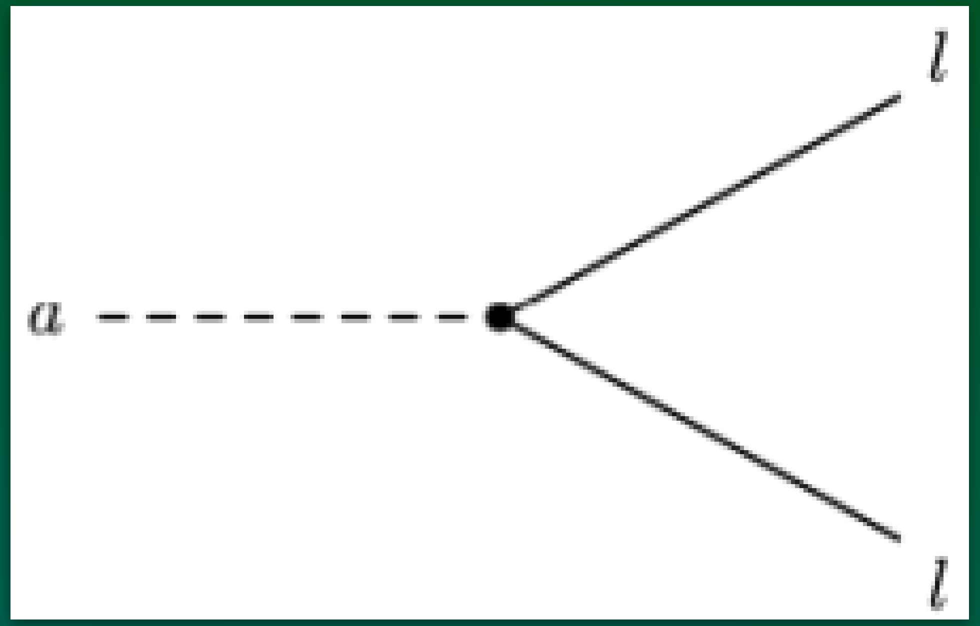

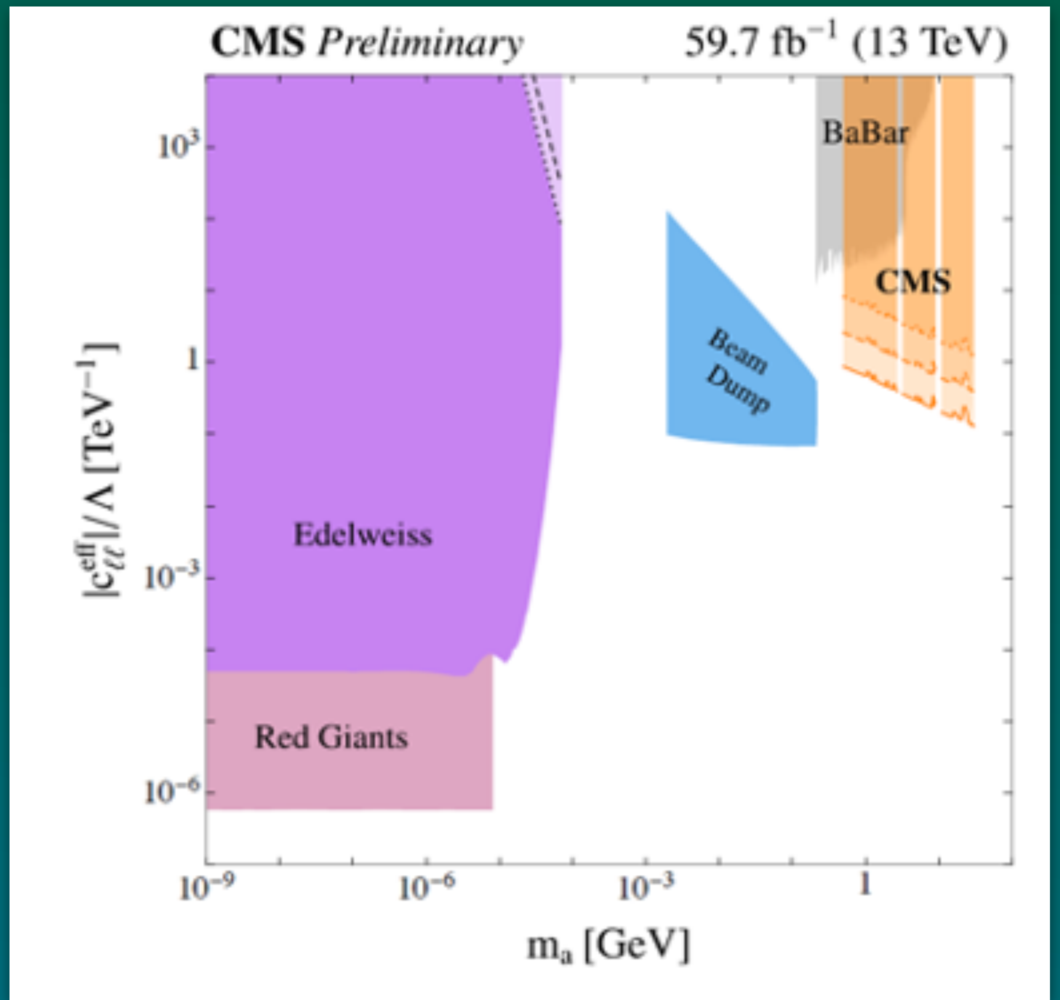

Appendix B

Below ϒ Resonance 1D Mass Templates

From pre-approval talk given by Wei Shi

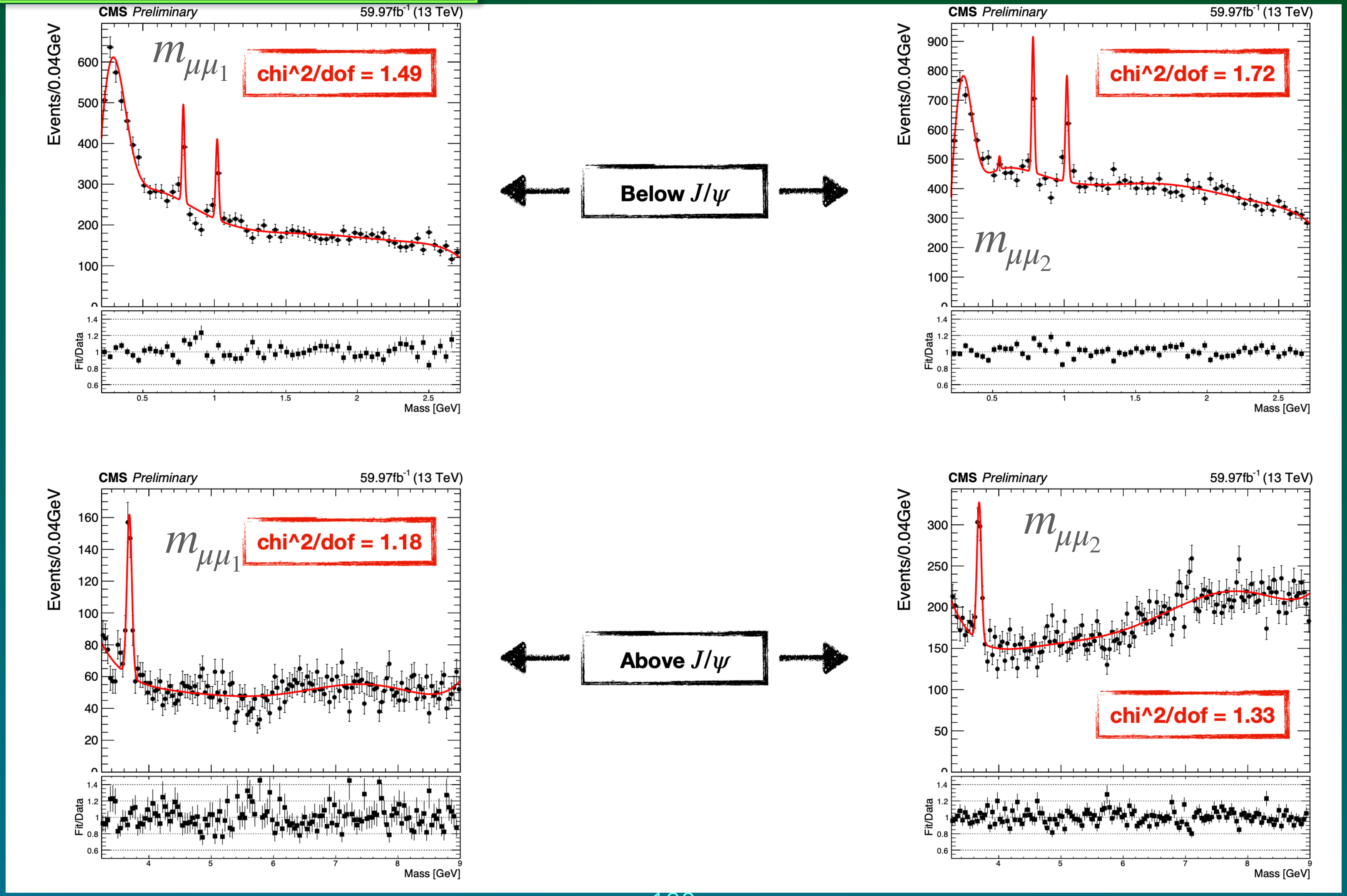

Appendix C

Kernel Density Estimation Above Υ Resonance

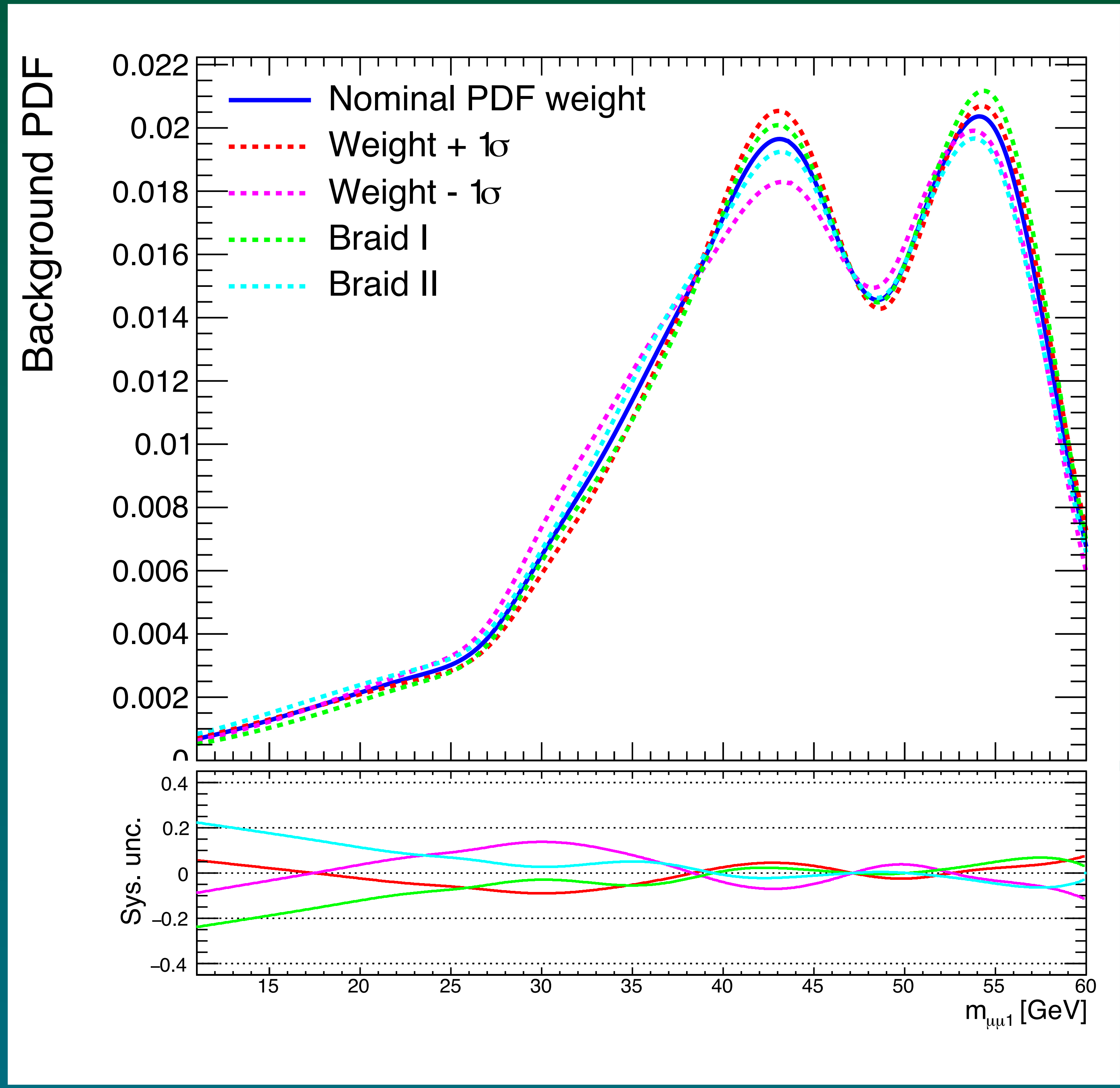

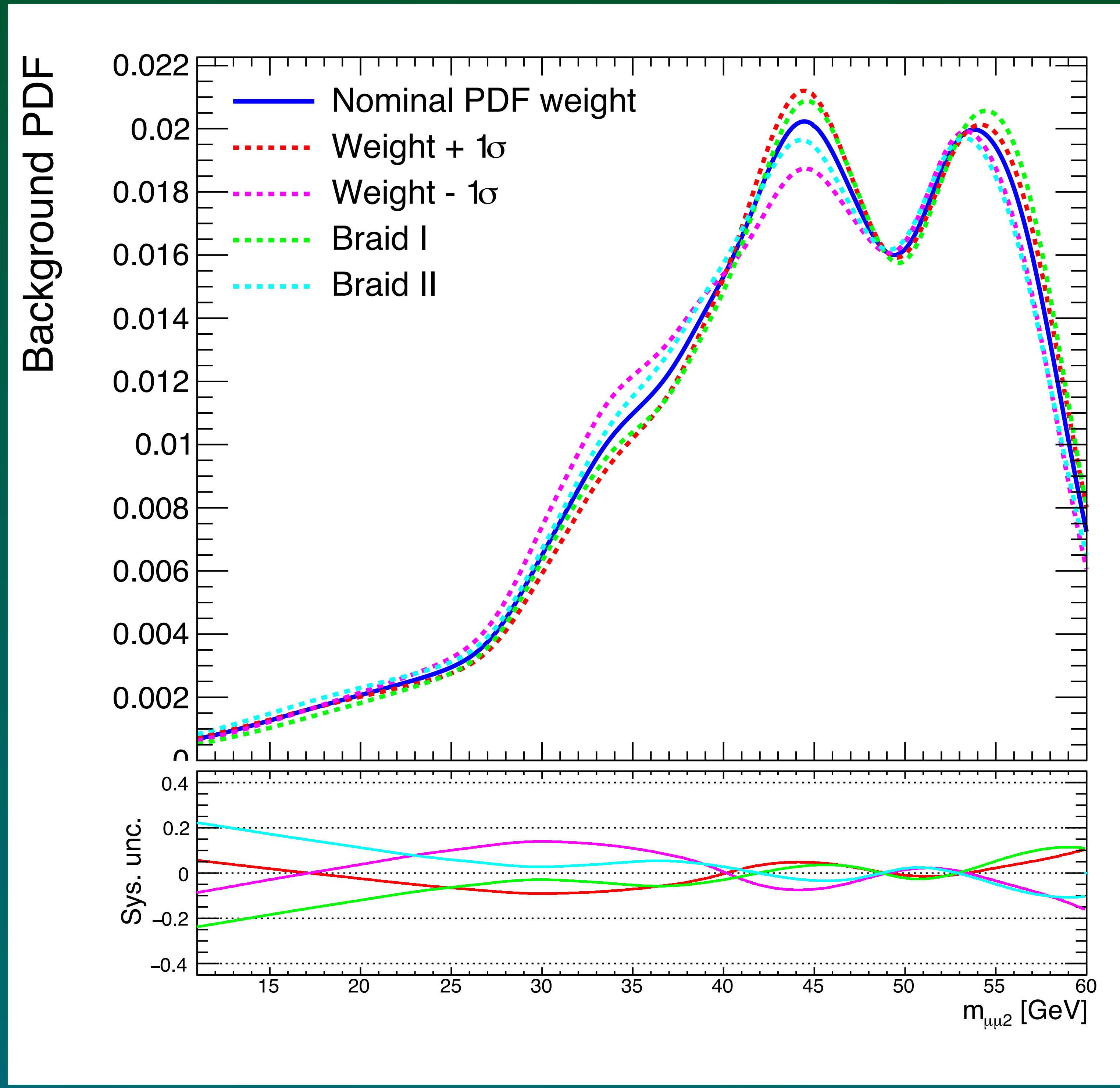

Appendix D

Triggers

- **HLT_DoubleL2Mu23NoVtx_2Cha**
  - Major contribution (70%-90%) to overall trigger efficiency,
    important for very boosted signals (low mass large cTau)
  - Only available for 2018
- **HLT_Mu18_Mu9_SS, HLT_TrkMu12, HLT_TripleMu_12_10_5**
  - Lower p_T improves trigger efficiency
- 2017 Analysis:
  - **HLT_Mu23_Mu12** replaced **HLT_DoubleL2Mu23NoVtx_2Cha**

2018

Trigger Paths
HLT_DoubleL2Mu23NoVtx_2Cha
HLT_Mu18_Mu9_SameSign
HLT_TrkMu12_DoubleTrkMu5NoFiltersNoVtx,
HLT_TripleMu_12_10_5

2017

Trigger Paths
HLT_Mu23_Mu12
HLT_Mu18_Mu9_SameSign
HLT_TrkMu12_DoubleTrkMu5NoFiltersNoVtx
HLT_TripleMu_12_10_5

Appendix D

Triggers

- **HLT_DoubleL2Mu23NoVtx_2Cha**
  - Major contribution (70%-90%) to overall trigger efficiency,
    important for very boosted signals (low mass large cTau)
  - Only available for 2018
- **HLT_Mu18_Mu9_SS, HLT_TrkMu12, HLT_TripleMu_12_10_5**
  - Lower p_T improves trigger efficiency
- 2017 Analysis:
  - **HLT_Mu23_Mu12** replaced **HLT_DoubleL2Mu23NoVtx_2Cha**

From pre-approval talk given by Wei Shi

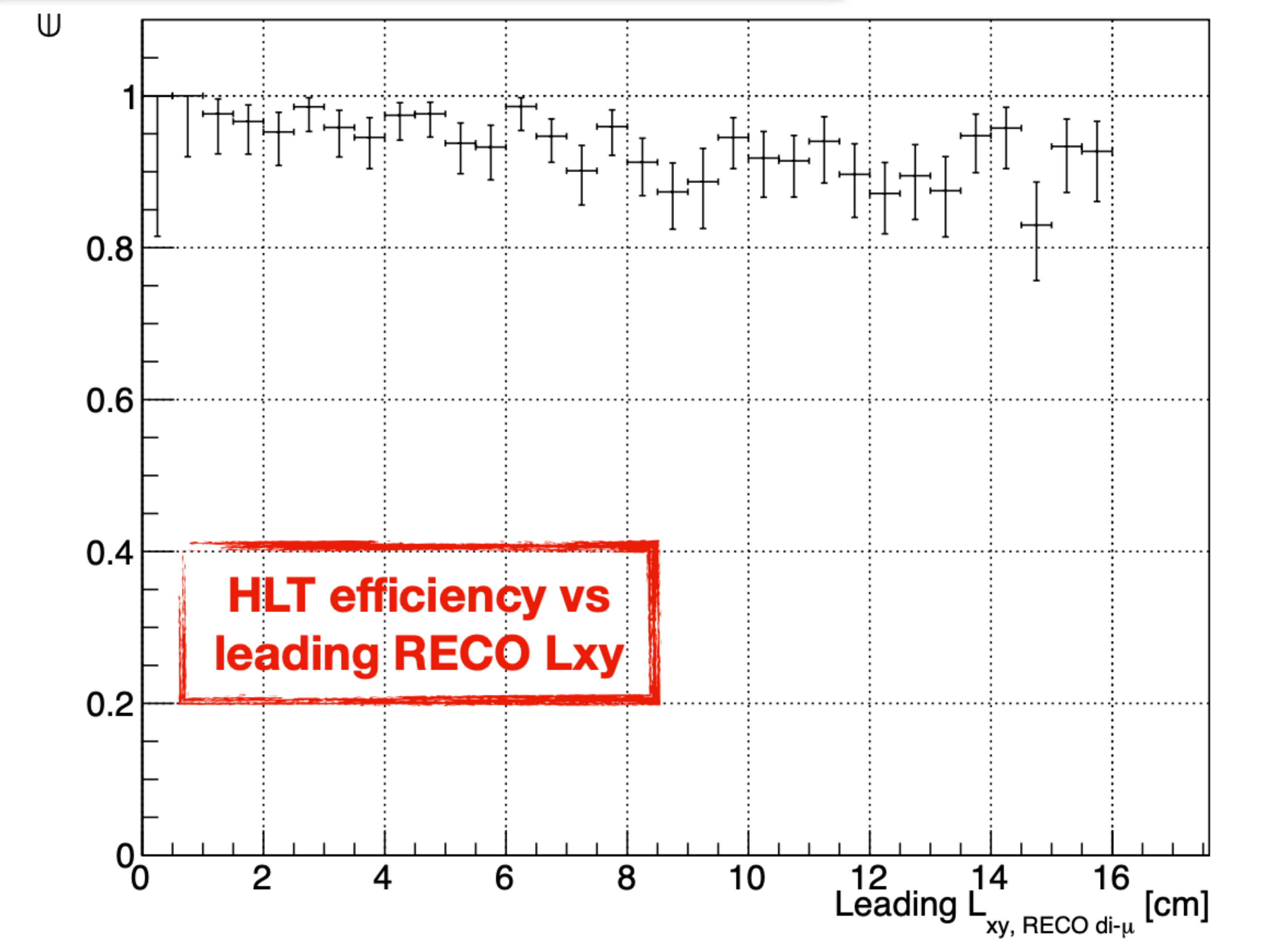

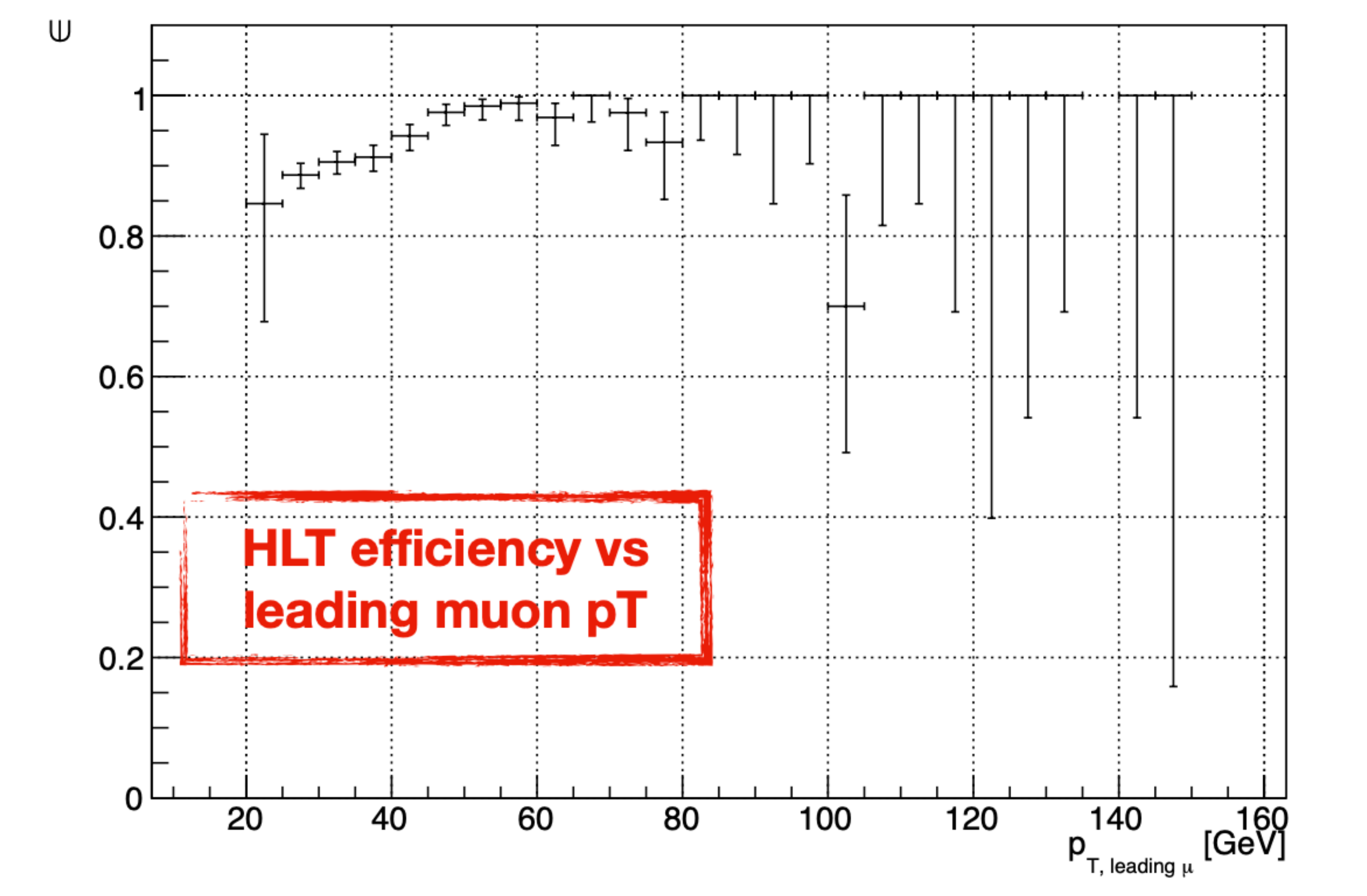

Appendix E

Pixel Hit

- Pixel detector went through and upgrade in 2016
- We require a valid pixel hit in phase-1 detector for at least one muon of each pair
- 4 barrel layers L_{xy} up 16 cm, and 3 forward layers $|L_z|$ up to 51.6 cm

Left: comparative layout of the pixel detector between the layers and disks, before and after the upgrade of pixel detectors.
Right: Transverse-oblique view comparing the pixel barrel layers in the upgraded detector versus pre-upgrade

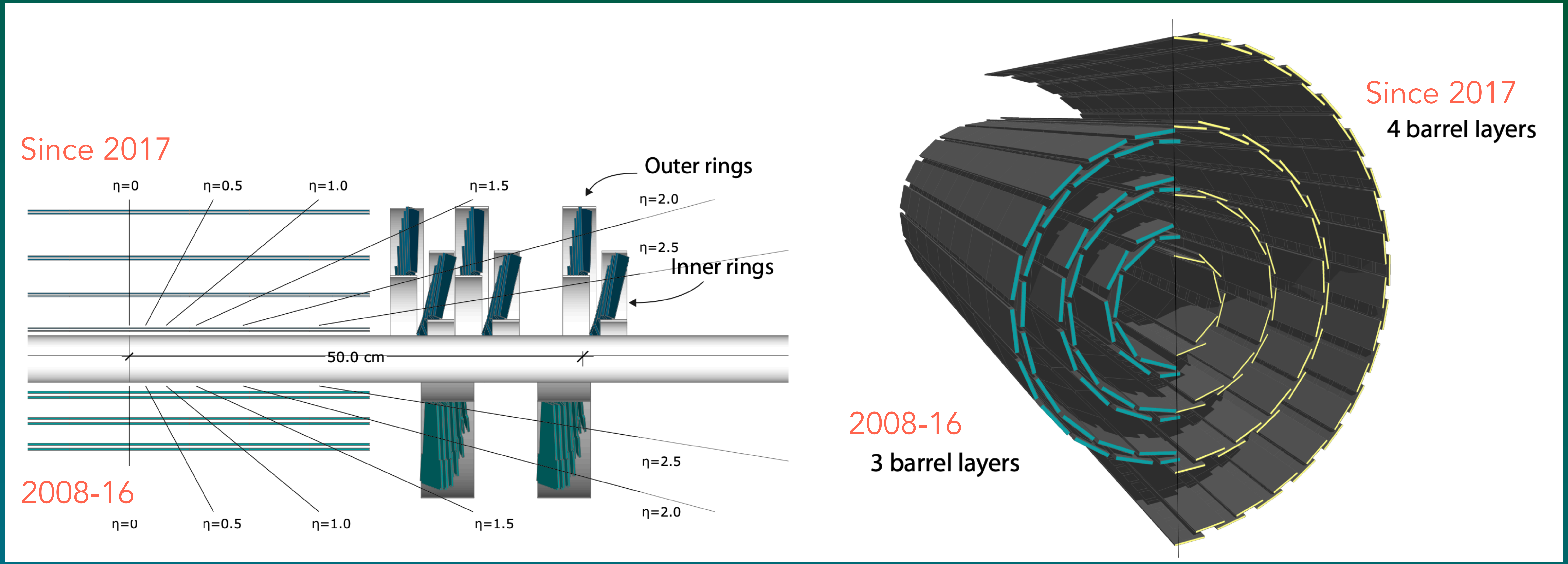

Appendix E

Dimuon Vertex

- dimuon vertex fit probability from KalmanVertexFitter

$$P_{\mu\mu} > P(L_{xy}, f\sqrt{\Delta R}, N_{SA-\mu})$$

$$P(L_{xy}, f\sqrt{\Delta R}, N_{SA-\mu}) = P_0 \times (1 - N_{SA\mu}) \times \exp[-(\frac{L_{xy}}{R_0})^2 \times f(\sqrt{\Delta R})]$$

$$f(\Delta R) = p_0 + p_1 \times \sqrt{\Delta R} + p_2 \times (\Delta R)^2 + p_3 \times (\Delta R)^3 + p_4 \times (\Delta R)^4$$

$p_0 = 0.2,\ R_0 = 10cm,\ p_0 = 8.54,\ p_1 = -50.46,\ p_2 = 109.83,\ p_3 = -92.74,\ p_4 = 36.84$

Appendix E

Mass window

- Choose desired efficiency: calculate the signal significance ($s/\sqrt{S+B}$)
- Significance drops at higher masses
- We chose 90% signal efficiency
- Window size is determined based on desired 90% efficiency

$$f(\frac{m_1 + m_2}{2})$$

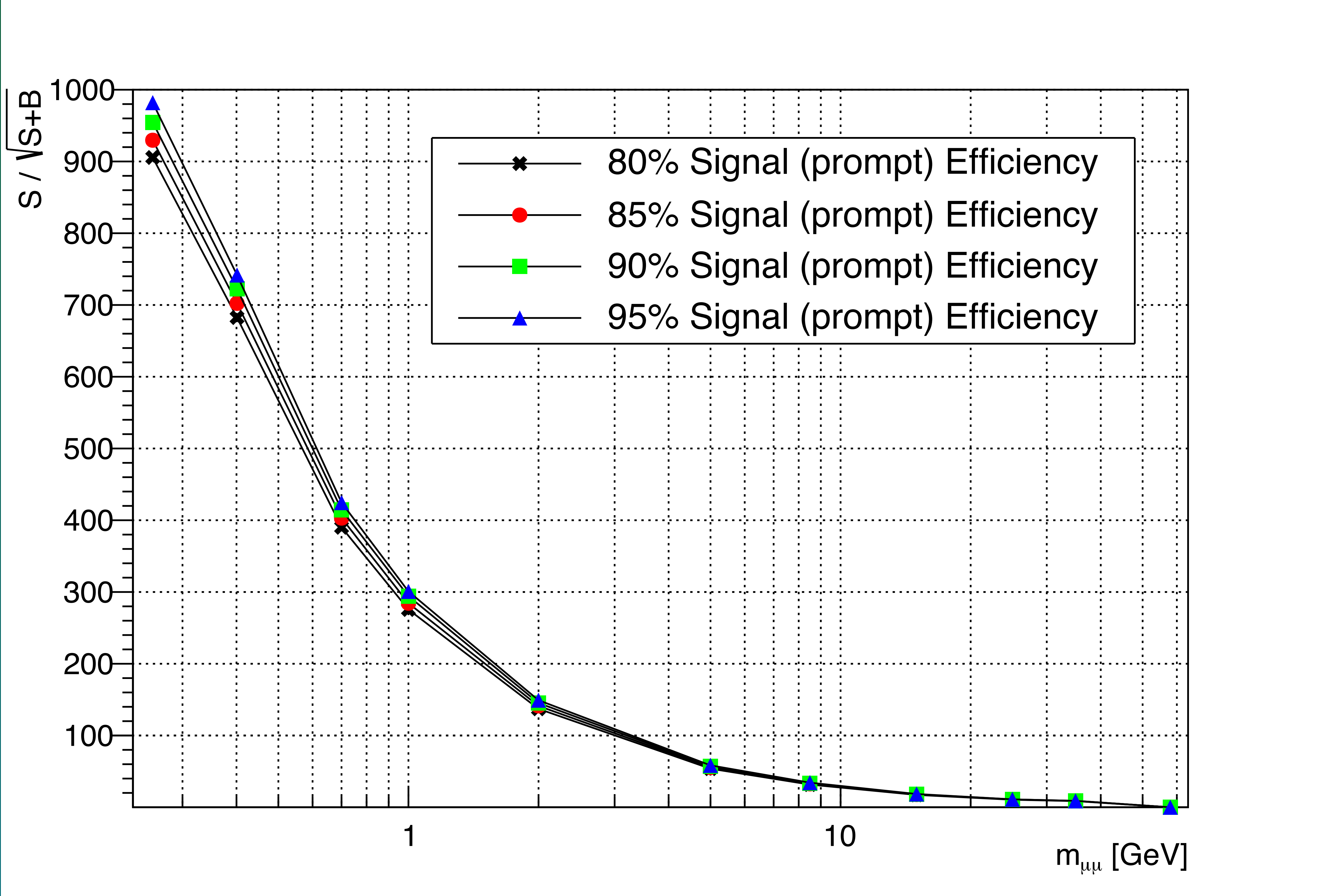

Appendix F

HLT Scale Factor 2018

- Using orthogonal triggers on SingleMuon control dataset and MC simulated events.
- The efficiency of the signal triggers is determined on events passing a set of selection criteria optimized to select WZTo3LNu and ZZTo4l events.
- This is done both on the data and on the MC simulated events. Then the signal HLT efficiency is calculated on the surviving events.
- The cut-flow table of this process is shown on the right.
- The efficiency of the signal HLT on both MC samples is ~0.99, while the efficiency of data is 0.986.
- This results in a trigger scale factor of SF = 0.986/0.99 = 99.6% ± 0.6% (stat.)

Selection	WZTo3LNu	ZZTo4Mu	Data
Pre-selection (if applicable)	301245.23	70517.53	18051620
Passes at least one orthogonal trigger	118895.45	22794.27	18014171
Exactly three muons	22819.88	4019.38	3405670
$\|\eta_i\| < 2.4$	22819.88	4019.38	3405670
$p_{T,1} > 20$ GeV, $p_{T,2} > 20$ GeV, $p_{T,3} > 10$ GeV	1007.26	116.17	373507
Two muons with opposite charge	999.81	115.70	337040
$\|m_{\mu\mu} - m_Z\| < 10$ GeV	835.89	73.05	222817
Medium muon ID	748.68	56.47	12627
$\|d_{xy,i}\| < 0.005$ cm	706.08	48.94	5269
$\|d_{z,i}\| < 0.01$ cm	603.32	39.64	3059
$\mathrm{RelIso}_i < 0.1$	406.95	25.71	437
Passes at least one signal trigger	402.72	25.42	431

Appendix F

HLT Scale Factor 2017

- For 2017 we separate the run eras and emulate the triggers
- The cross-section weighted total MC is calculated
- For each run:
  - $Total\ MC_{eff} = \frac{\sigma_{WZ} \times WZ_{\#events} + \sigma_{ZZ} \times ZZ_{\#events}}{\sigma_{WZ} + \sigma_{ZZ}}$
  - $SF = \frac{data_{eff}}{total\ MC_{eff}}$
- The lumi weighted total SF:
- $Total\ SF = \frac{(4.79 \times 0.908) + (23.19 \times 0.996) + (13.53 \times 0.956)}{41.5}$
- That results in an overall **SF = 0.972**

	Lumi fb^{-1}	WZ eff	ZZ eff	Total MC eff	Data eff	SF
Run B	4.79	0.902	0.912	0.904	0.821	0.908
Run C-E	23.19	0.95	0.96	0.955	0.95	0.994
Run F	13.53	0.996	0.995	0.996	0.953	0.956

Appendix G

Brazilian Plot - Post Fit Observed Limits -2018

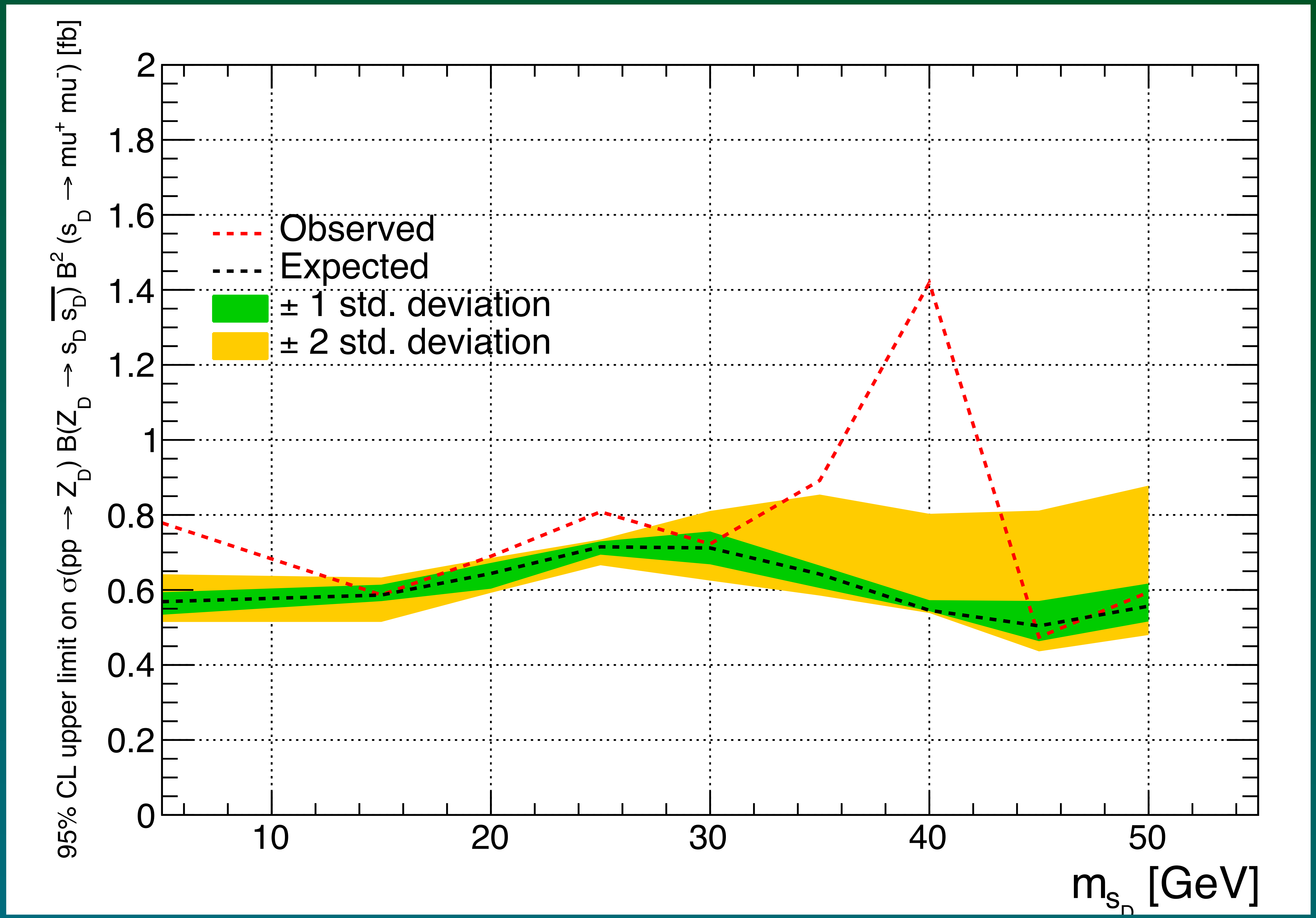

Figure20: Brazilian bands for m_{ZD} =100 GeV. Expected limits after unblinding

Appendix G

Brazilian Plot - Post Fit Observed Limits -2018

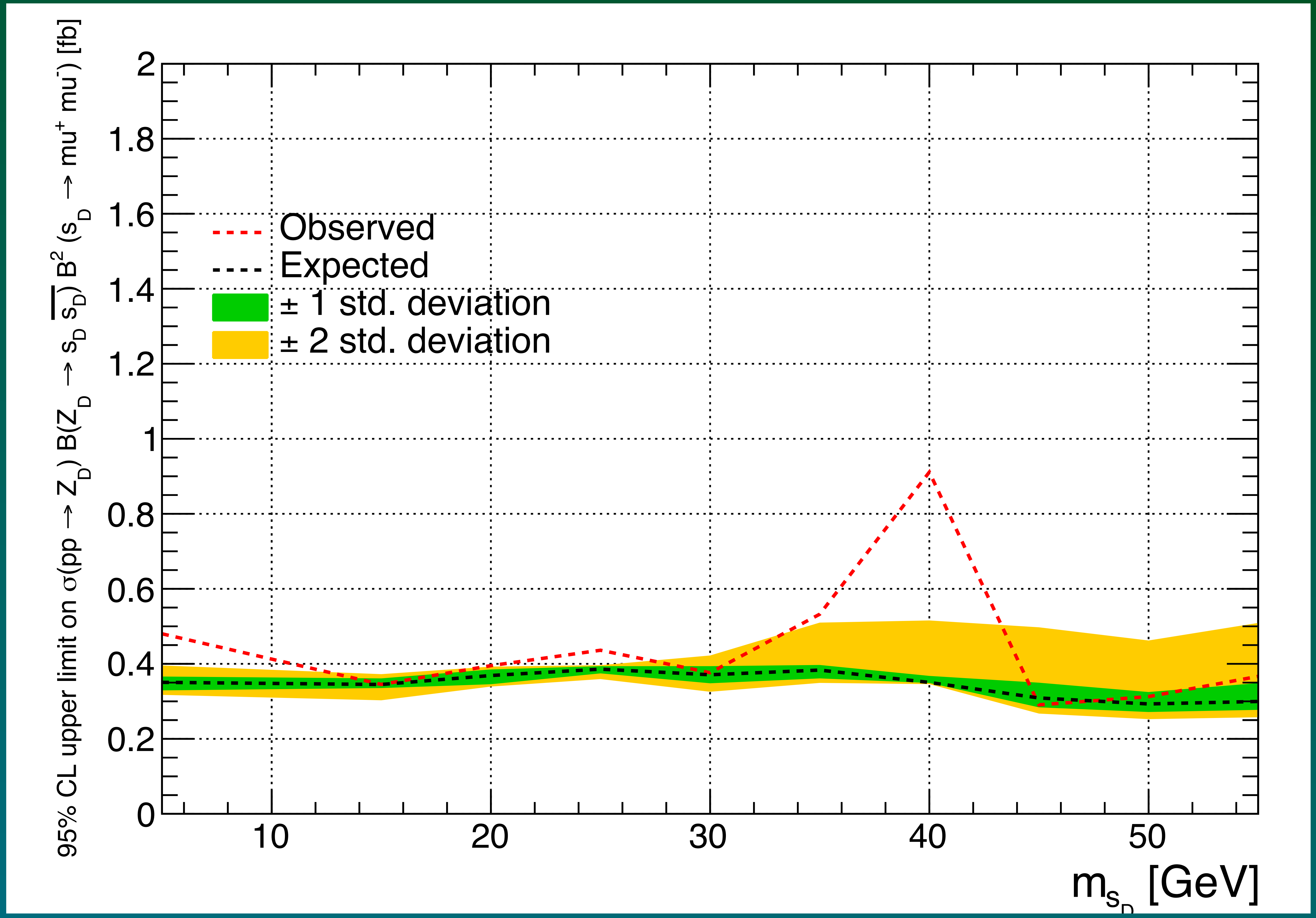

Figure22: Brazilian bands for m_{ZD} =125 GeV. Expected limits after unblinding

Appendix G

Brazilian Plot - Post Fit Observed Limits -2018

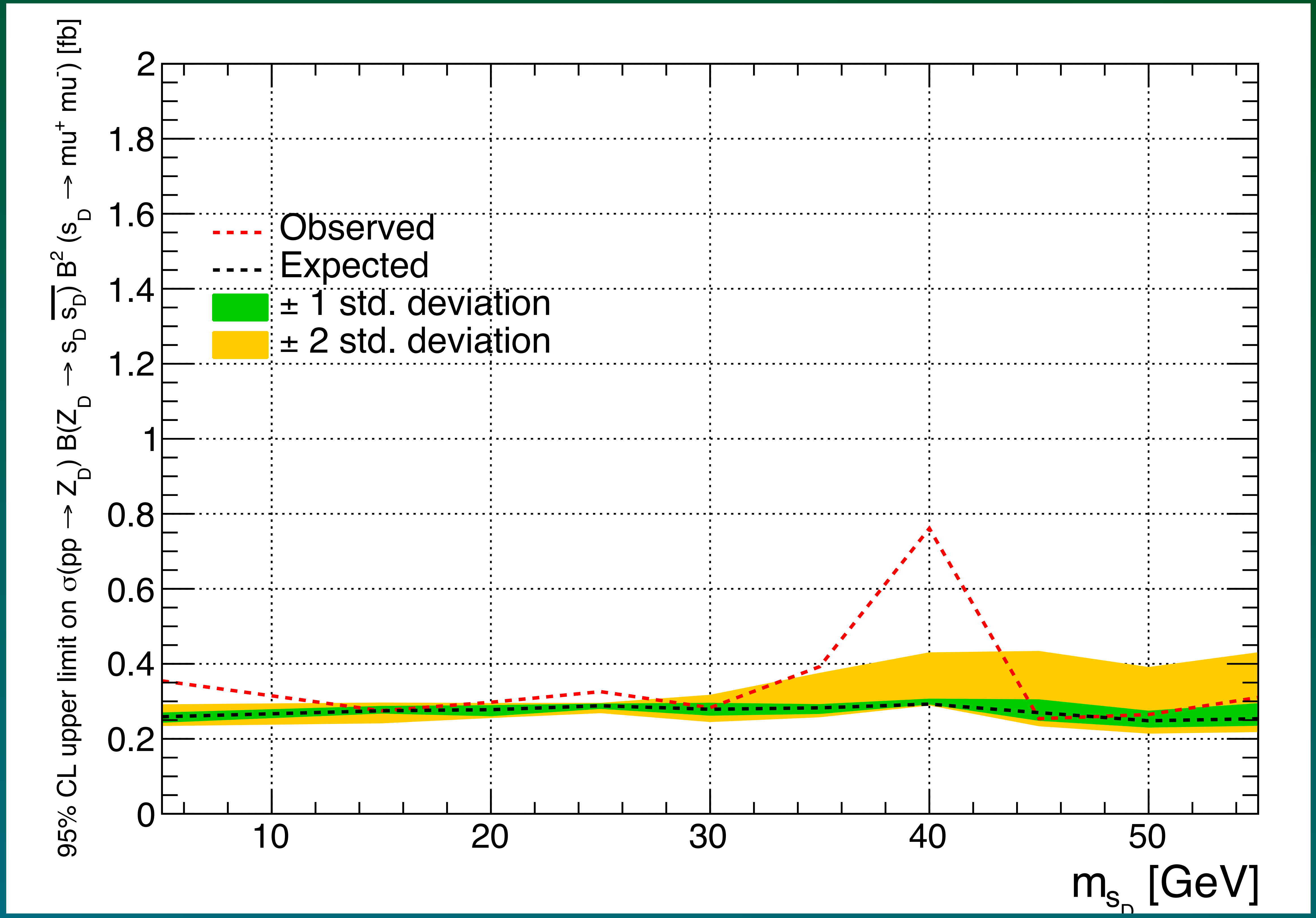

Figure26: Brazilian bands for m_{ZD} =150 GeV. Expected limits after unblinding

Appendix G

Brazilian Plot - Post Fit Observed Limits -2018

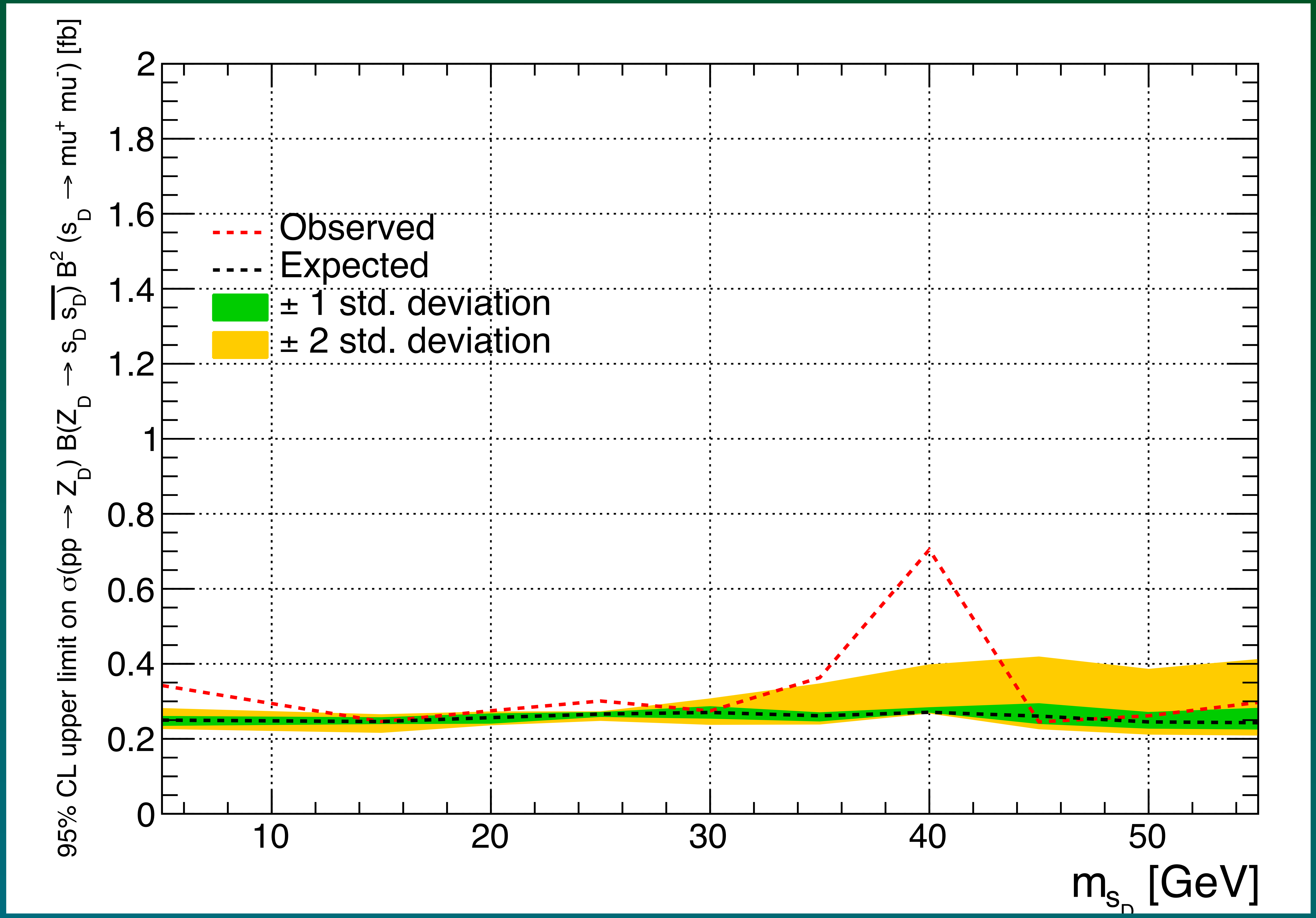

Figure27: Brazilian bands for m_{ZD} =160 GeV. Expected limits after unblinding

Appendix G

Brazilian Plot - Post Fit Observed Limits -2018

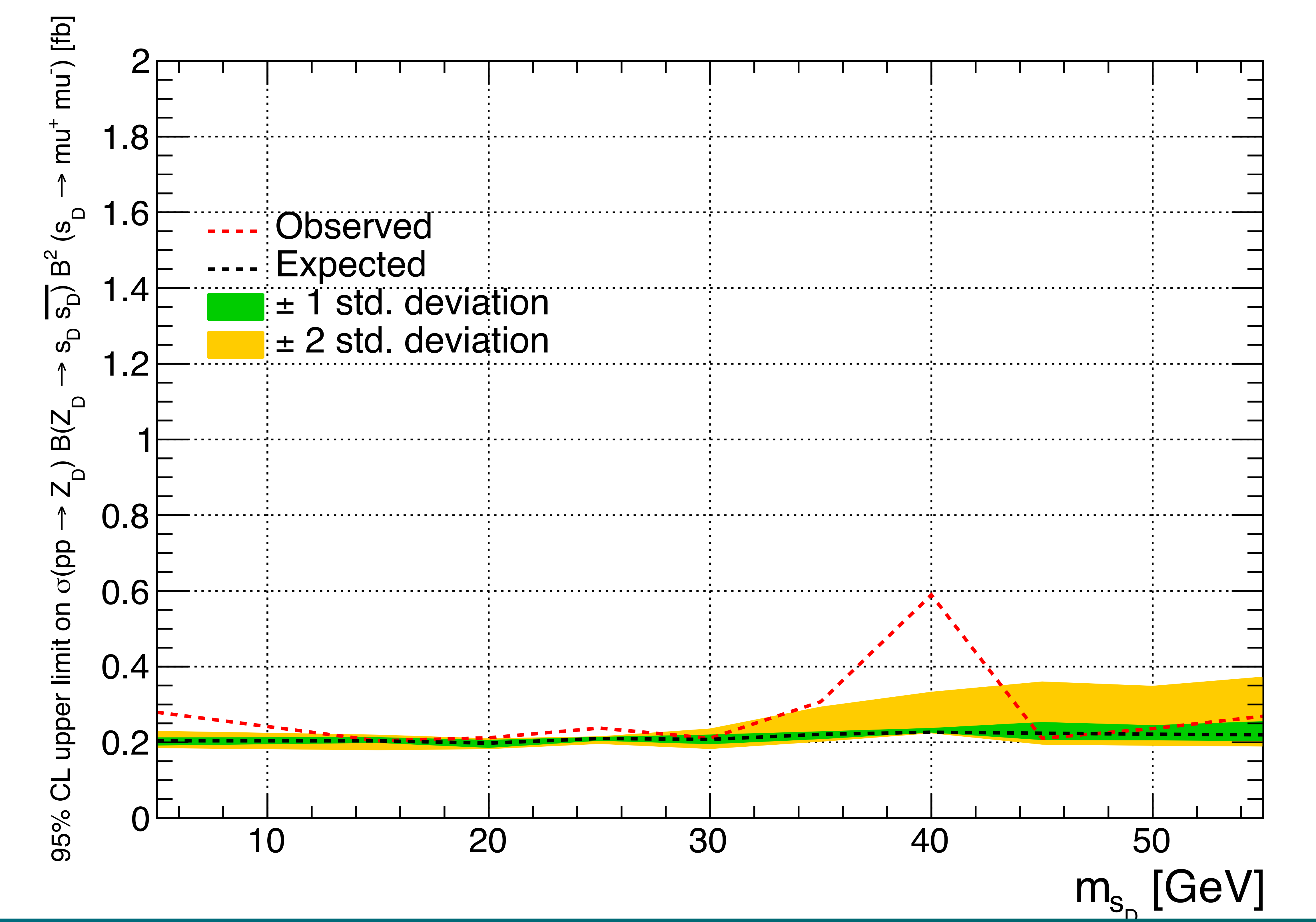

Figure31: Brazilian bands for m_{ZD} =200 GeV. Expected limits after unblinding